

**INVESTIGATION OF PLASTIC DEFORMATION AND
RESIDUAL STRESSES OCCURRED AFTER DEEP
ROLLING PROCESS ON ALUMINUM 6082 ALLOY
USING FINITE ELEMENT ANALYSIS**

**DERİN OVALAMA İŞLEMİ SONRASINDA 6082
ALÜMİNYUM ALAŞIMI ÜZERİNDE OLUŞAN PLASTİK
DEFORMASYON VE ARTIK GERİLMELERİN SONLU
ELEMENLAR ANALİZİ İLE İNCELENMESİ**

RUHİ BATUHAN SAVAŞKAN

Asst. Prof. MEHMET OKAN GÖRTAN

Supervisor

Submitted to

Graduate School of Science and Engineering of Hacettepe University

as a Fulfillment to the Requirements

for the Award of the Degree of Master of Science

in Mechanical Engineering.

2019

This work titled "INVESTIGATION OF PLASTIC DEFORMATION AND RESIDUAL STRESSES OCCURRED AFTER DEEP ROLLING PROCESS ON ALUMINUM 6082 ALLOY USING FINITE ELEMENT ANALYSIS" by RUHİ BATUHAN SAVAŞKAN has been approved as a thesis for the degree of **Master of Science in Mechanical Engineering** by the Examining Committee Members mentioned below.


Prof. Dr. Bora Yıldırım

Head



Asst. Prof. Dr. Mehmet Okan Görtan

Supervisor



Assoc. Prof. Dr. Benat Koçkar

Member



Assoc. Prof. Dr. Barış Sabuncuoğlu

Member



Asst. Prof. Dr. Osman Selim Türkbaş

Member



This thesis has been approved as a thesis for the degree of **Master of Science in Mechanical Engineering** by Board of Directors of the Institute of Graduate School of Science and Engineering on / /

Prof. Dr. Menemşe GÜMÜŞDERELİOĞLU

Director of the Institute of
Graduate School of Science and Engineering

ETHICS

In this thesis study, prepared in accordance with the spelling rules of Institute of Graduate School of Science and Engineering of Hacettepe University,

I declare that

- all the information and documents have been obtained in the base of academic rules
- all audio, visual and written information and results have been presented according to the rules of scientific ethics
- in the case of using others works, related studies have been cited in accordance with scientific standards
- all cited studies have been fully referenced
- I did not do any distortion in the data set and any part of this thesis has not been presented as another thesis study at this or any other university.

30 / 06 / 2019

Ruhi Batuhan Savaşkan

YAYIMLAMA VE FİKRİ MÜLKİYET HAKLARI BEYANI

Enstitü tarafından onaylanan lisansüstü tezimin/raporumun tamamını veya herhangi bir kısmını, basılı (kağıt) ve elektronik formatta arşivleme ve aşağıda verilen koşullarla kullanıma açma iznini Hacettepe üniversitesine verdiğimi bildiririm. Bu izinle Üniversiteye verilen kullanım hakları dışındaki tüm fikri mülkiyet haklarım bende kalacak, tezimin tamamının ya da bir bölümünün gelecekteki çalışmalarda (makale, kitap, lisans ve patent vb.) kullanım hakları bana ait olacaktır.

Tezin kendi orijinal çalışmam olduğunu, başkalarının haklarını ihlal etmediğimi ve tezimin tek yetkili sahibi olduğumu beyan ve taahhüt ederim. Tezimde yer alan telif hakkı bulunan ve sahiplerinden yazılı izin alınarak kullanması zorunlu metinlerin yazılı izin alarak kullandığımı ve istenildiğinde suretlerini Üniversiteye teslim etmeyi taahhüt ederim.

Yükseköğretim Kurulu tarafından yayınlanan "*Lisansüstü Tezlerin Elektronik Ortamda Toplanması, Düzenlenmesi ve Erişime Açılmasına İlişkin Yönerge*" kapsamında tezim aşağıda belirtilen koşullar haricince YÖK Ulusal Tez Merkezi / H. Ü. Kütüphaneleri Açık Erişim Sisteminde erişime açılır.

- Enstitü / Fakülte yönetim kurulu kararı ile tezimin erişime açılması mezuniyet tarihimden itibaren 2 yıl ertelenmiştir.
- Enstitü / Fakülte yönetim kurulu gerekçeli kararı ile tezimin erişime açılması mezuniyet tarihimden itibaren ay ertelenmiştir.
- Tezim ile ilgili gizlilik kararı verilmiştir.

30 / 06 / 2019

Ruhi Batuhan Savaşkan



ÖZET

DERİN OVALAMA İŞLEMİ SONRASINDA 6082 ALÜMİNYUM ALAŞIMI ÜZERİNDE OLUŞAN PLASTİK DEFORMASYON VE ARTIK GERİLMELERİN SONLU ELEMANLAR ANALİZİ İLE İNCELENMESİ

Ruhi Batuhan Savaşkan

Yüksek Lisans, Makina Mühendisliği Bölümü

Tez Danışmanı: Dr. Öğr. Üyesi Mehmet Okan Görtan

Haziran 2019, 127 Sayfa

Bu çalışmanın amacı, farklı geometrilere sahip örneklerde derin ovalama işleminden hemen sonra meydana gelen artık gerilmelerin sonlu elemanlar analizi metodunu kullanarak, gerilmelerin yöne bağımlılığını araştırmaktır. Dinamik yüklemeye maruz kalan parçalarda, yorulma dayanımını arttırmanın en etkili yollarından biri, parça yüzeyinde ve belirli bir derinlikte baskısal artık gerilmelerin oluşturulmasıdır [1]. Derin ovalama, baskısal artık gerilmelerin oluşturulmasında en etkili yöntemdir [2]. Bu işlem sırasında, parçaların yüzeyinde bir hidrolik küre veya silindir vasıtasıyla bölgesel plastik deformasyon oluşturulur. Derin ovalamanın asıl amacı, parçanın geometrisini değiştirmek değil, yalnızca yüzeyde plastik deformasyon oluşturarak malzemenin mekanik özelliklerini geliştirmektir [3]. Bu araştırma sırasında, süspansiyon parçalarının imalatında sıkça kullanılan alüminyum alaşımı EN AW-6082 (AlSi1MgMn) incelenecektir.

Bu inceleme sırasında farklı örnekler üretilmiştir. İlk olarak; alüminyum örnekler T4 ve T6 olarak ısıl işleme tabi tutulmuştur. T4 ve T6 ısıl işlemi görmüş örneklerin ikisinin de hazırlanmasına rağmen; T6 ısıl işlem görmüş malzemeler endüstriyel yorulma uygulamalarında en sık kullanılan malzeme olması nedeniyle bu araştırmada sadece T6 kullanılmıştır.

İkinci olarak; T6 ısıt işlem görmüş örnekler, malzemenin akış eğrisini elde etmek için çekme testine tabi tutulmuştur. Çekme testi sırasında; örnek DIN 50125 çekme testi standardlarına göre tasarlanmıştır. Malzemenin akma ve çekme dayanımı çekme testi ile belirlenmiştir. Ek olarak; yakın tarihli çalışmalarda, prizmatik parçalarda derin ovalama sonrasında malzemenin enlemsel yönündeki baskısal artık gerilmelerin, derin ovalama doğrultusundaki baskısal artık gerilmelerden iki kat daha yüksek olduğu gösterilmiştir [4, 5]. Ancak, silindirik parçaların ($\varnothing 8$ mm, $\varnothing 14$ mm) hem boylamsal hem de enlemsel yönlerinde artık gerilmeler incelenmemiştir. Bu nedenlerden dolayı, artık gerilmelerin bu örnekler üzerindeki yönsel bağımlılığını araştırmak için farklı geometri örnekleri (prizmatik, silindirik) modellenmiştir. Ayrıca, artık gerilmelerin dağılımı, üç farklı ilerleme parametresine (0.1 mm, 0.2 mm, 0.3 mm) göre incelenmiştir. Sonuç olarak; bu örneklerdeki artık gerilme dağılımının sonuçları birbirleriyle karşılaştırılmıştır.

Anahtar Kelimeler: Derin Ovalama, Yüzey İşleme, Yorulma Ömrü, Artık Gerilme

ABSTRACT

INVESTIGATION OF PLASTIC DEFORMATION AND RESIDUAL STRESSES OCCURRED AFTER DEEP ROLLING PROCESS ON ALUMINUM 6082 ALLOY USING FINITE ELEMENT ANALYSIS

Ruhi Batuhan Savaşkan

Master of Science, Department of Mechanical Engineering

Supervisor: Asst. Prof. Mehmet Okan Görtan

June 2019, 127 Pages

The purpose of this study is to investigate the directional dependency of residual stresses on different sample geometries occurred just after deep rolling using finite element analysis (FEA). One of the most effective way to increase the fatigue strength in the parts subjected to dynamic loading is to create compressive residual stresses on the part surface and at a certain depth of the material [1]. Deep rolling is the most effective process in terms of ability to produce compressive residual stresses [2]. During this process, a local plastic deformation is generated on the surface of the parts by means of a hydraulic sphere or cylinder. The main purpose of deep rolling is not to change the geometry of the workpiece but to improve the mechanical properties of the material by plastic deformation of the surface only [3]. During this investigation, aluminum alloy EN AW-6082 (AlSi1MgMn), which is frequently used in the manufacturing of suspension parts, will be examined.

During this examination, different specimens were manufactured. Firstly; the aluminum samples were heat treated as T4 and T6. Despite T4 and T6 heat treated samples were prepared, only T6 was used for investigations, due to the fact that T6 is the commonly used material in the industrial fatigue applications. Secondly; T6 heat treated samples were subjected to tensile test to obtain flow curve of the material. During the tensile test;

material was designed according to the tensile test standards of DIN 50125. Ultimate tensile and yield stress of the material were determined by tensile test. Additionally, in the recent studies showed that the compressive residual stresses in transverse direction are twice as high as in rolling direction on prismatic samples after deep rolling [4, 5]. However, residual stresses were not examined on both the tangential and longitudinal directions of cylindrical parts ($\text{\O}8$ mm, $\text{\O}14$ mm). Due to these reasons, it is aimed to model different sample geometries (prismatic, cylindrical) to investigate directional dependency of residual stresses on these samples. Also, distribution of residual stresses was examined with respect to three different feed parameters (0.1 mm, 0.2 mm, 0.3 mm). Subsequently, the results of residual stress distribution in these samples were compared with each others.

Keywords: Deep Rolling, Surface Treatment, Fatigue Life, Residual Stress

TEŐEKKÜR

Lisans ve yüksek lisans eđitimim boyunca ilgi ve desteđini esirgemeyen, tez alıŐmamın her aŐamasında da bÜyÜk emeđi olan tez danıŐmanım Dr. Öđr. Üyesi Mehmet Okan Görtan'a

Hayatım boyunca her koŐulda desteđini esirgemeyen ve yanımda olan, emeđini ödeyemeyeceđim canım aileme;

Tez dönemim boyunca yanımda olan, sevgi ve desteđini esirgemeyen deđerli arkadaşım Esra Per'e;

Tez dönemim boyunca yardımlarını esirgemeyen iŐ yerindeki ekip liderim Hüseyin Erdoğan'a;

Sonsuz TeŐekkürler,

Ruhi Batuhan Savaşkan

Haziran 2019, Ankara

CONTENTS

ÖZET	i
ABSTRACT	iii
INVESTIGATION OF PLASTIC DEFORMATION AND RESIDUAL STRESSES OCCURRED AFTER DEEP ROLLING PROCESS ON ALUMINUM 6082 ALLOY USING FINITE ELEMENT ANALYSIS	iii
TEŞEKKÜR	v
LIST OF FIGURES	viii
1. INTRODUCTION.....	1
2. STATE OF THE ART.....	3
2.1. Fatigue	3
2.2. Surface Treatment Methods.....	4
2.2.1. Shot Peening.....	4
2.2.2. Laser Shock Peening	5
2.2.3. Roller Burnishing	6
2.2.4. Deep Rolling.....	7
3. MOTIVATION	16
4. FINITE ELEMENT MODEL	19
4.1. Material Model	19
4.1.1. Heat Treatment Process	20
4.2. Finite Element Models.....	25
4.2.1. Longitudinal Rolling Prismatic Model	25
4.2.2. Longitudinal Rolling 14mm Diameter Model.....	30
4.2.3. Longitudinal Rolling 8mm Diameter Model.....	33
4.2.4. Tangential Rolling 14mm Diameter Model.....	36
4.2.5. Tangential Rolling 8mm Diameter Model.....	40
5. RESULTS.....	43

6. SUMMARY AND OUTLOOK	62
7. APPENDIX	64
8. REFERENCES.....	124
ÖZGEÇMİŞ.....	128

LIST OF FIGURES

Figure 1 Fatigue Loading [30].....	4
Figure 2 Shot Peening [32].....	5
Figure 3 Laser Shock Peening [33]	6
Figure 4 Roller Burnishing [36]	7
Figure 5 Deep Rolling [3].....	8
Figure 6 Tool & Specimen Geometry for 2D Analysis [4]	9
Figure 7 Mesh and Analysis Results [4].....	10
Figure 8 Geometry specimen, Rolling Tool and Mesh View [38]	11
Figure 9 The Test Fixture and Rolling Tool [38]	12
Figure 10 Residual Stresses (Numerical, Experimental) in Axial Direction [38].....	12
Figure 11 Residual Stresses (Numerical, Experimental) in Tangential Direction [38].....	13
Figure 12 Comparison between non-treated, DR and LSP treated specimens at different temperatures [23].....	14
Figure 13 Comparison between different applications of SP and DR on fretting fatigue [23]	15
Figure 14 Longitudinal Deep Rolling on a Prismatic Geometry (Conventional) [4, 5].....	16
Figure 15 Tangential Deep Rolling on a Cylindrical Geometry (Conventional) [4, 5].....	17
Figure 16 Longitudinal Deep Rolling on a Cylindrical Geometry (Novel)	18
Figure 17 T4 and T6 Heat Treatment Process	20
Figure 18 Chemical Composition of 6082 Aluminum Alloy [42]	21
Figure 19 DIN 50125 Tensile Test Standard Sample Geometry.....	22
Figure 20 Tensile Test Results for AA 6082 T4 and T6	23
Figure 21 Flow Curves for T4 and T6 Materials	25
Figure 22 Prismatic Model Roller Translation, Rotation and Load Parameters	25
Figure 23 Prismatic Model Course Mesh Structure	26
Figure 24 Prismatic Model Fine Mesh Structure	26
Figure 25 Prismatic Model Z Direction Mesh Structure	27
Figure 26 Deep Rolling Roller Geometry	27
Figure 27 Feed Parameters Between Rollers in Square Model	28
Figure 28 Ø14 mm Model Roller Translation, Rotation and Load Parameters	30
Figure 29 Ø14 mm Model Course Mesh Structure	30

Figure 30 Ø14 mm Model Fine Mesh Structure.....	31
Figure 31 Feed Parameters Between Rollers in Ø14 mm Model.....	32
Figure 32 Ø8 mm Model Roller Translation, Rotation and Load Parameters	33
Figure 33 Ø8 mm Model Course Mesh Structure	33
Figure 34 Ø8 mm Model Fine Mesh Structure	34
Figure 35 Feed Parameters Between Rollers in Ø8 mm Model.....	35
Figure 36 Tangential Rolling Ø14 mm Model Roller Translation, Rotation and Load Parameters	36
Figure 37 Tangential Rolling Ø14 mm Model Course Mesh Structure	37
Figure 38 Tangential Rolling Ø14 mm Model Fine Mesh Structure	38
Figure 39 Tangential Rolling Model Z Direction Mesh Structure	38
Figure 40 Feed Parameters Between Rollers in Ø14 mm Tangential Rolling Model.....	39
Figure 41 Tangential Rolling Ø8 mm Model Roller Translation, Rotation and Load Parameters	40
Figure 42 Tangential Rolling Ø8 mm Model Course Mesh Structure	41
Figure 43 Tangential Rolling Ø8 mm Model Fine Mesh Structure	41
Figure 44 Feed Parameters Between Rollers in Ø8 mm Tangential Rolling Model.....	42
Figure 45 Residual Stress Distribution on Square Model, σ_z , 250 N, 0.2 mm feed.....	44
Figure 46 Residual Stress Distribution on Square Model, σ_x , 250 N, 0.2 mm feed.....	45
Figure 47 Residual Stress Results on Square Model, σ_z , σ_x , 125 N for All Feed Parameters	46
Figure 48 Residual Stress Results on Square Model, σ_z , σ_x , 250 N for All Feed Parameters	46
Figure 49 Residual Stress Results on Square Model, σ_z , σ_x , 500 N for All Feed Parameters	47
Figure 50 Residual Stress Distribution on Ø14 Model, σ_z , 250 N, 0.2 mm feed	48
Figure 51 Residual Stress Distribution on Ø14 Model, σ_x , 250 N, 0.2 mm feed	49
Figure 52 Residual Stress Distribution on Ø8 Model, σ_z , 250 N, 0.2 mm feed	50
Figure 53 Residual Stress Distribution on Ø8 Model, σ_x , 250 N, 0.2 mm feed	51
Figure 54 Residual Stress Results on Ø14 Model, σ_z , σ_x , 125 N for All Feed Parameters .	52
Figure 55 Residual Stress Results on Ø14 Model, σ_z , σ_x , 250 N for All Feed Parameters .	52
Figure 56 Residual Stress Results on Ø14 Model, σ_z , σ_x , 500 N for All Feed Parameters .	53
Figure 57 Residual Stress Results on Ø8 Model, σ_z , σ_x , 125 N for All Feed Parameters ...	53
Figure 58 Residual Stress Results on Ø8 Model, σ_z , σ_x , 250 N for All Feed Parameters ...	54

Figure 59 Residual Stress Results on Ø8 Model, σ_z , σ_x , 500 N for All Feed Parameters ...	54
Figure 60 Residual Stress Results on Ø14 mm Longitudinal and Tangential Model, σ_z , 0.1 mm Feed for All Force Parameters	55
Figure 61 Residual Stress Results on Ø14 mm Longitudinal and Tangential Model, σ_x , 0.1 mm Feed for All Force Parameters	55
Figure 62 Residual Stress Results on Ø8 mm Longitudinal and Tangential Model, σ_z , 0.1 mm Feed for All Force Parameters	56
Figure 63 Residual Stress Results on Ø8 mm Longitudinal and Tangential Model, σ_x , 0.1 mm Feed for All Force Parameters	56
Figure 64 Total Equivalent Plastic Strain Results on Square Model for All Feed and Force Parameters	57
Figure 65 Total Equivalent Plastic Strain Results on Ø14 mm Model for All Feed and Force Parameters	57
Figure 66 Total Equivalent Plastic Strain Results on Ø8 mm Model for All Feed and Force Parameters	58
Figure 67 Total Equivalent Plastic Strain Results on Ø8 mm and Ø14 mm Model for 0.1mm Feed and Force Parameters	58
Figure 68 Square Model, 125 N, 250 N, 500 N, 0.1 mm Feed Parameter, σ_z , σ_x	59
Figure 69 Square Model, 125 N, 250 N, 500 N, 0.2 mm Feed Parameter, σ_z , σ_x	60
Figure 70 Square Model, 125 N, 250 N, 500 N, 0.3 mm Feed Parameter, σ_z , σ_x	60
Figure 71 Square, Ø14 mm, Ø8 mm Model, 125 N, 0.1 mm Feed Parameter, σ_z , σ_x	61
Figure 72 Square, Ø14 mm, Ø8 mm Model, 500 N, 0.1 mm Feed Parameter, σ_z , σ_x	61
Figure 73 Residual Stress Distribution on Square Model, σ_z , 125 N, 0.1 mm Feed Parameter.....	64
Figure 74 Residual Stress Distribution on Square Model, σ_x , 125 N, 0.1 mm Feed Parameter.....	65
Figure 75 Residual Stress Distribution on Square Model, σ_z , 250 N, 0.1 mm Feed Parameter.....	66
Figure 76 Residual Stress Distribution on Square Model, σ_x , 250 N, 0.1 mm Feed Parameter.....	67
Figure 77 Residual Stress Distribution on Square Model, σ_z , 500 N, 0.1mm Feed Parameter	68
Figure 78 Residual Stress Distribution on Square Model, σ_x , 500 N, 0.1 mm Feed Parameter.....	69

Figure 79 Residual Stress Distribution on Square Model, σ_z , 125 N, 0.2 mm Feed Parameter.....	70
Figure 80 Residual Stress Distribution on Square Model, σ_x , 125 N, 0.2 mm Feed Parameter.....	71
Figure 81 Residual Stress Distribution on Square Model, σ_z , 500 N, 0.2 mm Feed Parameter.....	72
Figure 82 Residual Stress Distribution on Square Model, σ_x , 500 N, 0.2 mm Feed Parameter.....	73
Figure 83 Residual Stress Distribution on Square Model, σ_z , 125 N, 0.3 mm Feed Parameter.....	74
Figure 84 Residual Stress Distribution on Square Model, σ_x , 125 N, 0.3 mm Feed Parameter.....	75
Figure 85 Residual Stress Distribution on Square Model, σ_z , 250 N, 0.3 mm Feed Parameter.....	76
Figure 86 Residual Stress Distribution on Square Model, σ_x , 250 N, 0.3 mm Feed Parameter.....	77
Figure 87 Residual Stress Distribution on Square Model, σ_z , 500 N, 0.3 mm Feed Parameter.....	78
Figure 88 Residual Stress Distribution on Square Model, σ_x , 500 N, 0.3 mm Feed Parameter.....	79
Figure 89 Residual Stress Distribution on $\emptyset 14$ Model, σ_z , 125 N, 0.1 mm Feed Parameter.....	80
Figure 90 Residual Stress Distribution on $\emptyset 14$ Model, σ_x , 125 N, 0.1 mm Feed Parameter.....	81
Figure 91 Residual Stress Distribution on $\emptyset 14$ Model, σ_z , 250 N, 0.1 mm Feed Parameter.....	82
Figure 92 Residual Stress Distribution on $\emptyset 14$ Model, σ_x , 250 N, 0.1 mm Feed Parameter.....	83
Figure 93 Residual Stress Distribution on $\emptyset 14$ Model, σ_z , 500 N, 0.1 mm Feed Parameter.....	84
Figure 94 Residual Stress Distribution on $\emptyset 14$ Model, σ_x , 500 N, 0.1 mm Feed Parameter.....	85
Figure 95 Residual Stress Distribution on $\emptyset 14$ Model, σ_z , 125 N, 0.2 mm Feed Parameter.....	86

Figure 96 Residual Stress Distribution on Ø14 Model, σ_x , 125 N, 0.2 mm Feed Parameter	87
Figure 97 Residual Stress Distribution on Ø14 Model, σ_z , 500 N, 0.2 mm Feed Parameter	88
Figure 98 Residual Stress Distribution on Ø14 Model, σ_x , 500 N, 0.2 mm Feed Parameter	89
Figure 99 Residual Stress Distribution on Ø14 Model, σ_z , 125 N, 0.3 mm Feed Parameter	90
Figure 100 Residual Stress Distribution on Ø14 Model, σ_x , 125 N, 0.3 mm Feed Parameter	91
Figure 101 Residual Stress Distribution on Ø14 Model, σ_z , 250 N, 0.3 mm Feed Parameter	92
Figure 102 Residual Stress Distribution on Ø14 Model, σ_x , 250 N, 0.3 mm Feed Parameter	93
Figure 103 Residual Stress Distribution on Ø14 Model, σ_z , 500 N, 0.3 mm Feed Parameter	94
Figure 104 Residual Stress Distribution on Ø14 Model, σ_x , 500 N, 0.3 mm Feed Parameter	95
Figure 105 Residual Stress Distribution on Ø8 Model, σ_z , 125 N, 0.1 mm Feed Parameter	96
Figure 106 Residual Stress Distribution on Ø8 Model, σ_x , 125 N, 0.1 mm Feed Parameter	97
Figure 107 Residual Stress Distribution on Ø8 Model, σ_z , 250 N, 0.1 mm Feed Parameter	98
Figure 108 Residual Stress Distribution on Ø8 Model, σ_x , 250 N, 0.1 mm Feed Parameter	99
Figure 109 Residual Stress Distribution on Ø8 Model, σ_z , 500 N, 0.1 mm Feed Parameter	100
Figure 110 Residual Stress Distribution on Ø8 Model, σ_x , 500 N, 0.1 mm Feed Parameter	101
Figure 111 Residual Stress Distribution on Ø8 Model, σ_z , 125 N, 0.2 mm Feed Parameter	102
Figure 112 Residual Stress Distribution on Ø8 Model, σ_x , 125 N, 0.2 mm Feed Parameter	103

Figure 113 Residual Stress Distribution on Ø8 Model, σ_z , 500 N, 0.2 mm Feed Parameter	104
Figure 114 Residual Stress Distribution on Ø8 Model, σ_x , 500 N, 0.2 mm Feed Parameter	105
Figure 115 Residual Stress Distribution on Ø8 Model, σ_z , 125 N, 0.3 mm Feed Parameter	106
Figure 116 Residual Stress Distribution on Ø8 Model, σ_x , 125 N, 0.3 mm Feed Parameter	107
Figure 117 Residual Stress Distribution on Ø8 Model, σ_z , 250 N, 0.3 mm Feed Parameter	108
Figure 118 Residual Stress Distribution on Ø8 Model, σ_x , 250 N, 0.3 mm Feed Parameter	109
Figure 119 Residual Stress Distribution on Ø8 Model, σ_z , 500 N, 0.3 mm Feed Parameter	110
Figure 120 Residual Stress Distribution on Ø8 Model, σ_x , 500 N, 0.3 mm Feed Parameter	111
Figure 121 Residual Stress Distribution on Ø8 T. R. Model, σ_z , 125 N, 0.1 mm Feed Parameter	112
Figure 122 Residual Stress Distribution on Ø8 T. R. Model, σ_x , 125 N, 0.1 mm Feed Parameter	113
Figure 123 Residual Stress Distribution on Ø8 T. R. Model, σ_z , 250 N, 0.1 mm Feed Parameter	114
Figure 124 Residual Stress Distribution on Ø8 T. R. Model, σ_x , 250 N, 0.1 mm Feed Parameter	115
Figure 125 Residual Stress Distribution on Ø8 T. R. Model, σ_z , 500 N, 0.1 mm Feed Parameter	116
Figure 126 Residual Stress Distribution on Ø8 T. R. Model, σ_x , 500 N, 0.1 mm Feed Parameter	117
Figure 127 Residual Stress Distribution on Ø8 T. R. Model, σ_z , 125 N, 0.1 mm Feed Parameter	118
Figure 128 Residual Stress Distribution on Ø8 T. R. Model, σ_x , 125 N, 0.1 mm Feed Parameter	119
Figure 129 Residual Stress Distribution on Ø8 T. R. Model, σ_z , 250 N, 0.1 mm Feed Parameter	120

Figure 130 Residual Stress Distribution on Ø8 T. R. Model, σ_x , 250 N, 0.1 mm Feed Parameter.....	121
Figure 131 Residual Stress Distribution on Ø8 T. R. Model, σ_z , 500 N, 0.1 mm Feed Parameter.....	122
Figure 132 Residual Stress Distribution on Ø8 T. R. Model, σ_x , 500 N, 0.1 mm Feed Parameter.....	123

1. INTRODUCTION

Recent studies show that safety, fuel consumption, greenhouse effect regulations are getting stricter. These strict regulations force the manufacturer to produce much more efficient and lightweight designs [6]. Kleiner et.al. [7] stated that surface treatment methods aim to increase strength of materials while the thickness decreasing. Jeswiet et.al. [8] mentioned that production of dynamically loaded parts from aluminum alloys allow to a lightweight and durable designs. But if the fatigue life is considered, part sections should be thicker, and this causes weight increase on the parts [8]. As Kukielka et.al. [9] stated, most of the failures of the materials causing by cracks on the surface are fatigue failures. It is already known that the cracks which are causing fatigue failures, initiates from the surface of the material [10]. By these reasons, Kirkhope et. al. [1] stated that there are two main principles which increase fatigue life without changing the structure of material. These principles are decreasing surface roughness and creating residual stresses. Decreasing surface roughness weakens and postpones the notch effect on the part surfaces and that yields an improvement on the strength [1]. As Schulze [11] stated, two important methods for generation of compressive residual stresses on the material are deep rolling and shot peening. Also, there is a method called Laser Shock Peening. In this method, strain hardening and residual stresses (compressive) generated on the material surface by means of high energy laser beams [3]. In shot peening, small granules made of steel or glass are shot to materials by the mean of gears or pressurized air [12]. According to Miao et. al. [13] in the shot peening process, compressive residual stresses can occur at 0.2 mm depth under the surface for aluminum 2024. Consequently, aluminum alloys fatigue life can increase up to 28% [14]. Due to ease of application and increase of fatigue life, shot peening had been using for years on aircraft motor blades [15], medical implants [16] and piston rods [17]. But this process has also some disadvantages. According to study of Ludian and Wagner [18], on shot peening process to reach the desired fatigue life increase, process should be implemented all of the surfaces. Even for some applications, decrease of fatigue life occurs. Bagherifard et. al. [19] inform that excess application of shot peening process can cause surface cracks. These cracks can reduce the material life. Even in the normal applications, perfect control of residual stresses cannot be achieved. Because residual stresses occur randomly [19]. On the other hand, another surface treatment process which creates residual stress is deep rolling. As Klocke and Mader [20] explained that,

local plastic deformations are created by the means of hydrostatic sphere or cylinder. In this process, the main aim is not to change the material geometry, but to improve of the mechanical properties. During application of this method, three important phenomena should be explained. First one is strain hardening due to plastic deformation. Second one is, impurities on the surface mechanically rolled and this causes roughness decrease on the material [21]. The third and the most important one is, generation of compressive residual stresses as a reaction of plastically deformation [11]. Sticchi et. al. [2] suggest that the stress level of compressive residual stresses in deep rolling could be 5 times greater than in Shot Peening process. When the aluminum alloys considered, especially on 6xxx and 7xxx alloys, compressive residual stresses after deep rolling process can reach up to 1 mm depth [22, 23, 24, 25]. It is also reported; all the effects of deep rolling can cause a fatigue life increase between 60%-300 [22, 24]. For this reason, deep rolling can be counted as the most effective process for fatigue life increase [3]. Nowadays, for the same reason deep rolling is used on turbine blades [26], railway axles [27] and aircraft motor hanging bolts [28] very commonly.

In this study, structural dependency of residual stresses will be investigated on cylindrical parts by FEA analysis. Firstly, prismatic parts will be deep rolled. Secondly, cylindrical parts will be deep rolled in longitudinal direction. Thirdly, residual stresses on prismatic and cylindrical materials will be compared. Then, tangential rolling will be applied to these cylindrical parts.

In prismatic parts, it has been investigated that residual stresses are two times higher in transverse direction than in longitudinal direction. Occurrence of residual stresses cause a very high improvement on the mechanical properties and service life of material. If directional dependency and magnitude of residual stresses on cylindrical parts would be similar to the prismatic parts, deep rolling process can be applied very effectively for industrial parts, because most of the engineering parts have radii.

2. STATE OF THE ART

2.1. Fatigue

Fatigue can be expressed as; materials might fail when a cyclic loading is applied. This material failure can occur at a stress level under the material yield strength [29]. Fatigue failure is the frequently seen failure type for the engineering parts.

First loading type, amplitude is not changing (constant amplitude), and the second loading type, amplitude is changing (variable) (Fig. 1). Constant amplitude loading can be investigated as high cycle and low cycle fatigue. High cycle fatigue can be expressed by lower loads, longer life ($>10^5$ cyc.) This can be analyzed by the method of stress-life (S-N Curve). Deformation is in elastic range. Low cycle fatigue can be expressed by higher loads, shorter life ($<10^5$ cyc.). This is commonly analyzed by strain-life method. This also includes plastic deformation. In the variable amplitude loading; the loading amplitude is changing continuously. For deterministic loading, the properties of loading can be foreseen. Also, material properties are well known. In stochastic loading; the applied load is random variable such as; wind load, earthquake. Fatigue strength can be easily affected by some factors such as; loading type, material strength and type, surface finish and state of residual stresses [30].

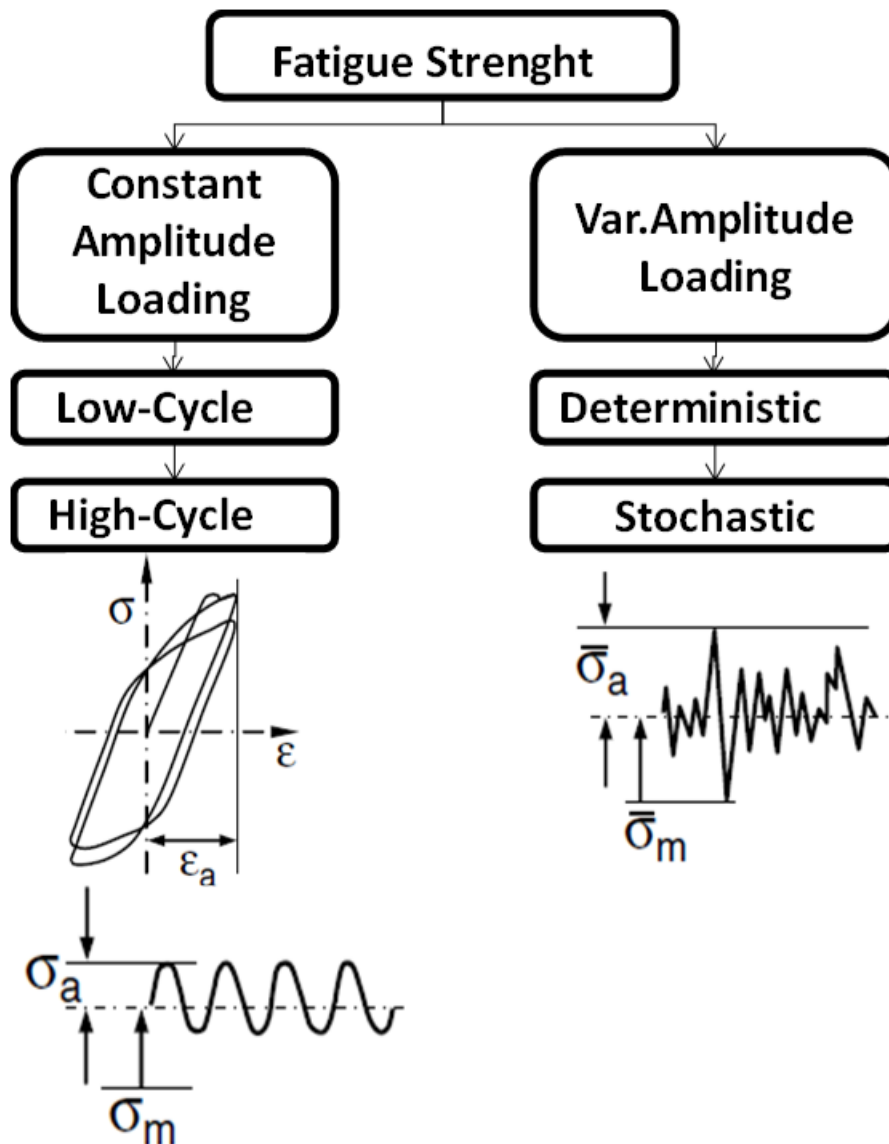


Figure 1 Fatigue Loading [30]

2.2. Surface Treatment Methods

There are multiple applications to improve fatigue strength of materials. These techniques are called as surface treatment methods. Conventional surface treatment methods will be presented in the following subchapters. Their advantages and disadvantages will be discussed. First important method is shot peening, the second one is laser shock peening and the third one is roller burnishing.

2.2.1. Shot Peening

Shot Peening (SP) is achieved by shooting tiny balls which are made of steel, glass or ceramic to the surface of the materials. Tiny balls are at high velocity during the process (20-100 m/s).

It has two major effects; compressive residual stresses in the surface and sub-surface, crack initiation prevention. Compressive residual stresses can increase the fatigue life of materials. However; the process parameters (large balls, high ball velocity, exaggerated application) should be selected and adjusted properly. Because these could result in high damage on the material and change the location of the surface layers. Also; this can increase the surface roughness. As a result, high cycle fatigue properties of the material are affected in negative manner [31]. Moreover, industrial parts have radii. So, it is hard to shot peen surfaces with radii properly. In Fig. 2; schematic of shot peening process can be seen. Small granules are shot with a specified velocity by a high frequency displacement generator to sample material which is held by a sample holder.

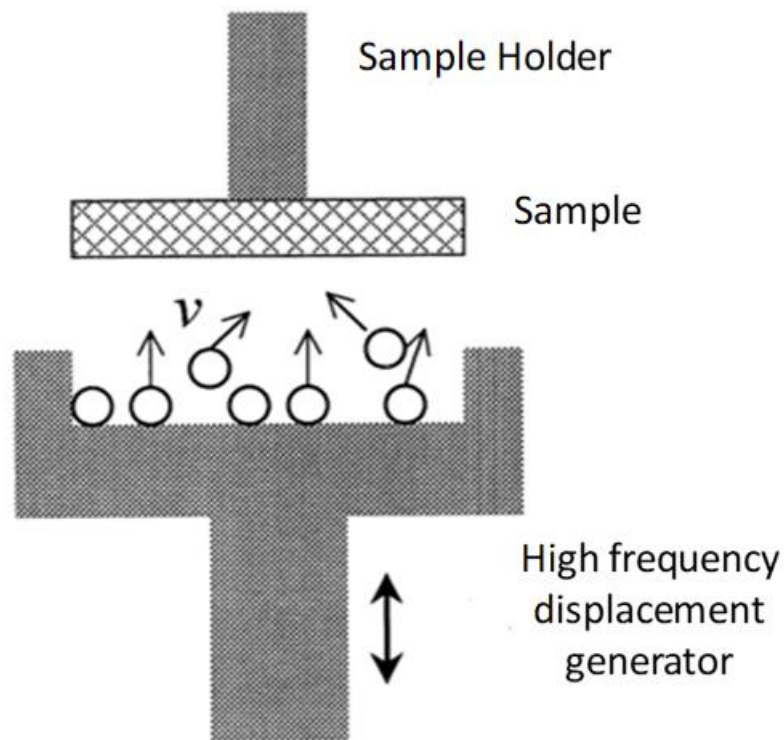


Figure 2 Shot Peening [32]

2.2.2. Laser Shock Peening

Laser Shock Peening (LSP) process is similar to traditional shot peening. In this method, residual stresses (compressive) can be induced at the surface and sub-surface of the sample. Perforation depth is much higher in this process than shot peening.

For LSP process, a black paint is painted on the desired peening location of the material. A thin layer of water is poured over this painted surface. High energy laser beam is sent to the sample material. By the one shot of laser beam, paint layer vaporizes, and plasma phase

of paint layer occurs. Shock waves with high pressure are generated on the surface of the material, while the plasma layer growing. The water layer has an advantage of limiting the energy and increasing the pressure intensity on the material surface. This pressure pulse is applied approximately for 50 nanosecond (ns), and the magnitude of the pressure can be two times of the material yield strength. Pressure pulses cause plastic deformation and compressive residual stresses on the surface and sub-surface of the material. Because of high pressure values in LSP, thin sections can be damaged during one-sided LSP application. So, LSP application should be made for two-sided. However, in peening application for two sides, the material can has difficulties on the complex geometries (turbine). In addition to that; two-sided peening could result in complex stress field through the material thickness.

When the application of LSP taken into account, comparison should not be made between SP. However, LSP can be used when the SP application is not suitable for some reasons such as; more improved properties, application on complex geometries, better control of quality, better surface finish. For some cases, LSP can also be used with SP for further fatigue property improvement [33, 34].

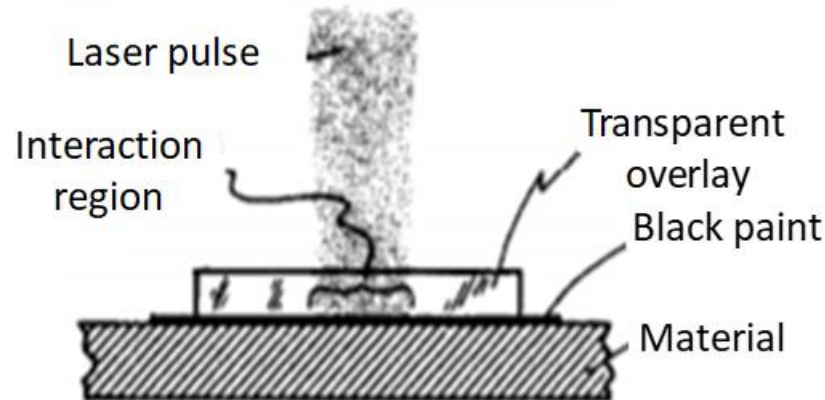


Figure 3 Laser Shock Peening [33]

2.2.3. Roller Burnishing

The valuable goals of this process are to decrease roughness of the surface, to increase to material hardness via plastic strain and to obtain residual stresses (compressive) on the material surface. Thus, wear and corrosion resistance, tensile as well as fatigue strength improves. It is succeeded by creating plastic deformation on the surface of material with very low forces. A normal force is applied to the material by the means of cylindrical or

spherical rollers. It is also affected by roller geometry, applied force, relative tangential velocity between the roller and the part and the feed at each part revolution.

This process is very similar to deep rolling process, but it should not be confused with deep rolling. Conventional burnishing operations are applied to raw cylindrical materials, bolts or screws threads. Roller burnishing is only applied to decrease the surface roughness. This process can supersede grinding operation as a low-cost operation [35]. Schematic of roller burnishing process is shown in Fig. 4.

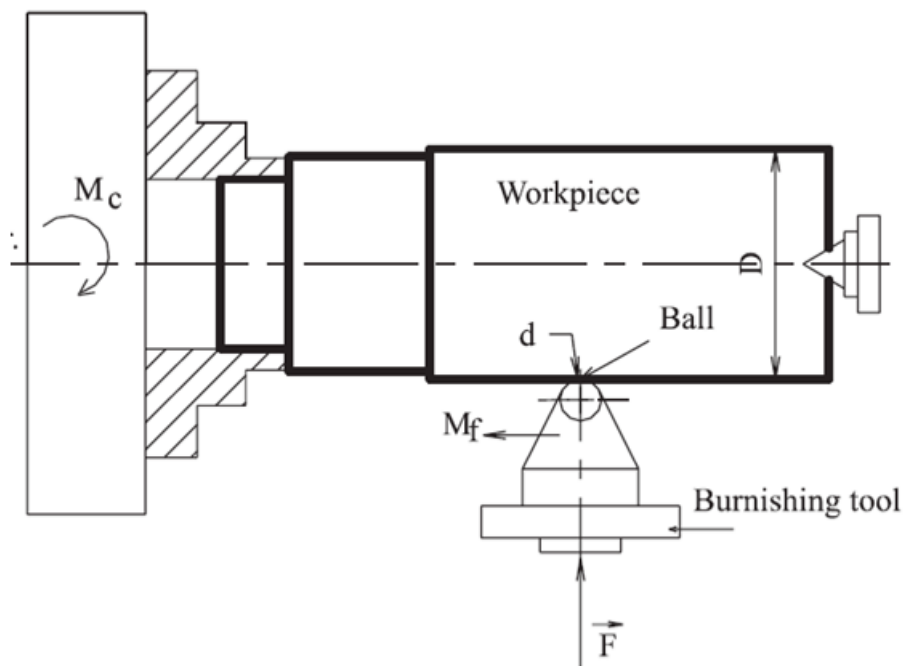


Figure 4 Roller Burnishing [36]

2.2.4. Deep Rolling

Deep rolling (DR) process is applied by mechanically or hydraulically actuated rollers or balls. By the means of these rollers or balls, a specific load is applied on the surface of the material. This causes surface and sub-surface local plastic deformation and compressive residual stresses (1-2 mm depth). In addition to that, DR yields strain hardening and surface roughness decrease. These results in fatigue life improvement [23]. DR can be applied by three equally placed rollers around its circumference for circular geometries (Fig. 5). On the other hand, force is applied along the surface by a ball or roller for planar geometries [3]. So as not to bend thin section materials, DR can be applied as two-sided. Application of deep rolling on more complex geometries is very similar, some special rolling tools can be designed, and it can be used by attaching another tool for flexibility of

the process application. The key process parameters are: feed value, applied pressure, number of repetitions and the friction between rollers and the material [37].

If deep rolling is compared with shot peening; deep rolling creates lower surface roughness. DR is able to generate deeper and higher residual stresses (compressive) on the surface and sub-surface of the material. DR also causes surface roughness decrease. When DR is compared with LSP, LSP is able to decrease surface roughness very little. It is important to express that high cycle fatigue (HCF) properties of DR is higher, while low cycle fatigue (LCF) properties of LSP is better [3].

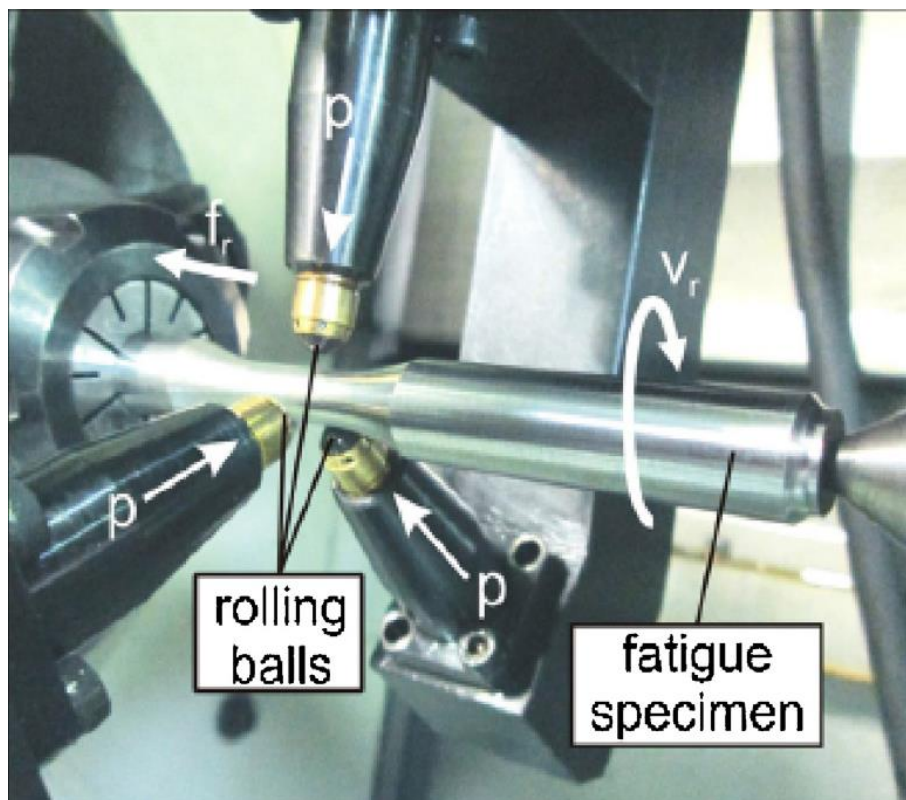


Figure 5 Deep Rolling [3]

It is also important to discuss finite element simulations on deep rolling process. M. Beghini et.al. [4] applied rolling operations on wide straight surface as in prismatic deep rolling process operation. Analysis done by plane strain elements, because of geometry simplification and reduced element size. Also, in 2D analyses, residual stress distribution can be assumed as uniform on the rolling direction for material surface. Thus, gradient of stress can be assumed in the depth of the material. Main limitation of the plane model is that, the residual stresses on longitudinal and transverse directions cannot be obtained at the same time.

Due to rolling tool geometry, the analysis model is set with plane strain elements which are placed on a cross section of the material along the rolling direction. In other words, analysis plane is perpendicular to rolling direction. The deep rolling roller which is made of steel is assumed as rigid due to its high stiffness compared to aluminum. For the material plastic behaviour, multilinear kinematic hardening material model is applied. The analysis results are taken from symmetry axis of the analysis plane. Also, results are taken after the last deep rolling application, in the case of no contact of rolling tool with the material surface. Optimum number of rolling is investigated by doing convergence analysis. The minimum used element size is 0.0025 mm and total element number is approximately 115000. In Fig. 6, roller geometry and rolling specimen is shown [4].

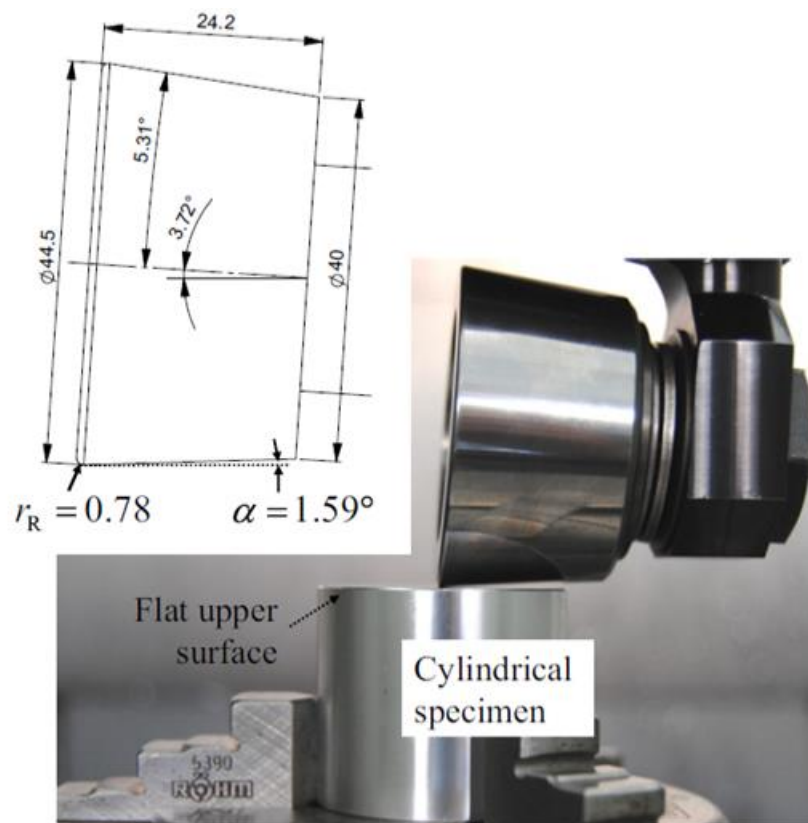


Figure 6 Tool & Specimen Geometry for 2D Analysis [4]

Also, analysis mesh and results view are shown below (Fig. 7). In Fig. 7, the feed direction and number of rolling operations can be seen. Near surface for the rolling process is meshed with fine elements. Far surface boundary meshes are much coarser than near surface, and it was getting coarser through depth direction. Furthermore, plastic deformation can be seen. Right hand side of Fig. 7, deep rolling residual stresses induced through multiple rolling paths [4].

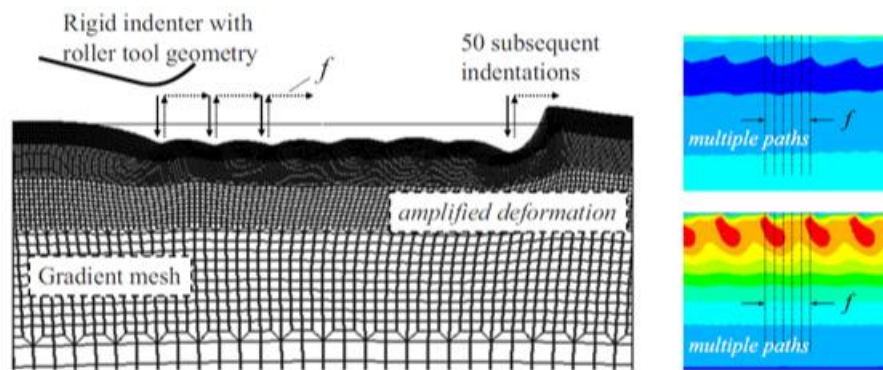


Figure 7 Mesh and Analysis Results [4]

Majzoobi et.al. [38] used round dog bone specimens for deep rolling analysis. The material which is used in this study is aluminum 7075- T6. Bending fretting fatigue test is applied to the rolled samples. Also, deep rolling process parameters are studied such as; turning speed of sample, applied force, number of process repetition and feed. For better and correct distribution of residual stresses, 3D analyses are run by using Abaqus Program. A small part of the material is modelled so as to save computational time and cost. For model dimensions; L is selected as 3 mm, a is selected as 1 mm, β is selected as 50-degree, b is selected as 3.55 mm. Deep rolling model geometry and mesh is also shown in Fig. 8.

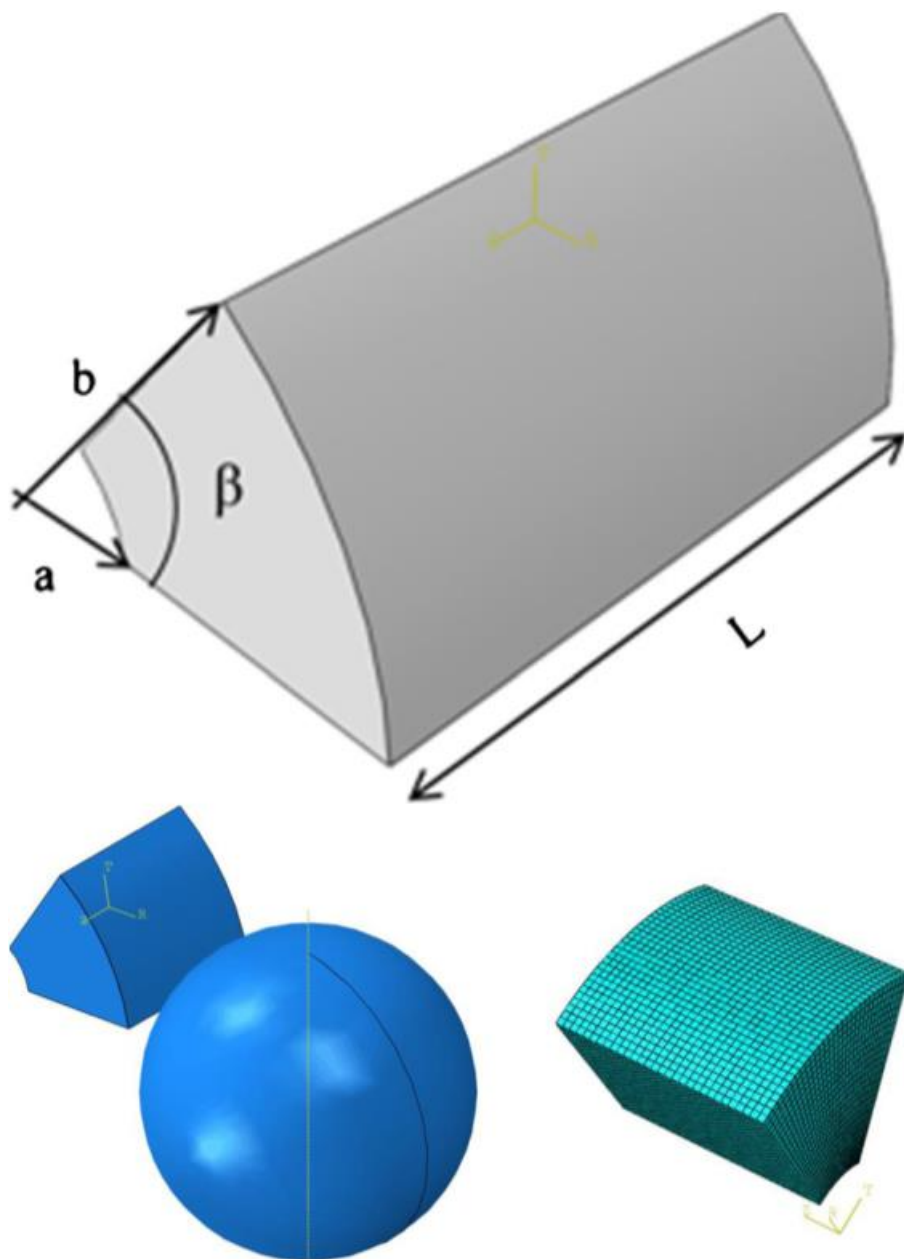


Figure 8 Geometry specimen, Rolling Tool and Mesh View [38]

Tangential rolling was applied on this study. Since the deep rolling material is subjected to alternating loading (compression-tension); material plasticity model is achieved by Chaboche Plasticity Model. 23040 number of elements are used for the analysis. The deep rolling tool can be assumed as rigid [38]. Lathe machine, deep rolling process fixture, rolling specimen and rolling tools can be seen in Fig. 9.



Figure 9 The Test Fixture and Rolling Tool [38]

After the application of deep rolling process, measurement process is made for two directions, tangential and axial. Moreover, the obtained numerical and experimental stress results are compared.

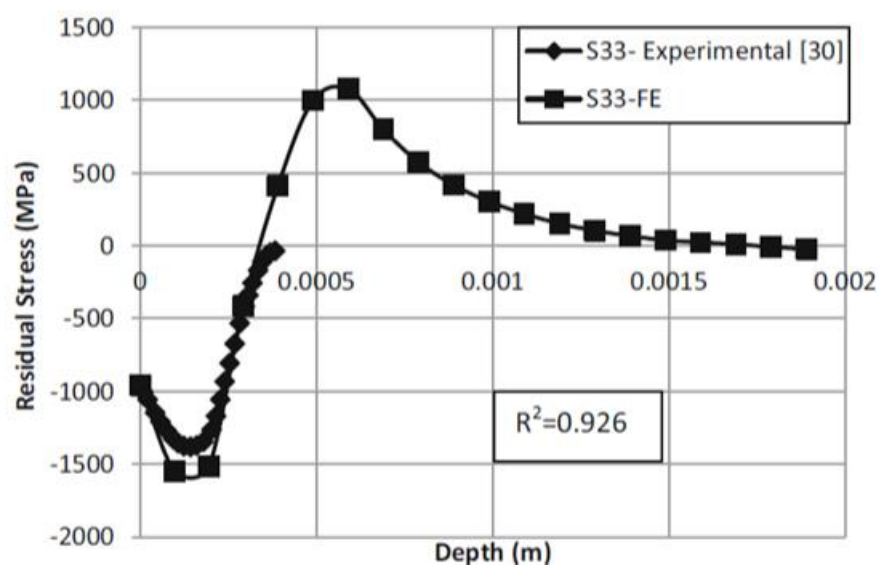


Figure 10 Residual Stresses (Numerical, Experimental) in Axial Direction [38]

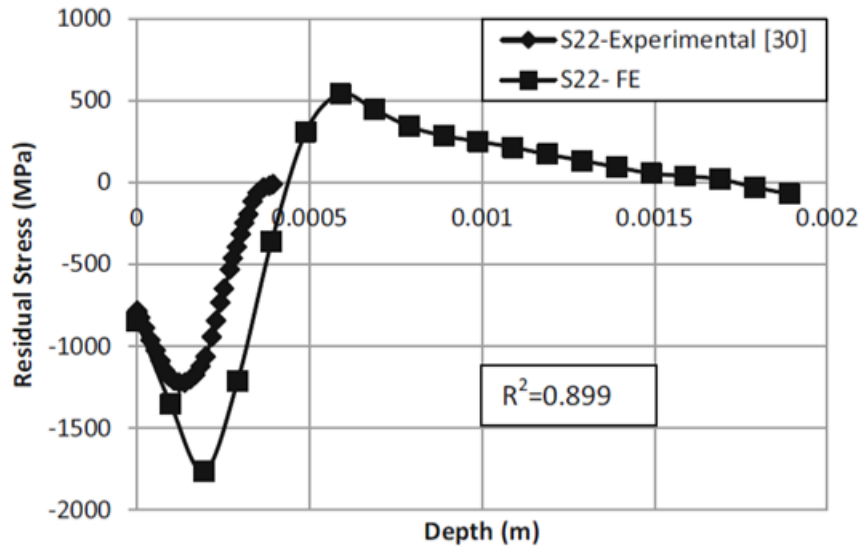


Figure 11 Residual Stresses (Numerical, Experimental) in Tangential Direction [38]

In Fig. 10 and 11, numerical and experimental residual stresses in axial and tangential were shown. Tangential direction corresponds the circumferential direction and axial direction corresponds the longitudinal direction of the specimen. In axial direction; results, experimental and numerical results are very close to each other. They start in the compressive region and turns into the tensile stresses after some depth. Measurement could be taken until the depth of 0.5 mm. In the tangential direction, experimental results are higher than the numerical results. This could occur due to insufficient measurement techniques. Again, stresses started in the compressive region and turns into tensile region. In both direction, stresses were obtained in higher magnitudes. For tangential direction, measurements were taken until the depth of 0.5 mm and numerical were taken until 2 mm of depth [38].

Some experiments are done for fatigue behaviour on different treated or non-treated Ti-6Al-4V materials at different specified temperatures in Fig. 12. If the fretting fatigue properties of LSP and DR are considered, deep rolling can be very advantageous even at elevated temperatures [23].

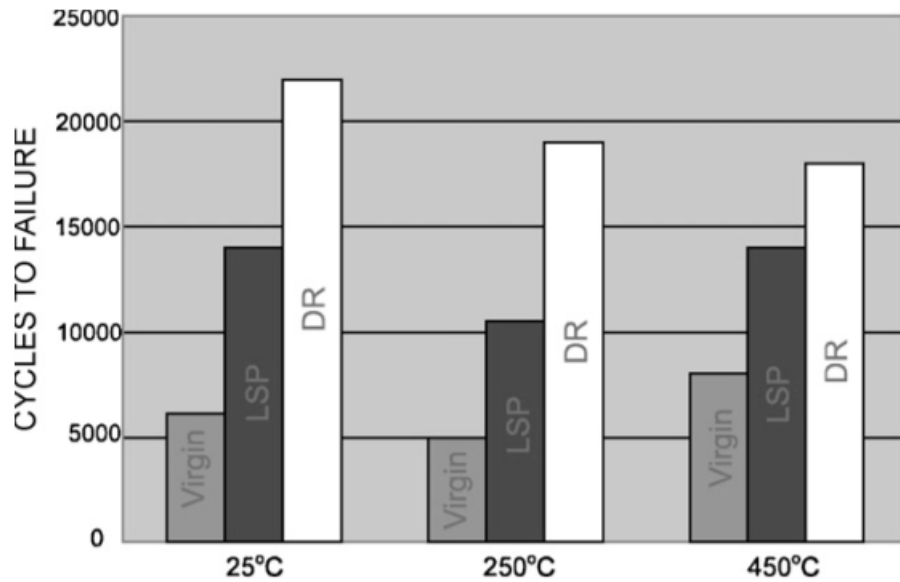


Figure 12 Comparison between non-treated, DR and LSP treated specimens at different temperatures [23]

Fig. 13 shows that the lowest fatigue life is obtained on non-treated specimens for fretting fatigue tests. However, the situation is different for the treated specimens. Different numbers of tests are done for different stress levels for normal and fretting fatigue. SP low cycle fretting fatigue ($<10^5$ cyc.) properties are better than DR. 300% fretting fatigue life increase can be obtained by SP. Therefore; SP high cycle fatigue (HCF) properties are counted as advantageous until 300000 cycles. When the cycles are higher than 300000, DR is obtained as more advantageous with the 700% life increase [23].

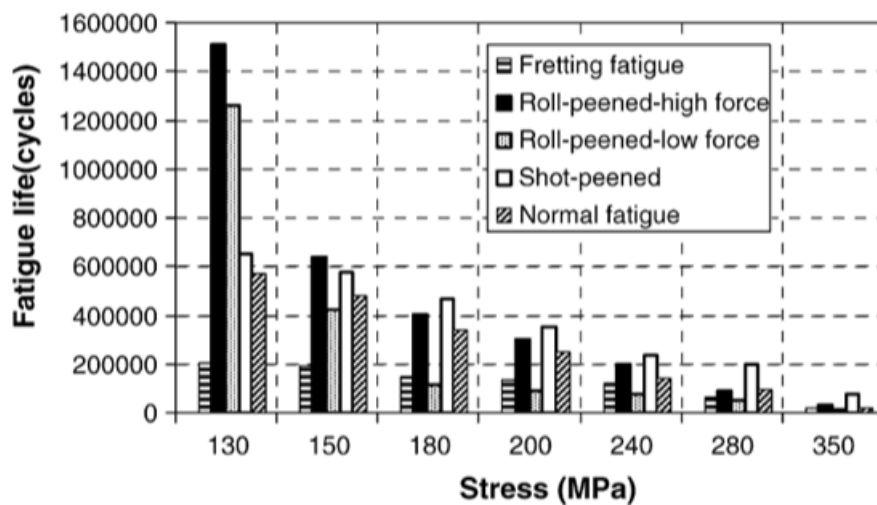


Figure 13 Comparison between different applications of SP and DR on fretting fatigue [23]

3. MOTIVATION

The main aim of this study is to investigate the directional dependency of the residual stresses on cylindrical parts. Because; most of the researches have studied cylindrical parts for tangential rolling operations and prismatic parts for longitudinal rolling operations. Also, these operations are easy to apply and conventional. In addition to that, studies have showed when the deep rolling is applied to prismatic parts; the residual stresses on the transverse direction are as twice as the residual stresses on deep rolling direction. Within the scope of these investigations; only a few fatigue life investigations have been made on rolled parts [4]. If it could be investigated with this study that the residual stresses on cylindrical parts occurred in the same way on longitudinal direction and transverse direction, it could mean that fatigue life might be obtained, and the process can also be used in the industry. Because most of the industrial parts have radii which are exposed to fatigue loading. Basic schematic of deep rolling on prismatic geometries plane surface materials is shown in Fig. 14.

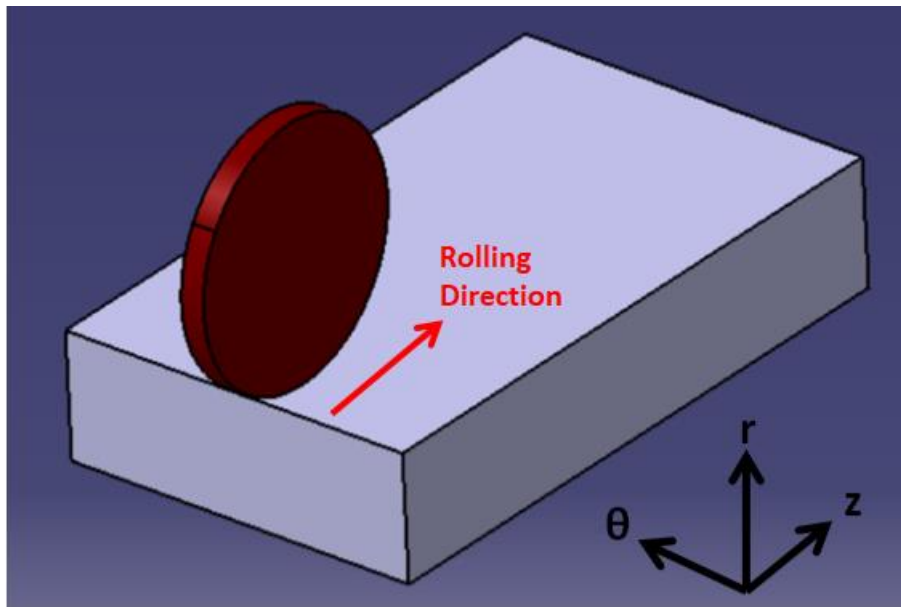


Figure 14 Longitudinal Deep Rolling on a Prismatic Geometry (Conventional) [4, 5]

Firstly, prismatic geometry model was created and analyzed on this study. Its aim was to compare created model with existing studies if there would be any difference between them. This helped to satisfy and validate created models for prismatic geometry.

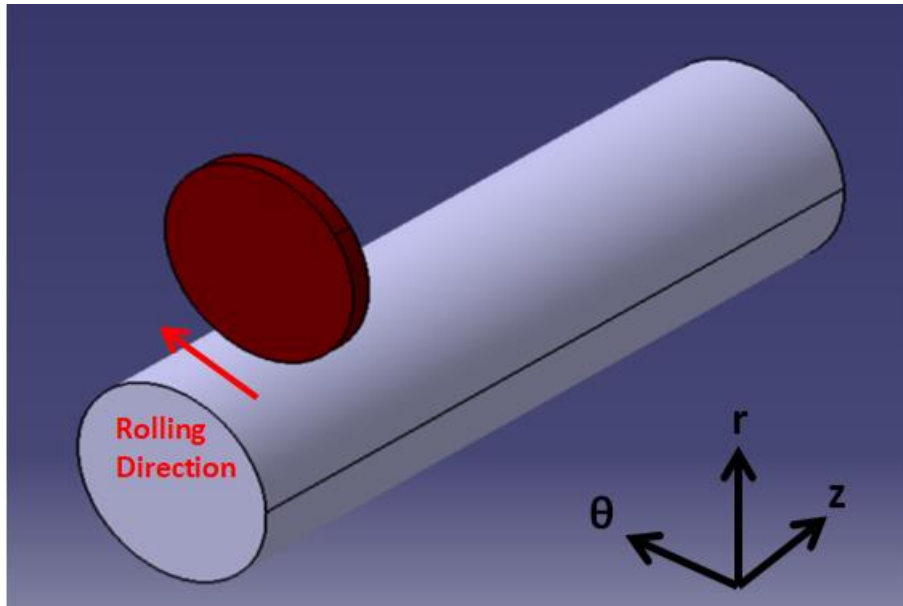


Figure 15 Tangential Deep Rolling on a Cylindrical Geometry (Conventional) [4, 5]

On the geometry above in Fig. 15; tangential rolling on cylindrical geometries were analyzed. Up to this point, when tangential rolling was taken into account, a few analyses were done as 3D tangential deep rolling and roller burnishing. Also, on AA6082 tangential rolling was investigated for the first time. But this rolling type requires also longitudinal rolling. Because, in the industry cylindrical parts are loaded in axial direction.

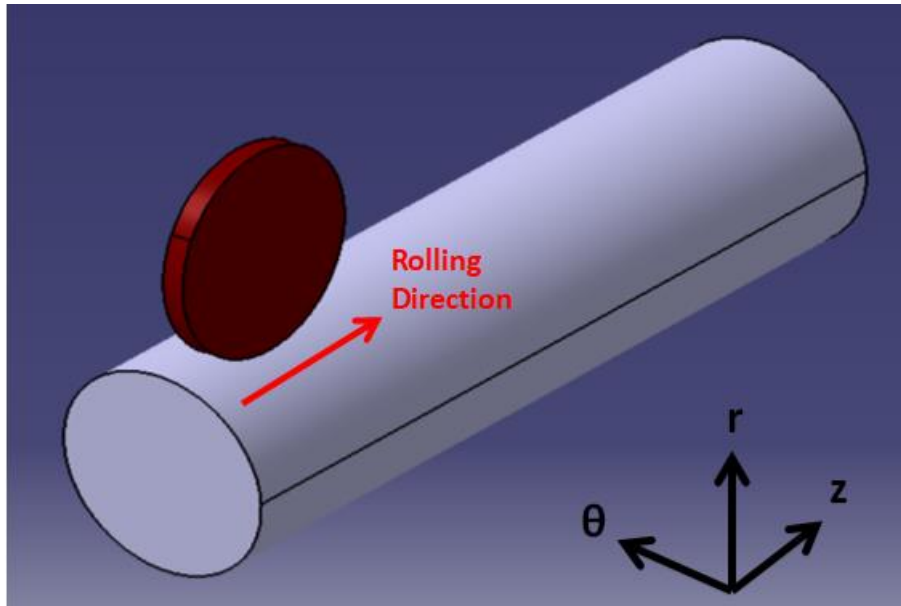


Figure 16 Longitudinal Deep Rolling on a Cylindrical Geometry (Novel)

Up to this time, the residual stress directional dependency had not been studied using finite element analysis method. Also, longitudinal deep rolling on cylindrical geometries had not been investigated by now. It was required because industrial parts have radii. The investigation done on the prismatic model must be implemented on cylindrical parts. These cylindrical parts were stationary on the analyses. Only rollers were mobile. It was aimed to investigate that whether the residual stresses on cylindrical parts occurs in the same way of residual stresses occurred on prismatic parts when deep rolling was applied. So, the main aim of this study is “investigation of the directional dependency of residual stresses on cylindrical parts”.

4. FINITE ELEMENT MODEL

In this chapter, material model and finite element models were introduced. Firstly, material flow curve was obtained for material plasticity. Deep rolling analyses were done on square geometry models, Ø14 mm and Ø8 mm geometry models. These models were named as S, Ø14, Ø8, TR_Ø14 and TR_Ø8, respectively. TR abbreviation was used for tangential rolling. 0125, 0250, 0500 indicates applied force parameters in Newtons. During model set up; first roller was placed in the middle section of the geometry. The others were placed equally with 0.1 mm, 0.2 mm and 0.3 mm gap. This gap annotation was shown after the force parameters on analysis naming. For all deep rolling analyses; five rollers were used starting from left hand to right hand side of the geometry on x-y plane. Secondly, prismatic model was introduced. Thirdly, 14 mm diameter and 8 mm diameter models were introduced. In these circular geometry models, longitudinal rolling and tangential rolling operations (only for cylindrical models) were applied.

4.1. Material Model

The tensile tests were applied to heat treated materials to obtain yield strength (Y.S.) and ultimate tensile strength (U.T.S.) and the flow curve of the material. In deep rolling process, materials were plastically deformed so it is required to investigate flow curve of the material. The flow curve of the material was obtained according to Swift equation. The tensile test sample geometry was designed according to DIN 50125 tensile test standards.

4.1.1. Heat Treatment Process

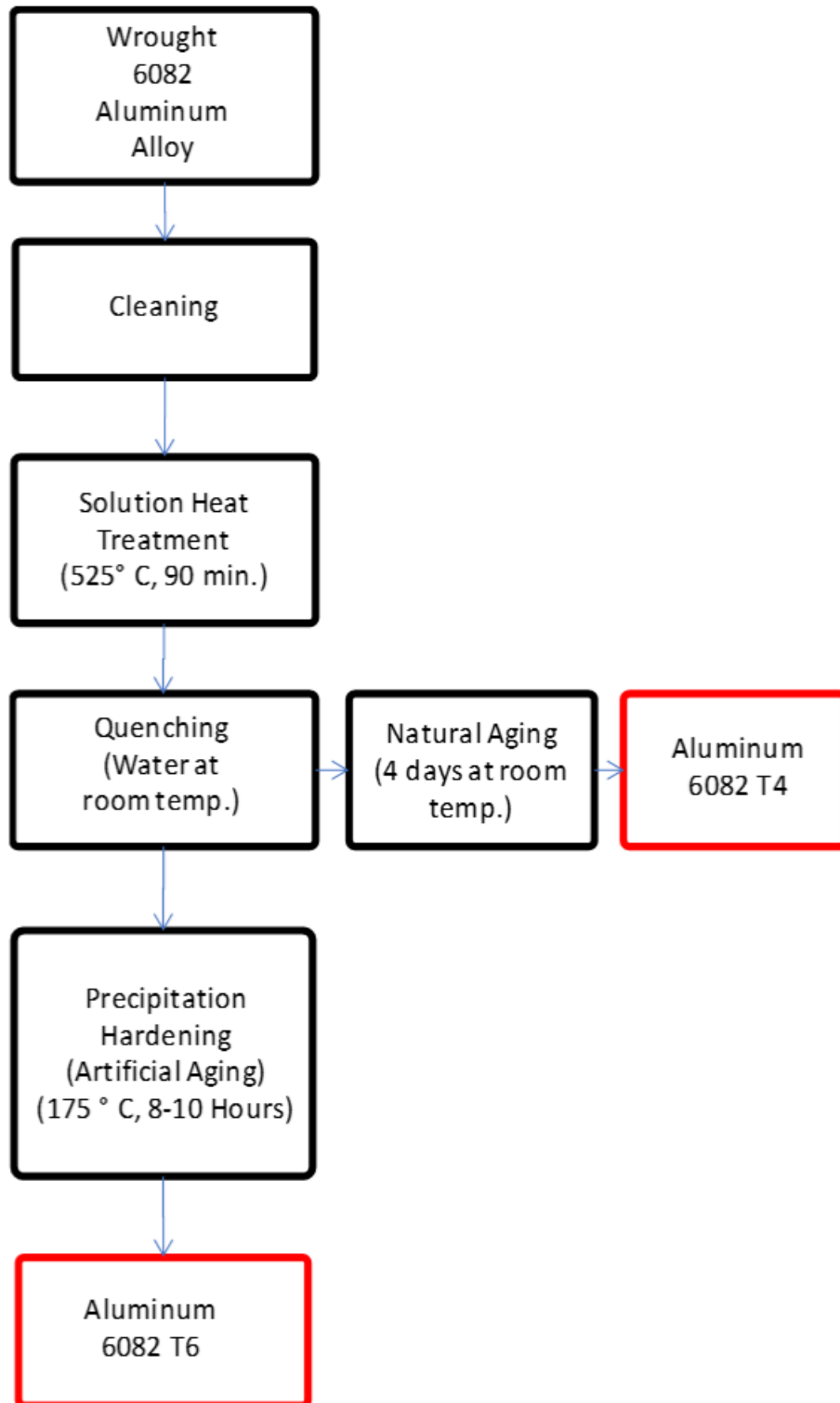


Figure 17 T4 and T6 Heat Treatment Process

AA 6082 was selected due to the fact that; this material is used for fatigue critical applications in automotive, aviation and power generation industries. This material is generally used as heat treated (T4 and T6), so heat treatment was applied to raw materials. To characterize the material, tensile tests were applied. For deep rolling analysis, the 3D geometries were modeled, and fem analysis were run. Finally, the residual stress results were investigated.

To apply heat treatment; firstly, samples were cleaned. Because in the heat treatment process, the dirt and dust on the material can solute into the material and harm the material. The samples were put into the oven for 90 minutes for 525 °C. After that, the samples were taken out of the oven and immediately sunk into the water at room temperature (25 °C). After 1 or 2 minutes, when they reached to room temperature, the samples were taken out of water and left to rest at room temperature for 4 days to obtain T4. To obtain T6, quenched samples were put into the oven again and artificial aged at 175 °C for 8-10 hours. All heat treatment processes were shown on Fig. 17. This artificial aging process were done so that all elements form solid solution when the material is quickly cooled from the solution heat treatment (SHT) temperature to 25 °C in order to keep that super saturated phase within the material. It was also known that Super Saturated Solid Solution (SSSS) ageing. Age hardening step helps to improve characteristic of the alloys which are heat treatable. This stage is the proper disintegration of the super saturated solid solution to achieve delicately spread elements.

When considering aluminum alloys, ductility property is gained during the solution heat treatment stage of T4 heat treatment and the strength property is gained during the ageing process during the T6 heat treatment process. During the age hardening process, elements in the alloy grow with the high temperature of artificial ageing. This growth increases the strength but reduces the ductility. For the heat treatment behavior of 6082 Aluminum Alloy under heat treatment, it was required to have a knowledge of material content of AA 6082 (Fig. 18) [39, 40, 41].

Chemical Composition of the AA 6082 (wt.%)								
Si	Fe	Cu	Mn	Mg	Cr	Zn	Others	Al
1.20	0.33	0.08	0.50	0.78	0.14	0.05	0.15	Bal

Figure 18 Chemical Composition of 6082 Aluminum Alloy [42]

As a next step; due to plastic deformation in deep rolling process, plasticity behavior of the material was determined. Flow curve is one of the plasticity models for the plastic behaviour of the materials. True stress versus true strain graph was used to obtain flow curve. True stress versus true strain graph was derived from engineering stress versus engineering strain curve by the help of Swift equation. This engineering stress versus engineering strain curve was obtained by tensile tests. The tensile test sample geometry was designed according to DIN 50125 tensile test standards [43].

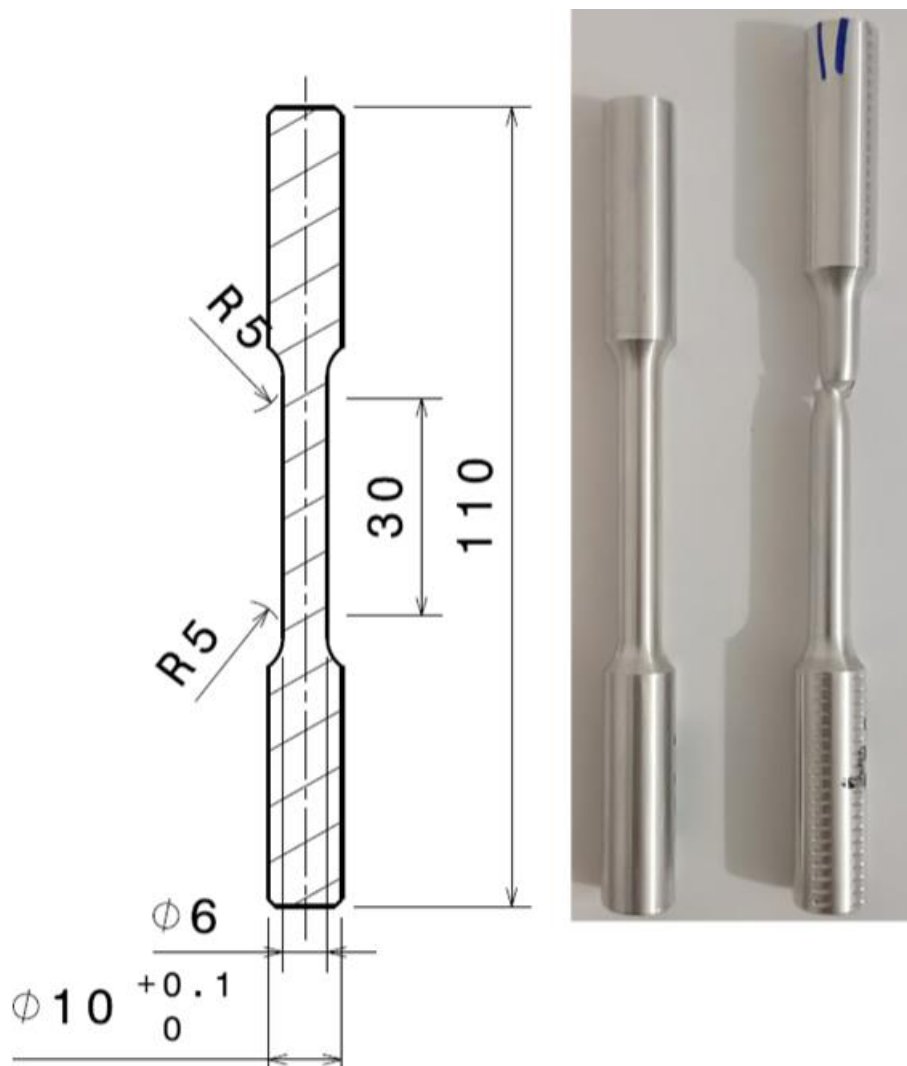


Figure 19 DIN 50125 Tensile Test Standard Sample Geometry

In Fig. 19, DIN 50125 tensile test geometry was shown. Also, view of the non-tested and tested samples can be seen. Tensile test application section diameter was 6 mm, and its length was 30 mm. While the diameter increasing, 5 mm fillet was applied. Total sample

length was 110 mm. Holding sections diameter was 10 mm. Test sample was held by grips of tensile test machine. Sample was pulled until it was broken off. A simple extensometer was used to measure extension on the material. Tensile test machine has also a load cell to measure the applied load.

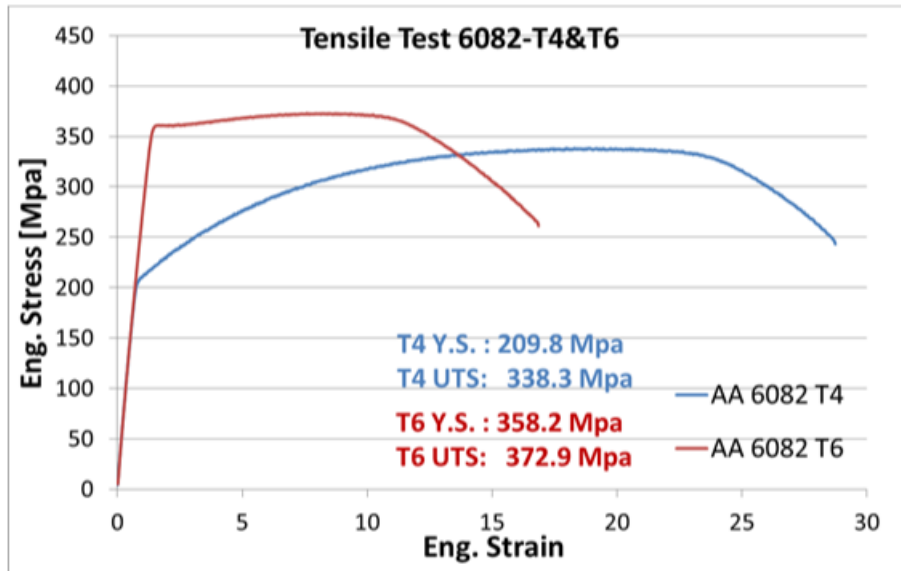


Figure 20 Tensile Test Results for AA 6082 T4 and T6

From the tensile test, only load and extension values of the sample were measured. Once obtaining these data, % elongation and engineering stress values were evaluated by using equations (1) and (2), respectively. Stress and strain values on the stress versus strain curve are called engineering stress and engineering strain (Fig. 20).

$$\left(\frac{\Delta l}{l_0}\right) \times 100 \quad (1)$$

$$\left(\frac{p}{\pi d^2}\right) \quad (2)$$

The yield strength and ultimate tensile strength values of the material were obtained from this graph (Fig. 20). Yield strength was evaluated by yield strength calculation technique on the stress-strain curve. Stress values are increasing up to some point and then decreasing after that level. This stress level is where the necking occurs and called ultimate tensile strength. While evaluating the flow curve, the engineering stress values after the yield stress level were taken into account. Furthermore, true stress values were evaluated by the following equation (3);

$$\frac{F \cdot l}{l_0 \cdot A_0} \quad (3)$$

Where F is the current load, l is the current length, l_0 and A_0 are the initial length and initial cross-sectional area, respectively. Next, true strain values were calculated by the following equation (4);

$$\ln\left(\frac{l_f}{l_0}\right) \quad (4)$$

Then, the difference between corresponding final true strain values and initial true strain values evaluated by the following equation (5);

$$\varepsilon_{tf} - \varepsilon_{to} \quad (5)$$

For the calculation of Swift equation parameters, the following equations (6) and (7) were used;

$$K = \sigma \cdot \left(\frac{e}{n}\right)^n \quad (6)$$

Where K is the strength coefficient, n is the strain hardening coefficient, σ is the ultimate tensile strength and e is the real number. Another strain constant for Swift equation is evaluated as;

$$\varepsilon_0 = \left(\frac{\sigma_y}{K}\right)^{\frac{1}{n}} \quad (7)$$

After all calculations Swift equation stress is evaluated by the equation (8);

$$\sigma_y = K \cdot (\varepsilon_0 + \varepsilon)^n \quad (8)$$

Where σ_y is the yield stress and the ε is the desired strain values for the flow curve. While evaluating the flow curve true stress versus $\varepsilon_{tf}-\varepsilon_{to}$ plot was created. A logical n constant was selected and flow curve by Swift equation versus strain graph was plotted. Then; by adjusting n value, these 2 curves were overlapped to each other. The best overlapped flow curve was determined to use for the material plasticity model. The strain hardening coefficient (n) for the best overlapped flow curve was 0.075 for T6 heat treated material flow curve. For T4 heat treated material best overlapped strain hardening coefficient (n) was 0.168. Evaluated flow curves for T4 and T6 heat treated materials can be seen in Fig. 21.

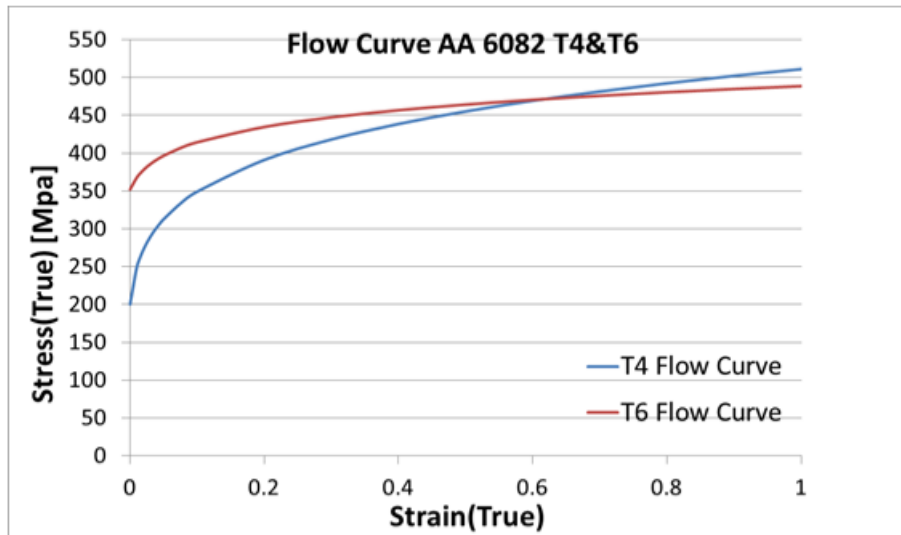


Figure 21 Flow Curves for T4 and T6 Materials

4.2. Finite Element Models

4.2.1. Longitudinal Rolling Prismatic Model

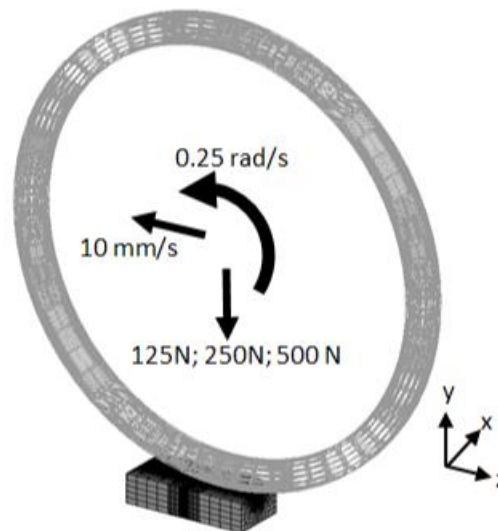


Figure 22 Prismatic Model Roller Translation, Rotation and Load Parameters

In this model (Fig. 22) prismatic geometry was used. In longitudinal rolling, 10 mm/s translational and 0.25 rad/s rotational speed were used. Applied load to the material through rollers were 125 N, 250 N and 500 N for different analysis models. Firstly; elements were created in 2D, expanded through -z direction and 3D mesh elements obtained.

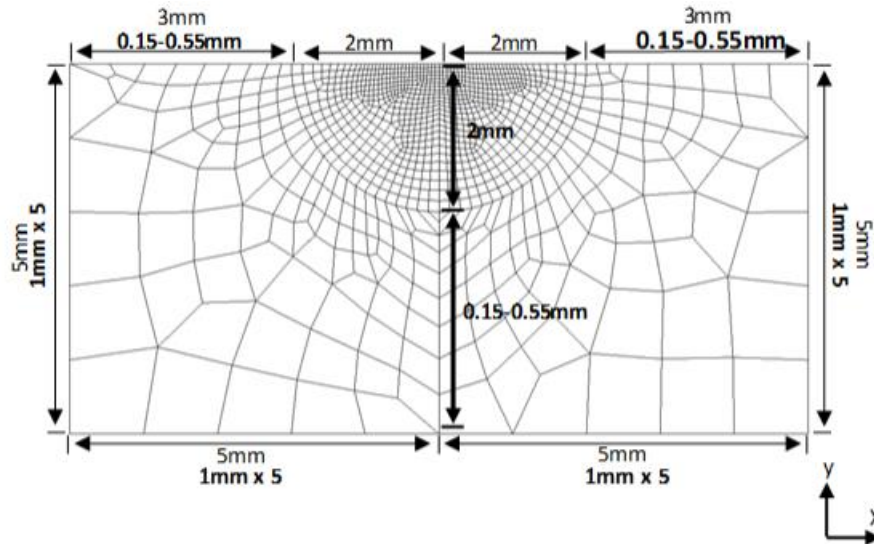


Figure 23 Prismatic Model Course Mesh Structure

Prismatic geometry (Fig. 23) was created as 5 mm length and 10 mm wide. In the middle of the geometry 2 mm radius circle was created for fine meshing where longitudinal rolling applied. At the top line, after the fine area, 3 mm length was divided into 0.15 mm-0.55 mm intervals. Length was divided into 5 equal intervals. Bottom line was divided into 10 equal intervals. Top surface of the geometry after the fine area, 3 mm length was divided into intervals starting from 0.15 mm to 0.55 mm. On this plane, total 2D mesh number was 1012 and total 3D mesh number was 64768.

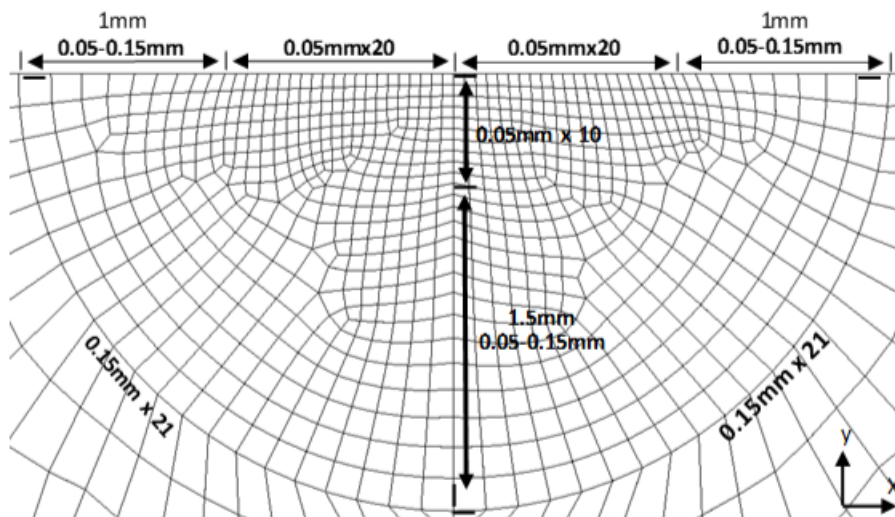


Figure 24 Prismatic Model Fine Mesh Structure

On 2 mm radius circle fine mesh section (Fig. 24), at the top line, 1 mm length starting from symmetry line was divided into 20 equal intervals as 0.05 mm. After that division, 1

mm length was divided into intervals starting from 0.05 mm to 0.15 mm. In y direction, 1 mm was divided into 10 equal intervals. Next, 1.5 mm was divided into intervals starting from 0.05 mm to 0.15 mm. Circle arc section was divided into 21 intervals as 0.15 mm.

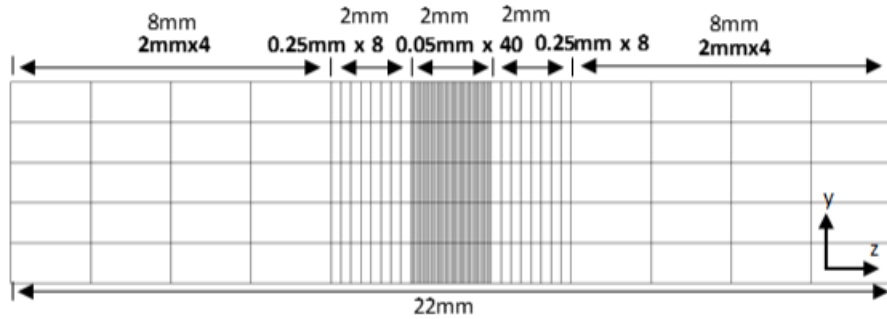


Figure 25 Prismatic Model Z Direction Mesh Structure

After creation of 2D mesh elements, elements were expanded through -z direction (Fig. 25). Rolling operation was started at -6 mm and finished at -16 mm in z direction. The area where the residual stress investigation made was very fine and element expansion size was 0.05 mm and 40 elements were used. The density of elements was decreased from middle point through the edges. Near the finest area, 0.25 mm expansion size and 40 elements used. The adjacent area was very course and 2 mm mesh size and 4 elements were used. Total expansion through -z direction was 22 mm, but application area was 10 mm. This was because the distribution of residual stresses should be observed properly in the middle of the material.

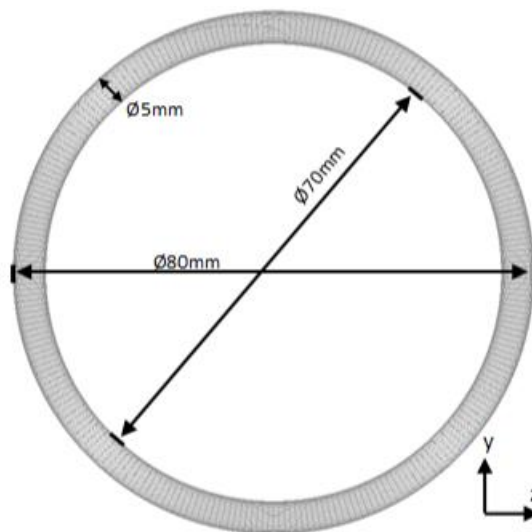


Figure 26 Deep Rolling Roller Geometry

The deep rolling tool had a ring geometry and its material was stainless steel (Fig. 26). This roller was controlled by a computer numerical control machine. Different load parameters were applied to material by these rollers during deep rolling process. Roller had 80 mm outer and 70 mm inner diameter. Cross section of the ring roller was circle and that circle diameter was 5 mm.

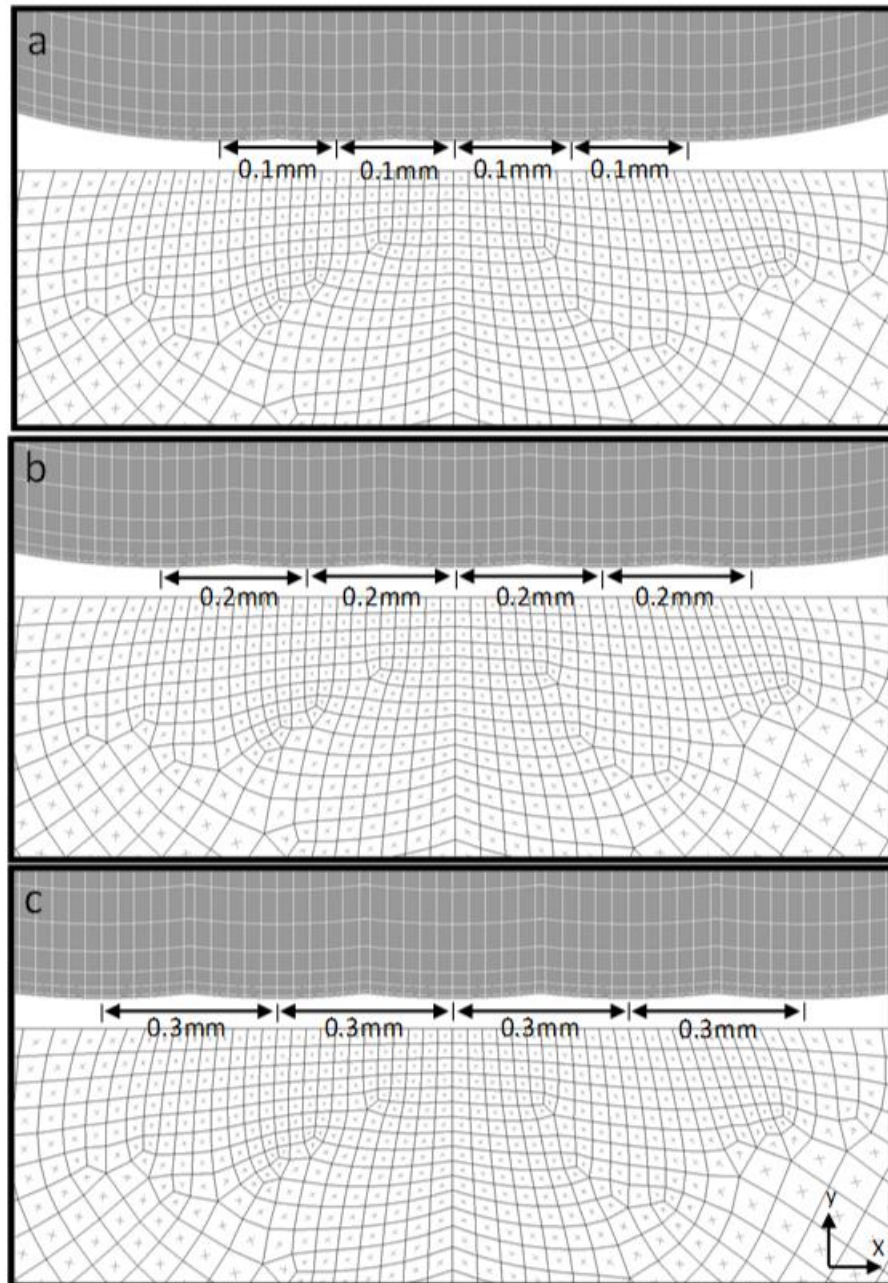


Figure 27 Feed Parameters Between Rollers in Square Model

Deep rolling operation was done with three feed parameters through x direction. Firstly; analysis was done with 0.1 mm distance between rollers. Secondly, gap between rollers increased to 0.2 mm and thirdly, gap increased to 0.3 mm for this analysis. Gap between rollers were shown in Fig. 27.

4.2.2. Longitudinal Rolling 14mm Diameter Model

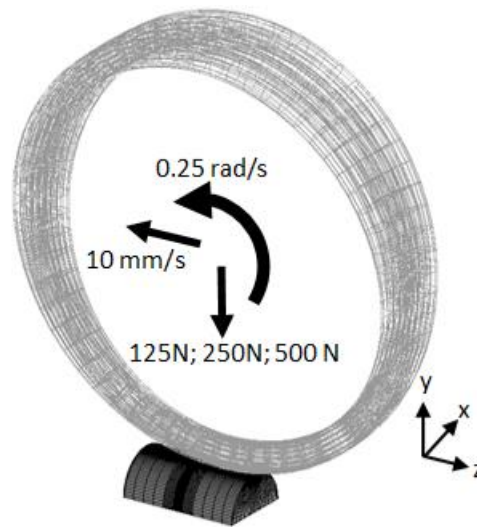


Figure 28 Ø14 mm Model Roller Translation, Rotation and Load Parameters

The next model was 14 mm diameter cylindrical part for longitudinal analysis. In this model, 10 mm/s translational and 0.25 rad/s rotational speed were used. Semi-circle model was created to decrease number of elements on the model. Applied load to the material through rollers were 125 N, 250 N and 500 N. Firstly; elements were created in 2D, expanded through -z direction and 3D mesh elements were obtained. Isometric view of the prepared 14 mm diameter model was shown in Fig. 28.

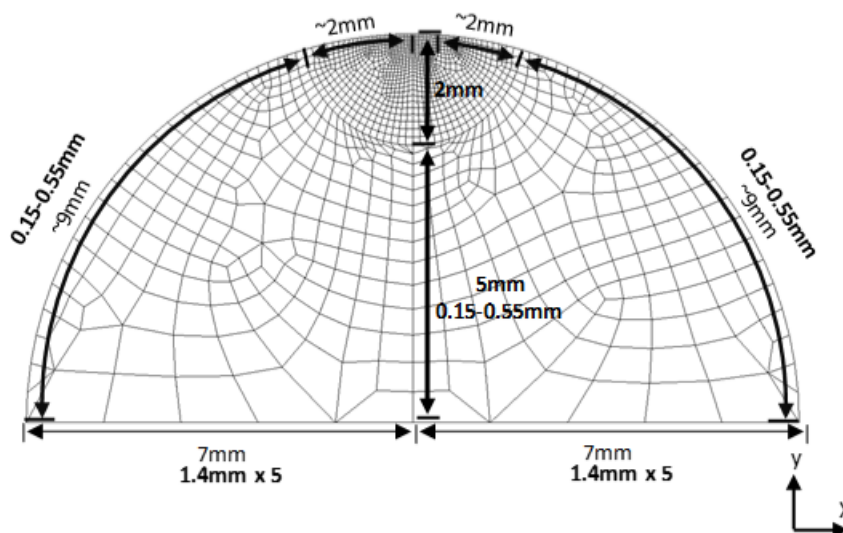


Figure 29 Ø14 mm Model Course Mesh Structure

14 mm diameter geometry was created as semi-circle model (Fig. 29). It had 7 mm length and 14 mm wide. In the middle of the geometry top surface, 2 mm radius circle was

created for fine meshing where longitudinal rolling applied. On the symmetry line, after the fine area, 5 mm length was divided into 0.15 mm-0.55 mm mesh intervals. On top surface of the geometry, after the fine area, arc length was approximately 9 mm and this arc length was divided into intervals as 0.15-0.55 mm. Bottom line of the geometry was divided into 10 equal intervals. On this plane, total 2D mesh number was 1282 and total 3D mesh number was 82048.

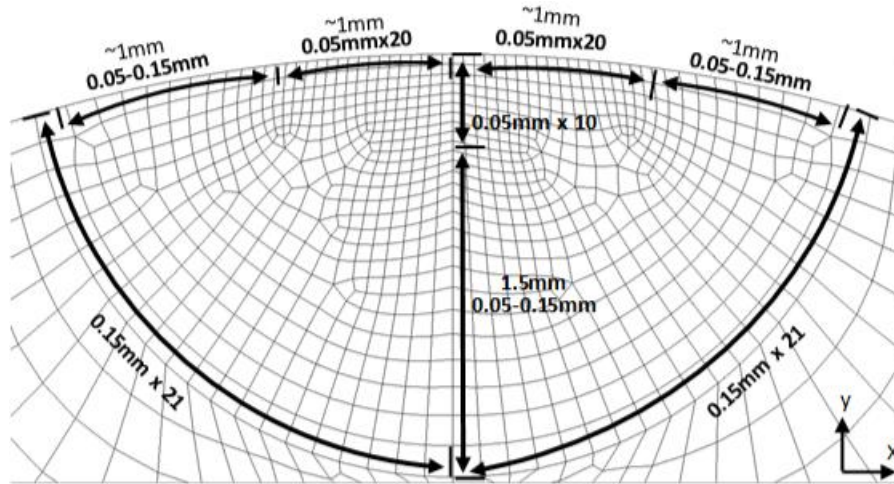


Figure 30 Ø14 mm Model Fine Mesh Structure

On 2 mm radius circle fine mesh section (Fig. 30), on the top line, 1 mm length to left and right side from symmetry line was divided into 20 equal intervals as 0.05 mm. After that division, 1 mm length was divided into intervals starting from 0.05 mm to 0.15 mm. In y direction, 1 mm was divided into 10 equal intervals. Next, 1.5 mm was divided into intervals starting from 0.05 mm to 0.15 mm. Circle arc section was divided into 21 intervals as 0.15 mm. After creation of 2D elements on x-y plane, these elements were expanded through -z direction in the same way with the square model analysis.

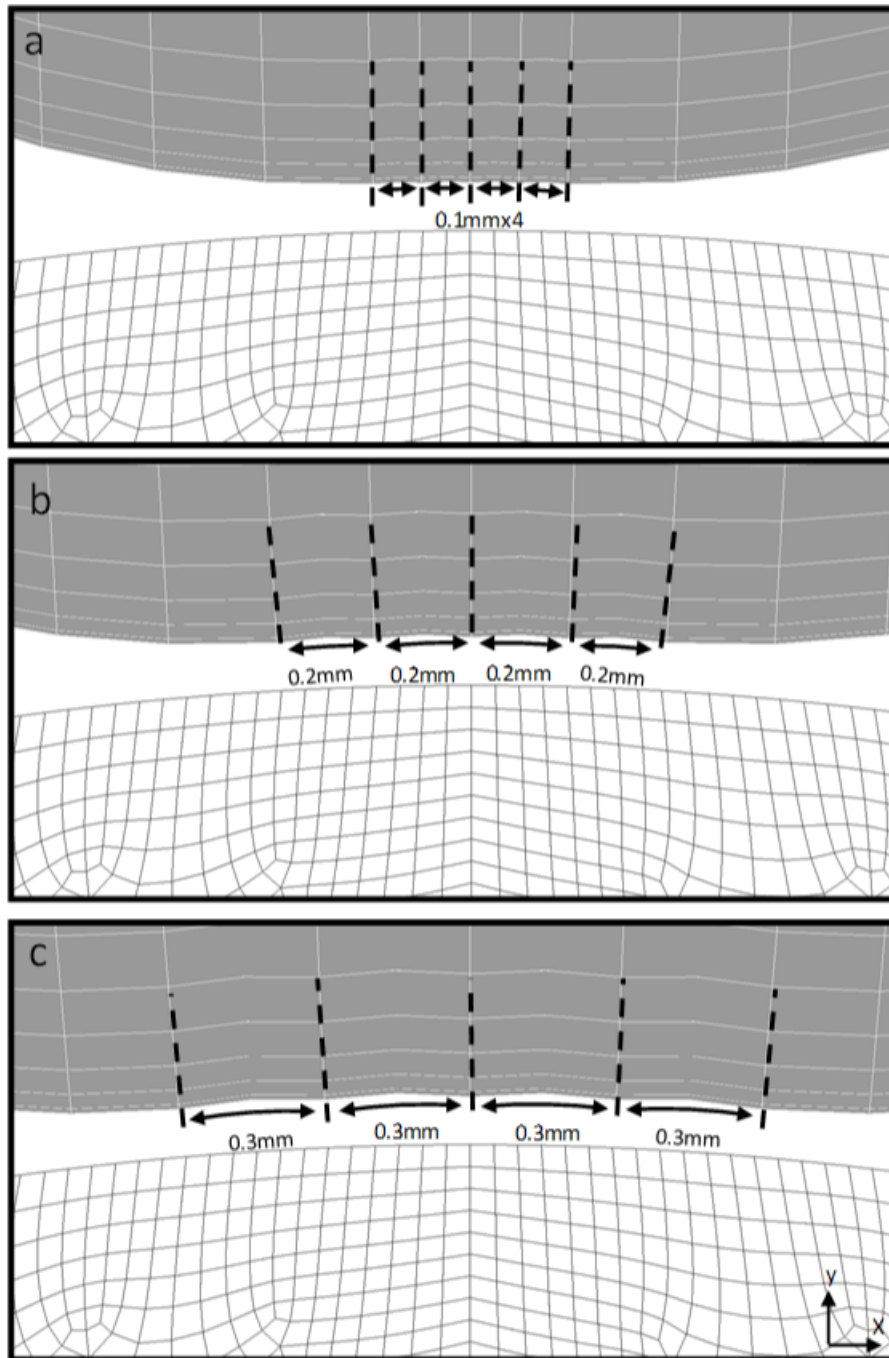


Figure 31 Feed Parameters Between Rollers in Ø14 mm Model

Deep rolling operation was done with three feed parameters through x direction. Firstly, analysis was done with 0.1 mm distance between rollers. Secondly, gap between rollers were increased to 0.2 mm and thirdly, gap was increased to 0.3 mm for this analysis. Rollers were rotated around the center of circle geometry with the appropriate angle to obtain these gaps. Gap between rollers were shown in Fig. 31.

4.2.3. Longitudinal Rolling 8mm Diameter Model

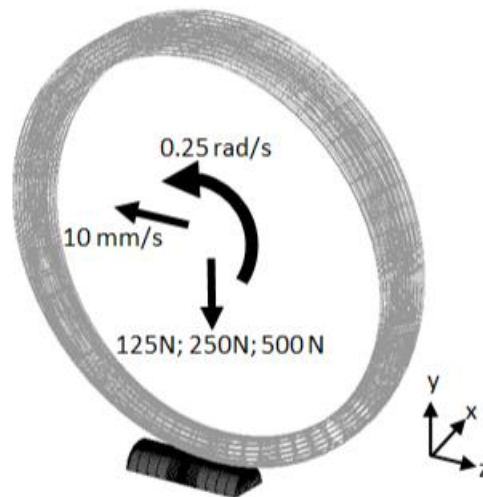


Figure 32 Ø8 mm Model Roller Translation, Rotation and Load Parameters

The next model was 8 mm diameter cylindrical part for longitudinal analysis. In this model, 10 mm/s translational and 0.25 rad/s rotational speed were used. Semi-circle model was created to decrease number of elements on the model. Applied load to the material through rollers were 125 N, 250 N and 500 N. Firstly, elements were created in 2D, expanded through -z direction and 3D mesh elements were obtained. Isometric view of the prepared 8 mm diameter model was shown in Fig. 32.

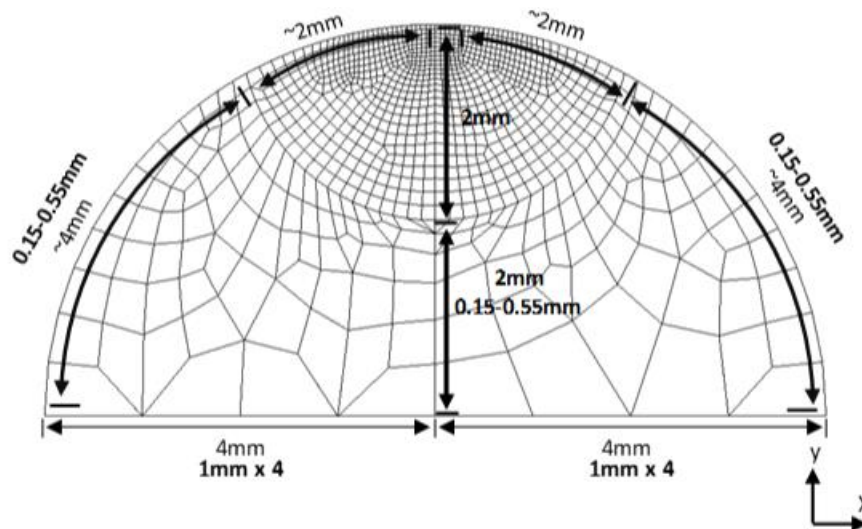


Figure 33 Ø8 mm Model Course Mesh Structure

8 mm diameter geometry was created as semi-circle model (Fig. 33). It had 4 mm length and 8 mm wide. In the middle top surface of the geometry, 2 mm radius circle was created

for fine meshing where longitudinal rolling applied. At the symmetry line, after the fine area, 2 mm length was divided into 0.15 mm-0.55 mm mesh intervals. On top surface of the geometry, after the fine area, arc length was approximately 4 mm and this arc length was divided into intervals as 0.15-0.55 mm. Bottom line of the geometry was divided into 8 equal intervals. On this plane, total 2D mesh number was 969 and total 3D mesh number was 62016.

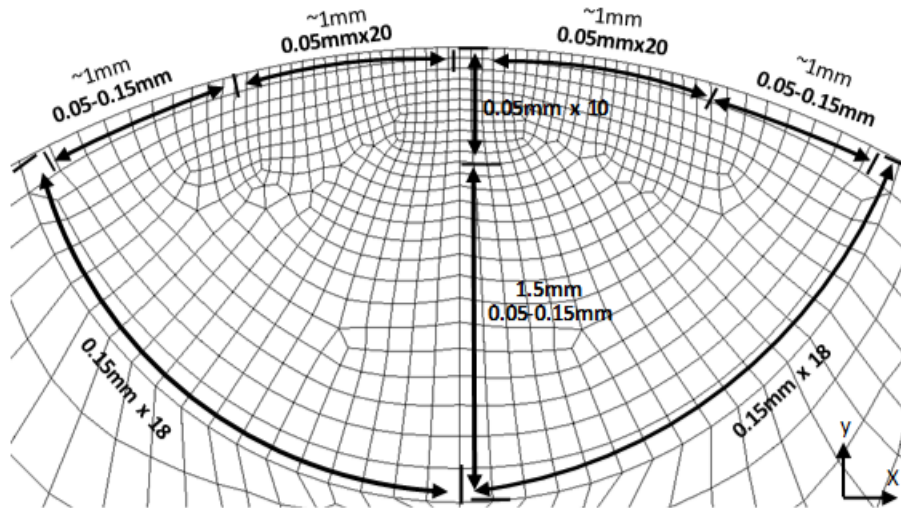


Figure 34 Ø8 mm Model Fine Mesh Structure

On 2 mm radius circle fine mesh section (Fig. 34), at the top line 1 mm length to left and right side from symmetry line was divided into 20 equal intervals as 0.05 mm. After that division, 1 mm length was divided into intervals starting from 0.05 mm to 0.15 mm. In y direction on symmetry line, 1 mm length was divided into 10 equal intervals. Next, 1.5 mm was divided into intervals starting from 0.05 mm to 0.15 mm. Circle arc section was divided into 18 intervals as 0.15 mm. After creation of 2D elements on x-y plane, these elements were expanded through -z direction in the same way with the square model analysis.

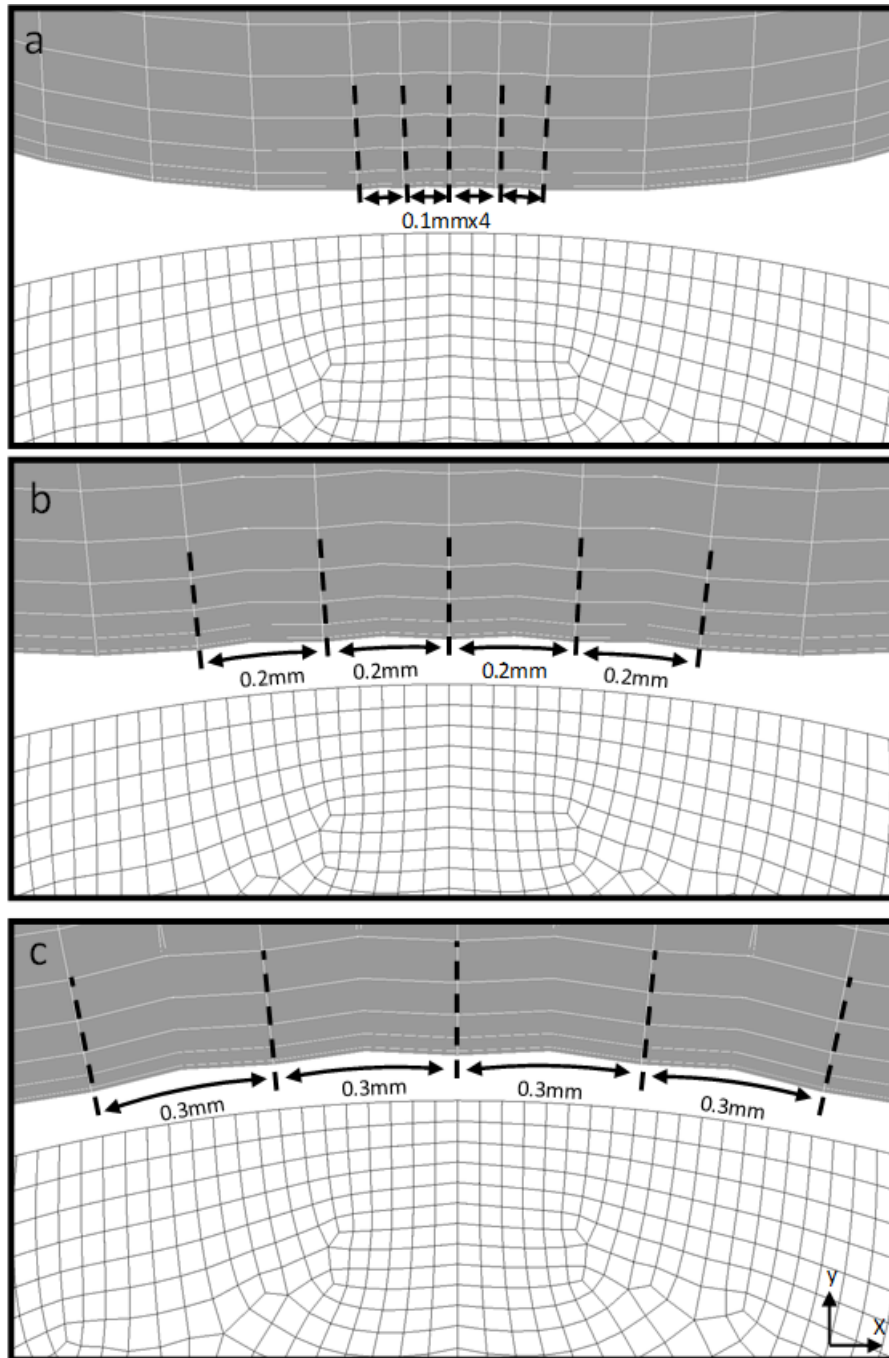


Figure 35 Feed Parameters Between Rollers in Ø8 mm Model

Deep rolling operation was done with three feed parameters through x direction. Firstly, analysis was done with 0.1 mm distance between rollers. Secondly, gap between rollers were increased to 0.2 mm and thirdly, gap was increased to 0.3 mm for this analysis. Rollers were rotated around the center of circle geometry with the appropriate angle to obtain these gaps. Gap between rollers were shown in Fig. 35.

4.2.4. Tangential Rolling 14mm Diameter Model

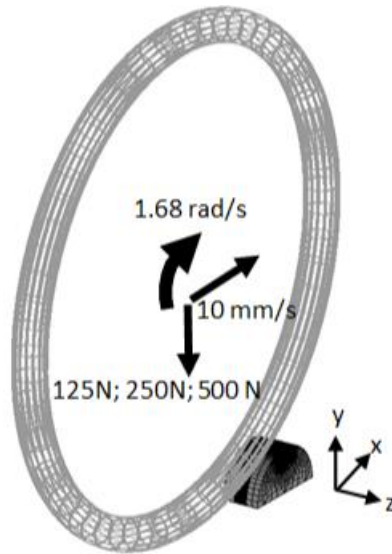


Figure 36 Tangential Rolling $\text{Ø}14$ mm Model Roller Translation, Rotation and Load Parameters

For the tangential rolling models firstly, 14 mm diameter workpiece model was introduced. In this model, 10 mm/s translational and 1.68 rad/s rotational speed were used. Rolling operation was applied around z axis. Only 60° section was rolled on the process which was symmetric with y axis. On this model, semi-circle model was created to decrease number of elements on the model. Applied load to the material through rollers were 125 N, 250 N and 500 N. In addition to that for tangential rolling only 0.1 mm feed gap was used between rollers. Firstly, elements were created in 2D, expanded through -z direction and 3D mesh elements were obtained. Isometric view of the prepared 14 mm diameter model was shown in Fig. 36.

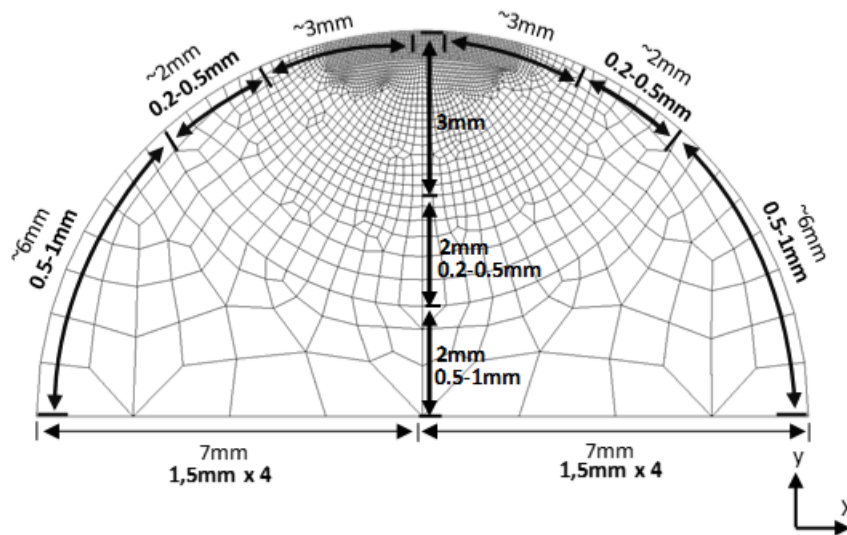


Figure 37 Tangential Rolling Ø14 mm Model Course Mesh Structure

14 mm diameter tangential rolling geometry was created as semi-circle model (Fig. 37). It had 7 mm length and 14 mm wide. In the middle surface of the geometry, 3 mm and 5 mm radius circles were created for fine meshing where tangential rolling was applied. On the symmetry line, after 3 mm length, 2 mm length was divided into 0.2 mm-0.5 mm mesh intervals. The next 2 mm was divided into 0.5 mm-1 mm intervals on symmetry line. On top surface of the geometry, after the fine area, arc length is approximately 8 mm. First arc length of 2 mm was divided into intervals as 0.2-0.5 mm and the next 6 mm arc length was divided into intervals as 0.5-1 mm. Bottom line of the geometry was divided into 8 equal intervals. Total mesh number on this plane was 350.

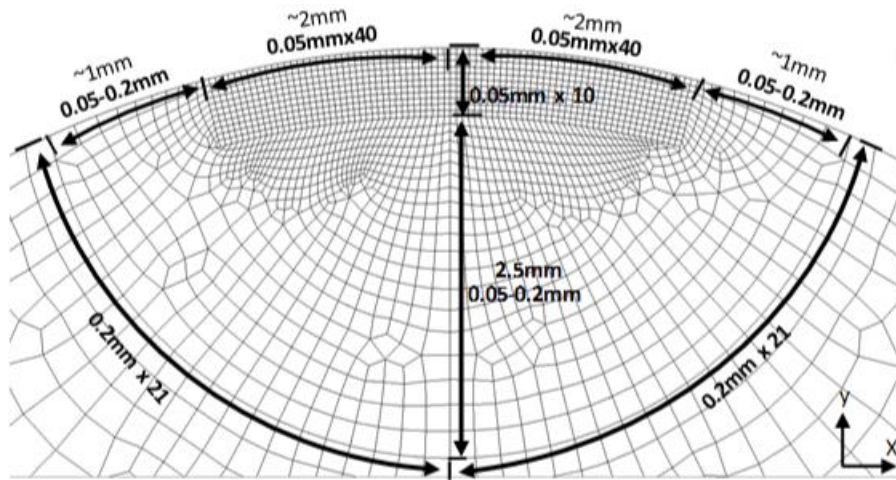


Figure 38 Tangential Rolling Ø14 mm Model Fine Mesh Structure

On this 3 mm radius circle model (Fig. 38), on the top surface of the model, 2 mm length from symmetry line to left and right side was divided into 40 equal intervals and the interval length was 0.05 mm. 6.5 mm radius circle on the geometry and 15° from symmetry line to clockwise and counterclockwise rotated lines were created and intersected. These were construction lines for fine meshing and cannot be seen in Fig. 38. The area limited with this arc and top surface was the tangential rolling examination area. This area was meshed 0.05 mm x 0.05 mm quadratic mesh elements. After that, intervals were divided into 0.05 mm to 0.2 mm for the next 1 mm length. In y axis, on symmetry line, first 0.5 mm length was divided into 10 equal intervals. Next 2.5 mm was divided into intervals starting from 0.05 mm to 0.2 mm. Circle arc section was divided 21 intervals in the length of 0.2 mm.

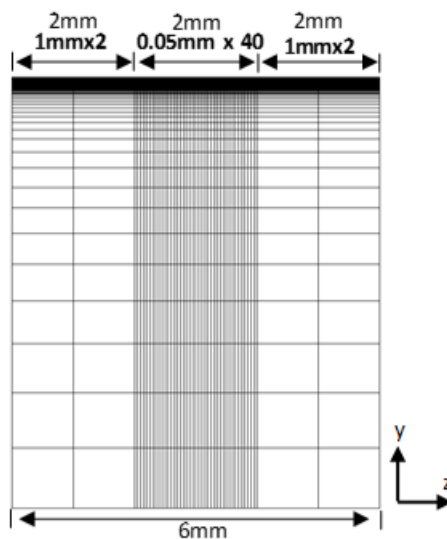


Figure 39 Tangential Rolling Model Z Direction Mesh Structure

After creation of 2D mesh elements, elements were expanded through -z direction (Fig. 39). This length was 6 mm through -z direction. Rolling operation was applied in the middle of the z direction mesh structure. In other words, first roller was placed at $z = -3$ mm and the others were 0.1 mm translated from first roller to the left and to the right. The area where the investigation of residual stresses made was very fine and element expansion size was 0.05 mm and 40 elements were used. The density of elements was decreased from middle point through the edges. Near the finest area 1 mm expansion size and 2 elements were used. Total expansion through -z direction was -6 mm, but application area was in the middle of z direction and its width was 0.5 mm. This was because sufficient material length allows sufficient expansion of residual stresses and diminish to zero through length and it is not desired to interrupt expansion of residual stresses properly.

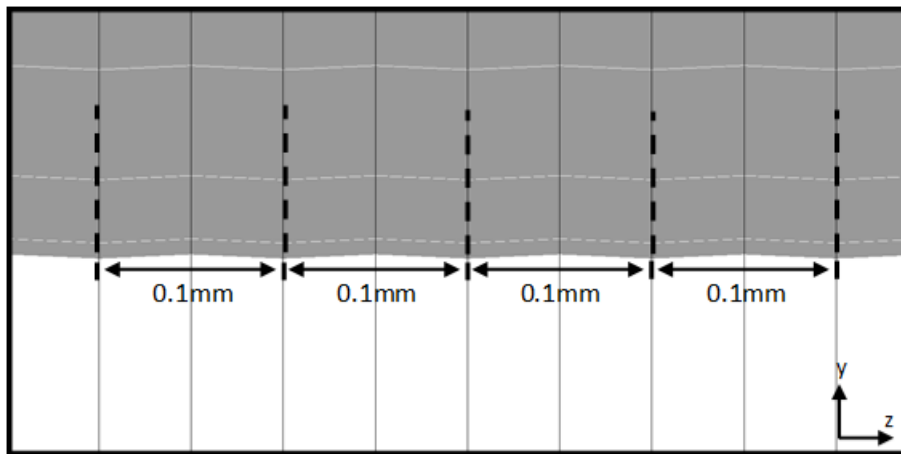


Figure 40 Feed Parameters Between Rollers in $\text{Ø}14$ mm Tangential Rolling Model

Tangential deep rolling operation was done with only 0.1 feed parameters through z direction. As mentioned before rollers were rotated around the center of circle geometry 30° . Total rolling area was 60° on the circular geometry. Gap between rollers were shown in Fig. 40.

4.2.5. Tangential Rolling 8mm Diameter Model

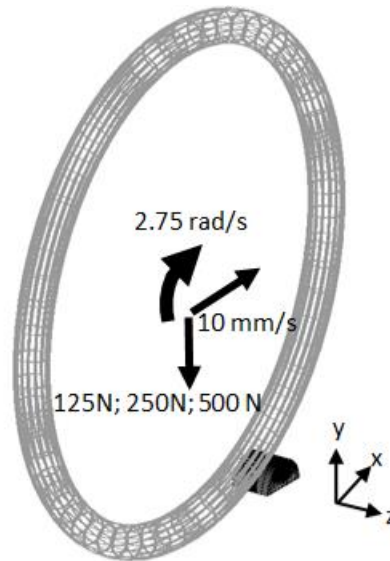


Figure 41 Tangential Rolling Ø8 mm Model Roller Translation, Rotation and Load Parameters

For the tangential rolling models, 8 mm diameter workpiece model was introduced. In this model, 10 mm/s translational and 2.75 rad/s rotational speed were used. Rolling operation was applied around z axis. Only 60° section was rolled on the process which was symmetric with y axis. On this model, semi-circle model was created to decrease number of elements on the model. Applied load to the material through rollers were 125 N, 250 N and 500 N. In addition to that, for tangential rolling only 0.1 mm feed gap was used between rollers. Elements were created in 2D, expanded through -z direction and 3D mesh elements were obtained. Isometric view of the prepared 8 mm diameter model was shown in Fig. 41.

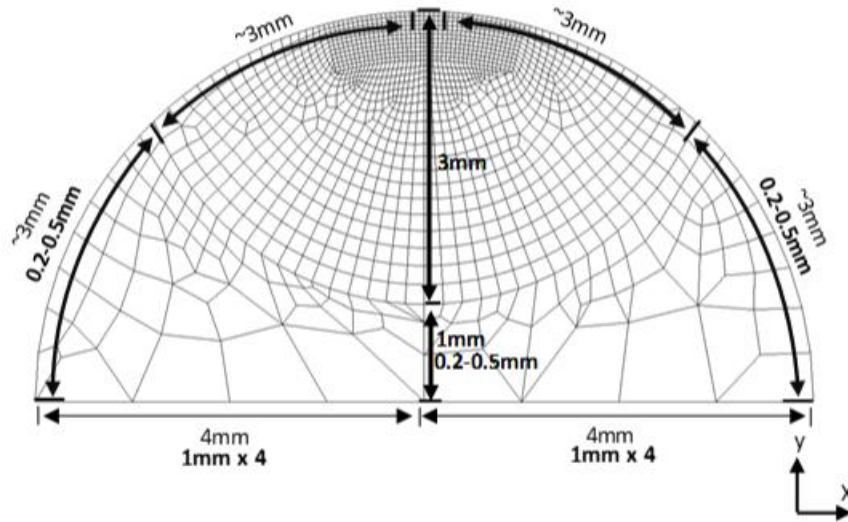


Figure 42 Tangential Rolling Ø8 mm Model Course Mesh Structure

8 mm diameter tangential rolling geometry was created as semi-circle model (Fig. 42). It had 4 mm length and 8 mm wide. In the middle surface of the geometry, only 3 mm radius circle was created for fine meshing where tangential rolling was applied. On the symmetry line after 3 mm length, 1 mm length was divided into 0.2 mm-0.5 mm mesh intervals. On top surface of the geometry, after the fine area, arc length was approximately 3 mm. This arc length of 3 mm was divided into intervals as 0.2-0.5 mm. Bottom line of the geometry was divided into 8 equal intervals. Total mesh number on this plane was 350.

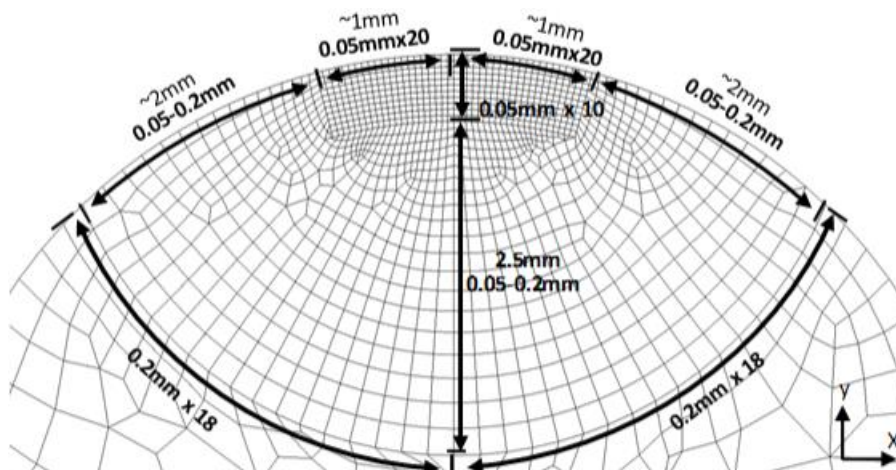


Figure 43 Tangential Rolling Ø8 mm Model Fine Mesh Structure

On this 3 mm radius circle model (Fig. 43), on the top surface of the model, 1 mm length from symmetry line to left and right side was divided into 20 equal intervals, and the interval length was 0.05 mm. 3.5 mm radius circle on the geometry and 15° from symmetry

line to clockwise and counterclockwise directions lines created and intersected. These were construction lines for fine meshing and cannot be seen in Fig. 43. The area limited with this arc and top surface was the tangential rolling examination area. This area was meshed with 0.05 mm x 0.05 mm quadratic mesh elements. After that, on the surface, intervals were 0.05 mm to 0.2 mm for the next 2 mm length. In y axis, on symmetry line or dept direction, first 0.5 mm length was divided into 10 equal intervals. Next 2.5 mm was divided into intervals starting from 0.05 mm to 0.2 mm. Circle arc section was divided into 18 intervals in the length of 0.2 mm. After creation of 2D elements on x-y plane, these elements were expanded through -z direction in the same way with the 14 mm diameter tangential rolling model analysis.

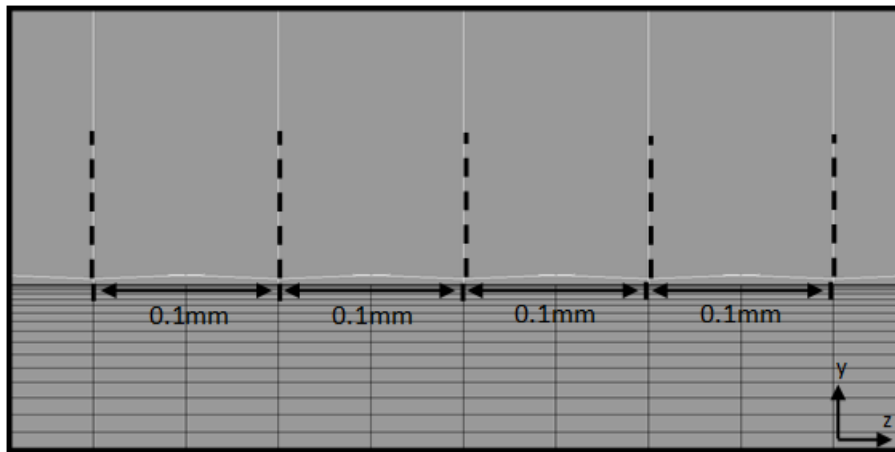


Figure 44 Feed Parameters Between Rollers in Ø8 mm Tangential Rolling Model

Tangential deep rolling operation was done with only 0.1 feed parameter through z direction. Rollers were rotated around the center of circle geometry around z axis by 30° starting from the middle of the geometry on x-y plane. Total rolling path was 60° on the circular geometry. Gap between rollers were shown in Fig. 44.

5. RESULTS

In this chapter, the finite element analysis results and obtained graphs were shown. Deep rolling analyses were done on square models, Ø14 mm and Ø8 mm models. These models were named as S, Ø14, Ø8, TR_Ø14 and TR_Ø8, respectively. 0125, 0250, 0500 indicates applied force parameters in Newtons. In these analyses; five rollers were used. First roller was placed in the middle section of the geometry. The others were placed equally with 0.1 mm, 0.2 mm and 0.3 mm gap. This annotation was shown after the force parameters on analysis naming.

Examination of residual stresses were done in directions x and z. σ_x and σ_z residual stress results were noted as X and Z, respectively. As mentioned before, analyses were done by 5 rolling operations, starting from left-hand side to right hand side of the geometry on x-y plane, and captures were taken at the end of each rolling operation. Furthermore, results were taken from the middle of the material on z direction with a distance of 2 mm left and 2 mm right from the symmetry line and 1mm depth from the surface of the material. Only 0.2 mm feed parameter results were shown for the first three analyses models. Because, on this feed parameter, saturated residual stress results were obtained. For tangential rolling, analyses were done only for 0.1 mm feed parameter and the results were plotted.

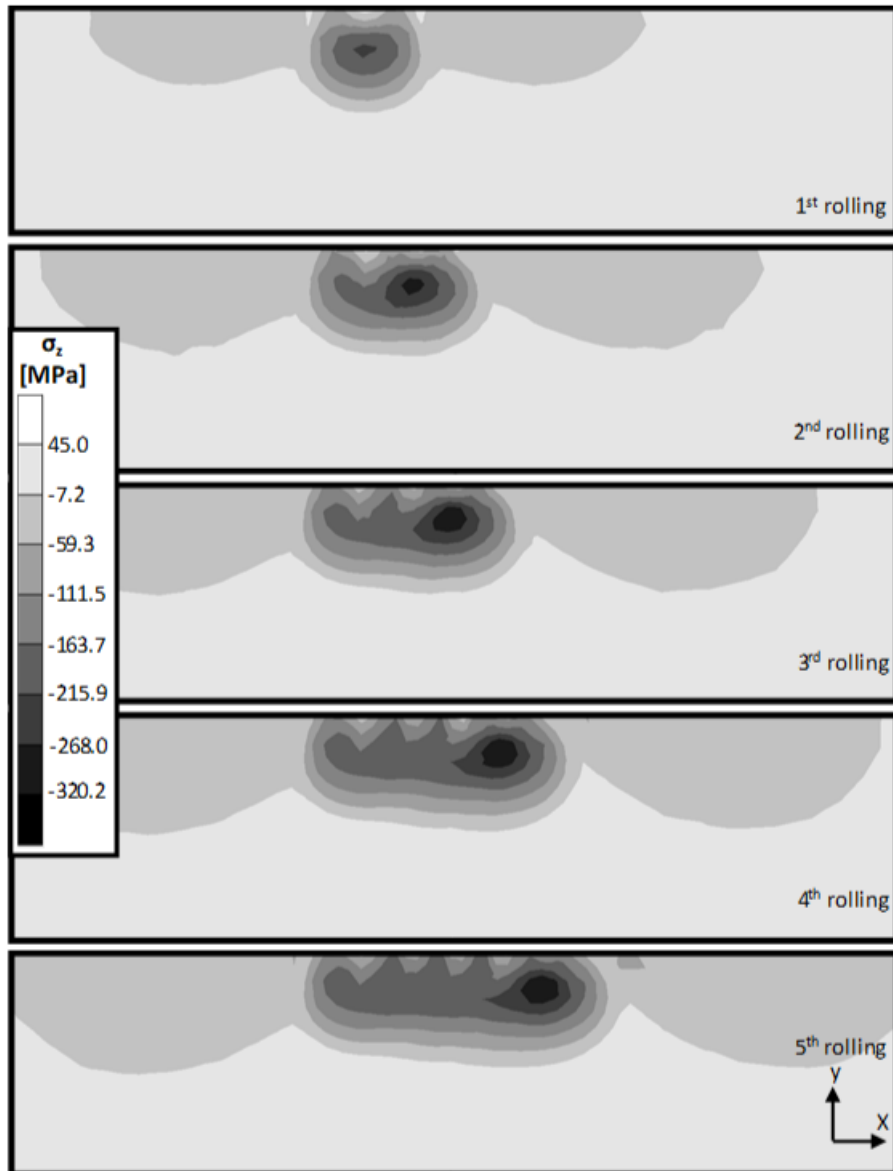


Figure 45 Residual Stress Distribution on Square Model, σ_z , 250 N, 0.2 mm feed

In Fig. 45, σ_z results were shown for each rolling operation on the square geometry with 250 N load and 0.2 mm roller gap. In that direction, depth of residual stresses reached through 5th rolling up to 0.5 mm and residual stress area width were obtained as almost 1.5-2 mm. Compressive residual stresses generally occurred but their magnitudes increased through 5th rolling in the range of 0-320 MPa. Tensile residual stresses also occurred very rarely in the range of 0-45 MPa. The dense area for compressive residual stresses occurred just after the surface in depth direction and this depth were almost 0.1-0.2 mm and the values decreased after this depth through 0.4 mm. As for the depth direction, residual stresses decreased in other direction starting from symmetry axis through width.

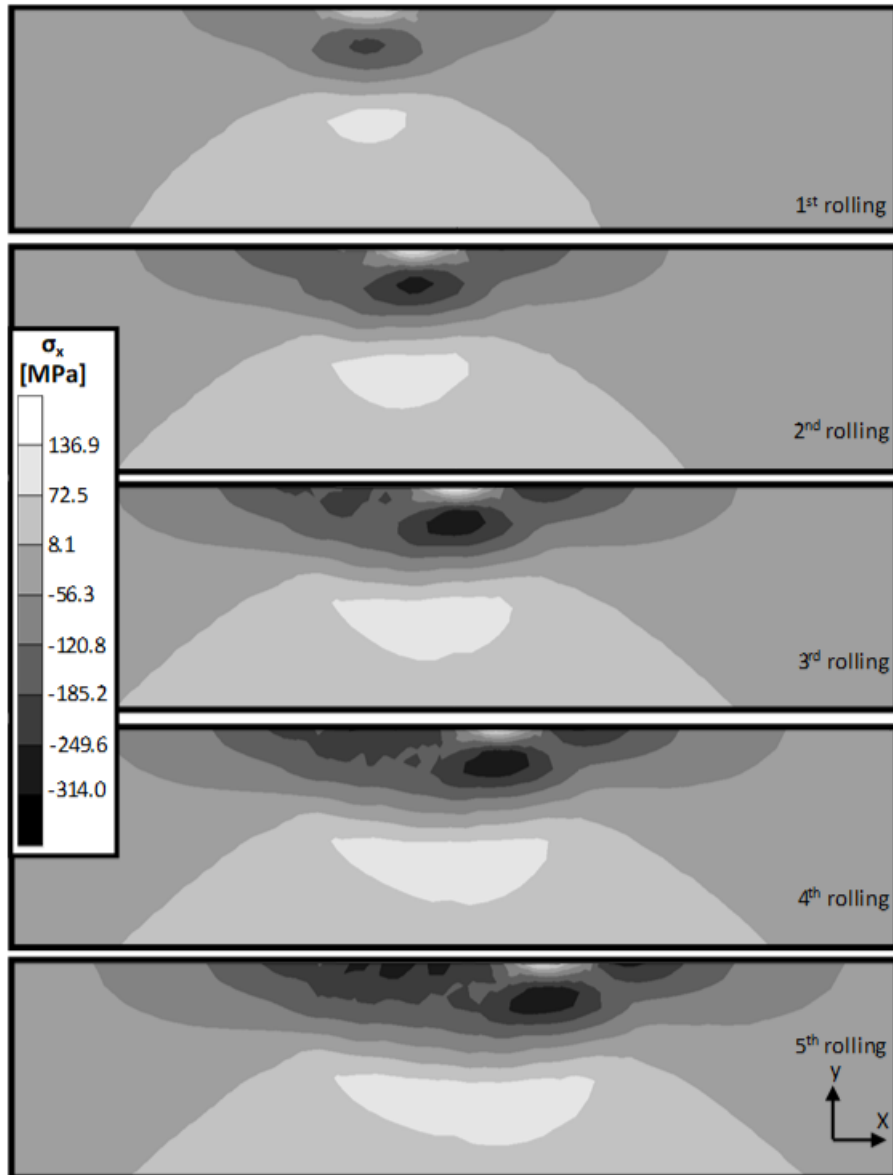


Figure 46 Residual Stress Distribution on Square Model, σ_x , 250 N, 0.2 mm feed

In Fig. 46, σ_x results were shown. In that direction, depth of residual stresses reached up to 0.9 mm through 5th rolling and residual stress area width were obtained as above the 2 mm. Compressive residual stresses generally occurred and their magnitudes increased through 5th rolling in the range of 0-315 MPa. Tensile residual stresses also occurred in a small area at a depth range of 0.6-0.9 mm from the surface in the range of 0-135 MPa. The dense area for compressive residual stresses occurred just after the surface in depth direction and this depth were almost 0.2-0.3 mm, same as in z direction results and the stress magnitudes decreased after this depth through 0.6 mm. As for the depth direction, residual stresses decreased in other direction starting from symmetry axis through width.

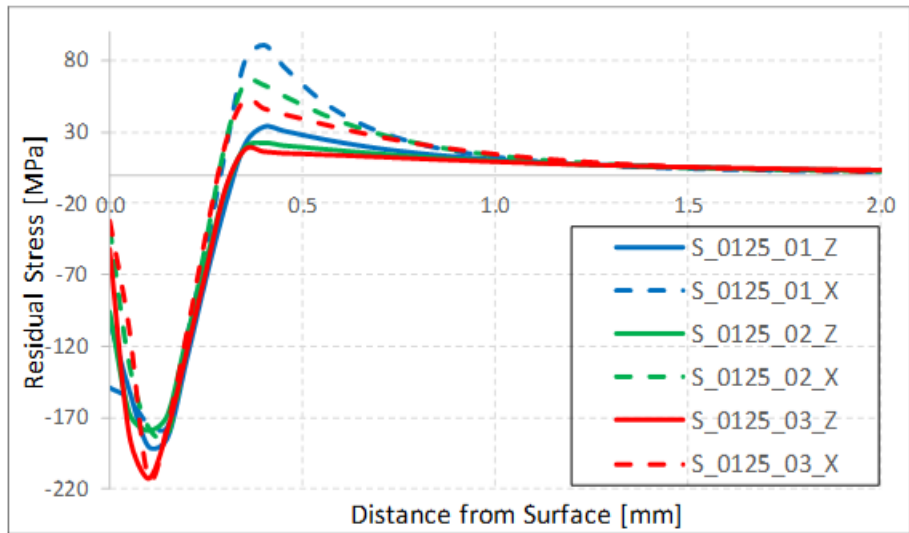


Figure 47 Residual Stress Results on Square Model, σ_z , σ_x , 125 N for All Feed Parameters

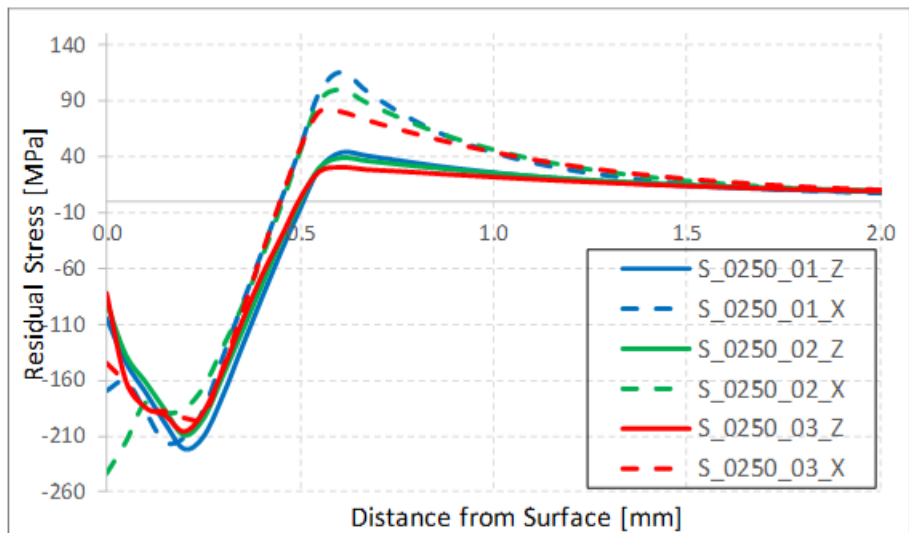


Figure 48 Residual Stress Results on Square Model, σ_z , σ_x , 250 N for All Feed Parameters

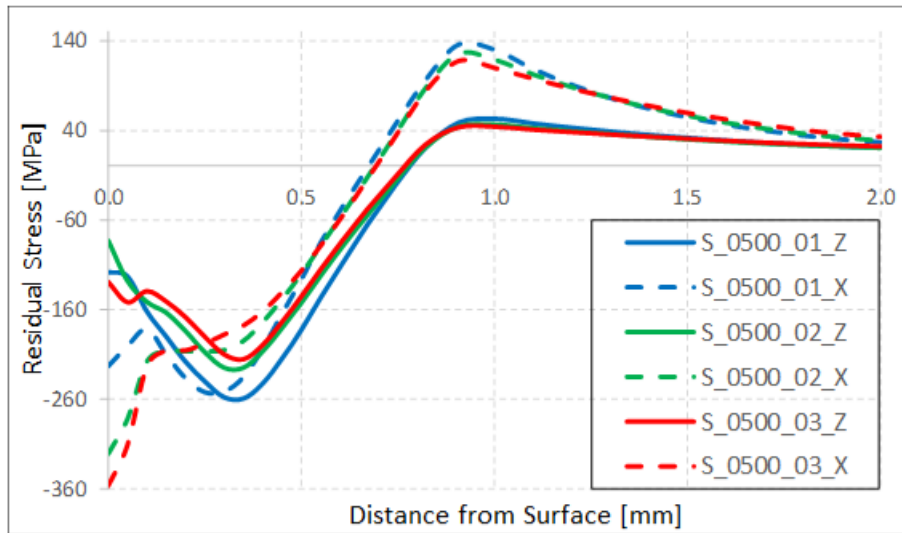


Figure 49 Residual Stress Results on Square Model, σ_z , σ_x , 500 N for All Feed Parameters

On the three graphs above (Fig. 47, 48, 49); the results were taken from symmetry axis from surface to 2 mm depth and at the end of the fifth rolling operation for square model for all feed parameters. All the force parameters were applied to the models. As can see from the graph label, blue lines show 125 N, green lines show 250 N, red lines show 500 N applications. Straight lines show σ_z , dashed lines show σ_x results. As can be seen from the graphs, all results started with compressive residual stress and made peaks in the depth range of 0-0.5 mm, turned into tensile residual stresses and made peaks again at different depths. σ_z and σ_x results followed each other in trend. It was also obvious that the more force was applied, the more residual stress results obtained. In addition to that, feed parameters of 0.1 mm, 0.2 mm and 0.3 mm did not significantly affect the residual stress values on the model.

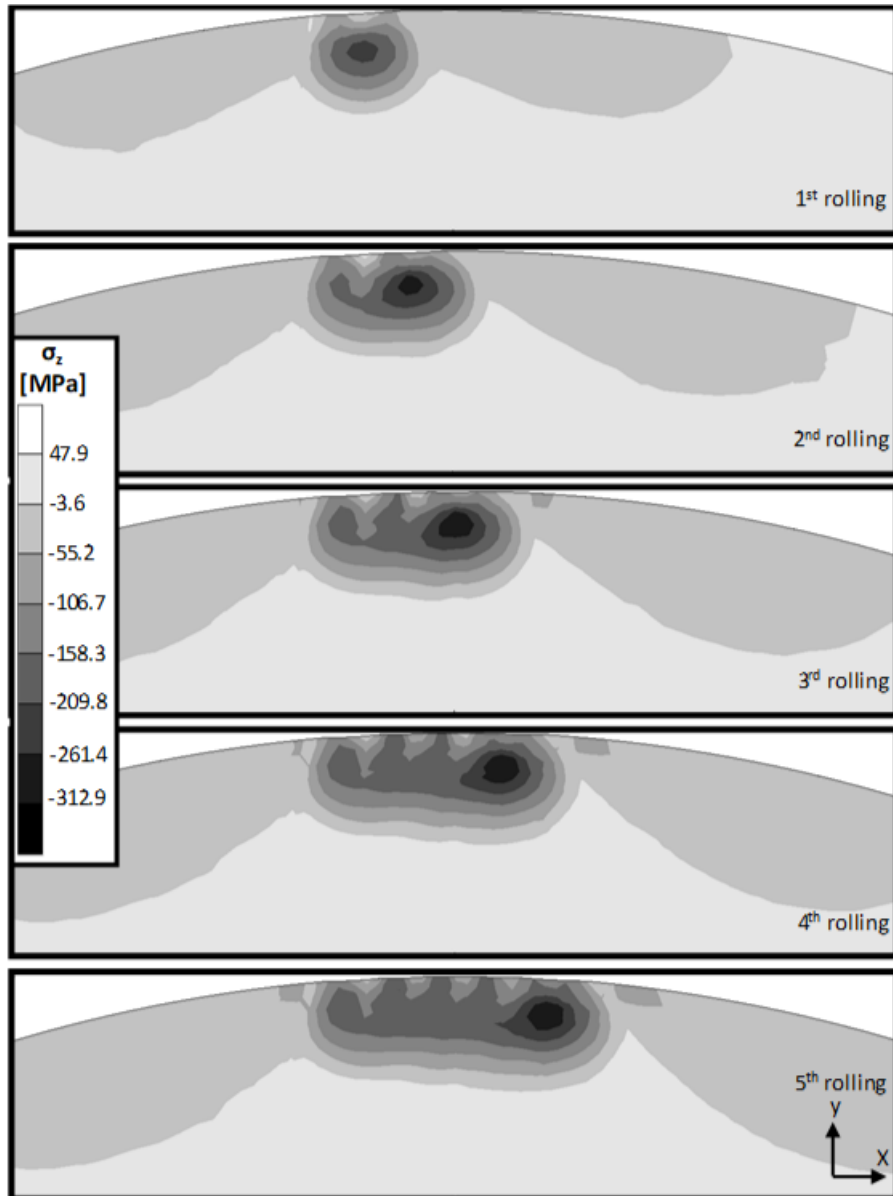


Figure 50 Residual Stress Distribution on Ø14 Model, σ_z , 250 N, 0.2 mm feed

In Fig. 50, σ_z results were shown for each rolling operation on the Ø14 model geometry with 250 N load and 0.2 mm roller gap. In that direction, depth of residual stresses reached up to 0.3 mm through 5th rolling and residual stress area width were obtained as in the range of 1-2 mm. Compressive residual stresses generally occurred, and their magnitudes increased through 5th rolling in the range of 0-312 MPa. Tensile residual stresses also occurred after the depth of 0.3 mm from the surface in the range of 0-50 MPa. The dense area for compressive residual stresses occurred just after the surface in depth direction and this depth were almost 0.1-0.2 mm and the stress magnitudes decreased after this depth through 0.3 mm. As for the depth direction, residual stresses decreased in other direction starting from symmetry axis through width.

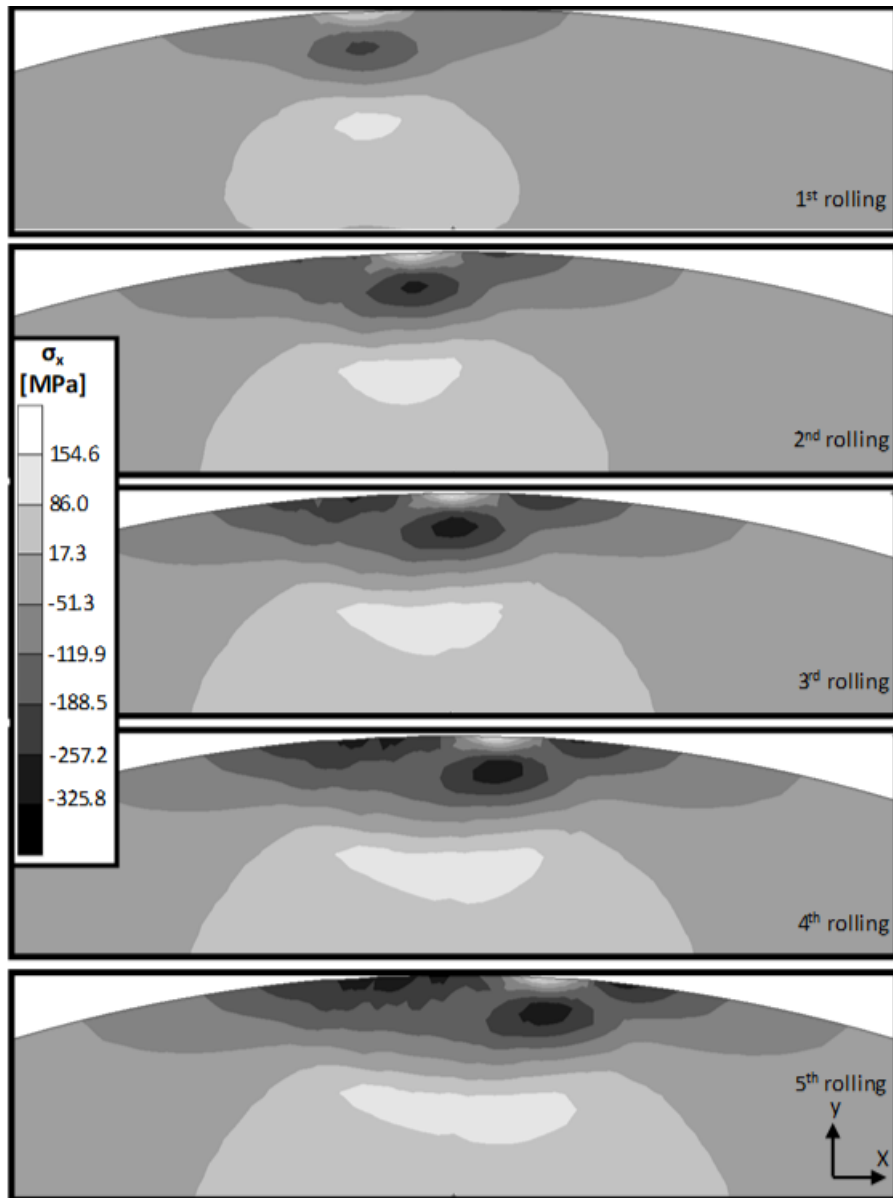


Figure 51 Residual Stress Distribution on Ø14 Model, σ_x , 250 N, 0.2 mm feed

In Fig. 51, σ_x results were shown for the same analysis. In that direction, depth of residual stresses reached up to 0.6 mm through 5th rolling and residual stress area width were obtained as almost 1 mm. Compressive residual stresses generally occurred, and their magnitudes increased through 5th rolling in the range of 0-325 MPa. Tensile residual stresses also occurred in a small area at a depth range of 0.3-0.6 mm from the surface in the range of 0-155 MPa. The dense area for compressive residual stresses occurred just after the surface in depth direction and this depth were almost 0.1-0.2 mm and the stress magnitudes decreased after this depth through 0.3 mm. As for the depth direction, residual stresses decreased in other direction through width. The results were very similar with the square model at same force and same feed parameters.

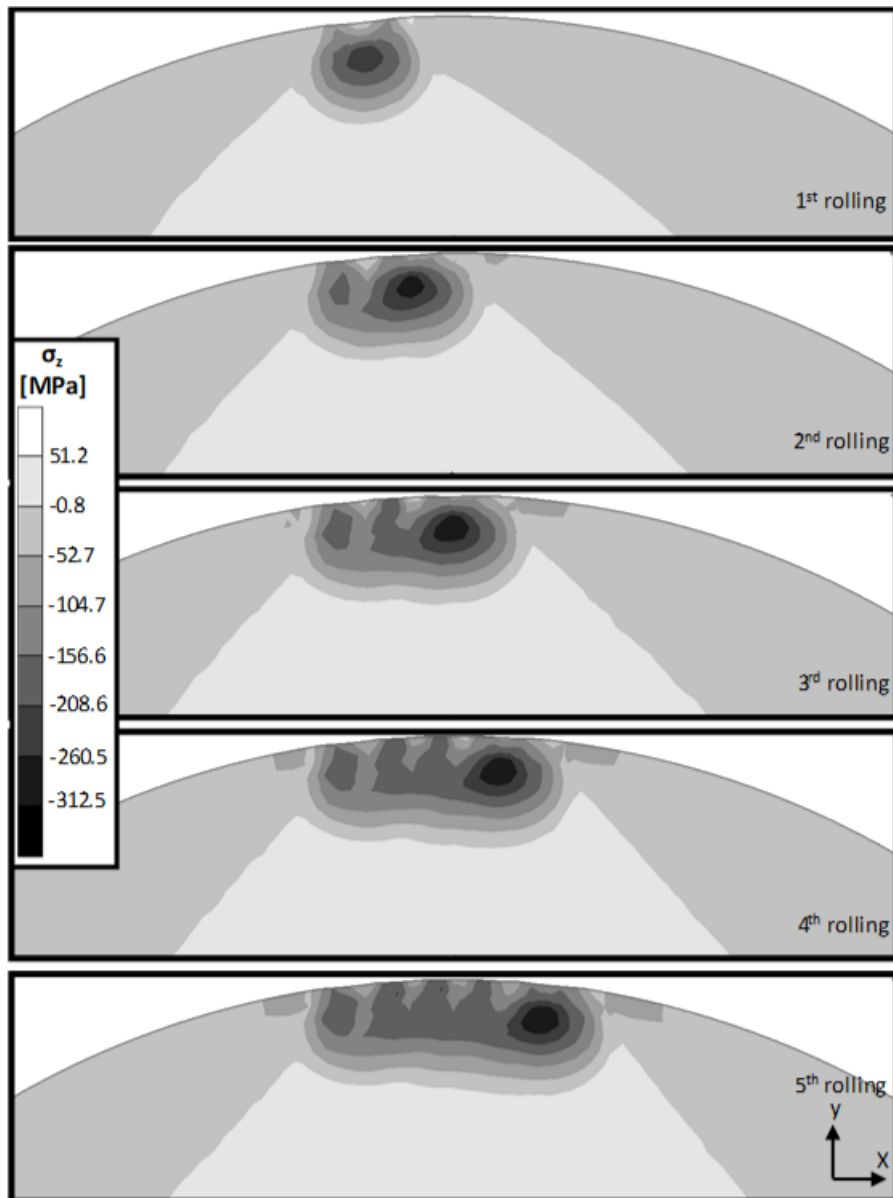


Figure 52 Residual Stress Distribution on Ø8 Model, σ_z , 250 N, 0.2 mm feed

In Fig. 52, σ_z results were shown for each rolling operation on the Ø8 model geometry with 250 N load and 0.2 mm roller gap. In that direction, depth of residual stresses reached through 5th rolling up to 0.4 mm and residual stress area width were obtained as in the range of 1-2 mm. Compressive residual stresses generally occurred, and their magnitudes increased through 5th rolling in the range of 0-312 MPa. Tensile residual stresses also occurred after the depth of 0.3 mm from the surface in the range of 0-50 MPa. The dense area for compressive residual stresses occurred just after the surface in depth direction and this depth were almost 0.1-0.2 mm and the magnitudes decreased after this depth through 0.3 mm. As for the depth direction, residual stresses decreased in other direction through

width. These results were very similar to 14 mm diameter model for the same direction, load and feed parameters.

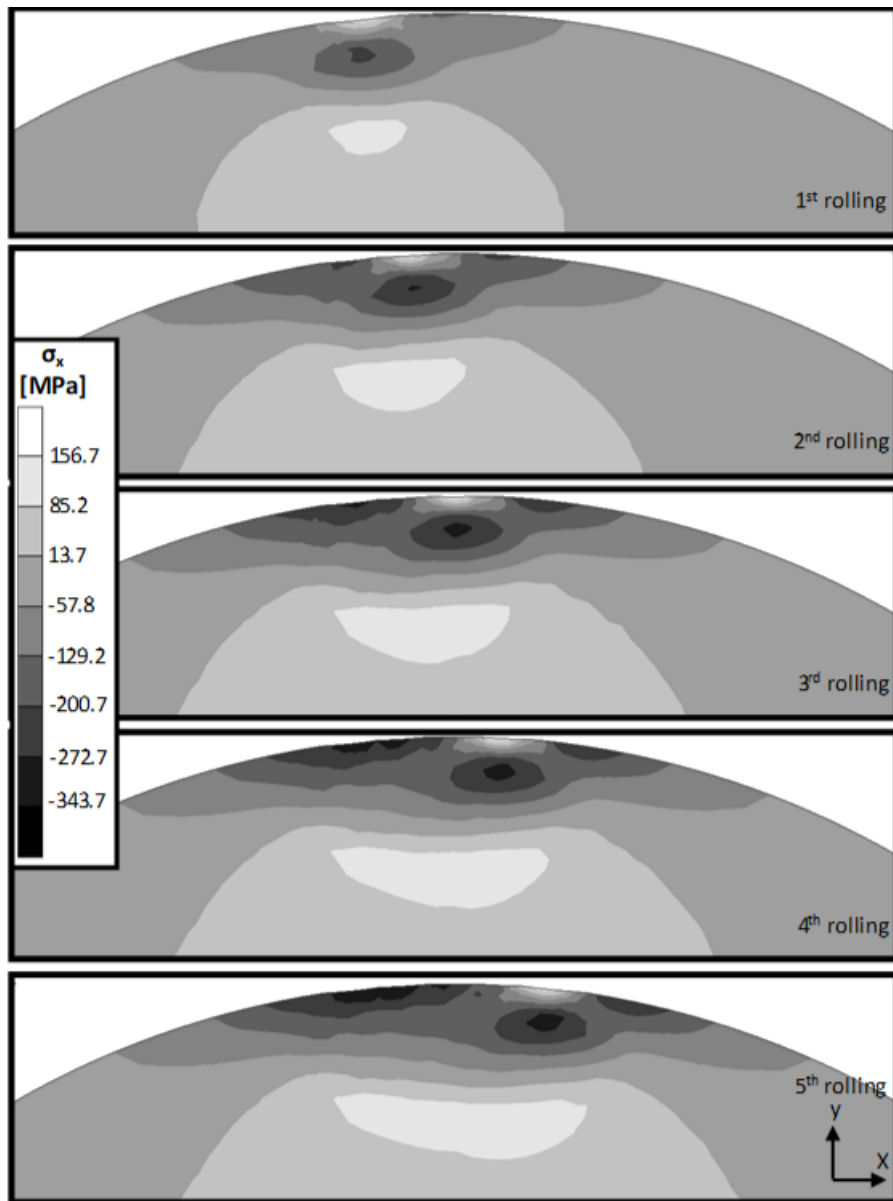


Figure 53 Residual Stress Distribution on Ø8 Model, σ_x , 250 N, 0.2 mm feed

In Fig. 53, σ_x results were shown for the same analysis. In that direction, depth of residual stresses reached up to 0.8 mm through 5th rolling and residual stress area width were obtained as almost 1 mm. Compressive residual stresses generally occurred, and their magnitudes increased through 5th rolling in the range of 0-343 MPa. Tensile residual stresses also occurred in a small area at a depth range of 0.6-0.8 mm from the surface in the range of 0-156 MPa. The dense area for compressive residual stresses occurred just after the surface in depth direction and this depth were almost 0.1-0.2 mm and the stress

magnitudes decreased after this depth through 0.3 mm. As for the depth direction, residual stresses decreased in other direction through width. The results were similar with the square model at same force and same feed parameters.

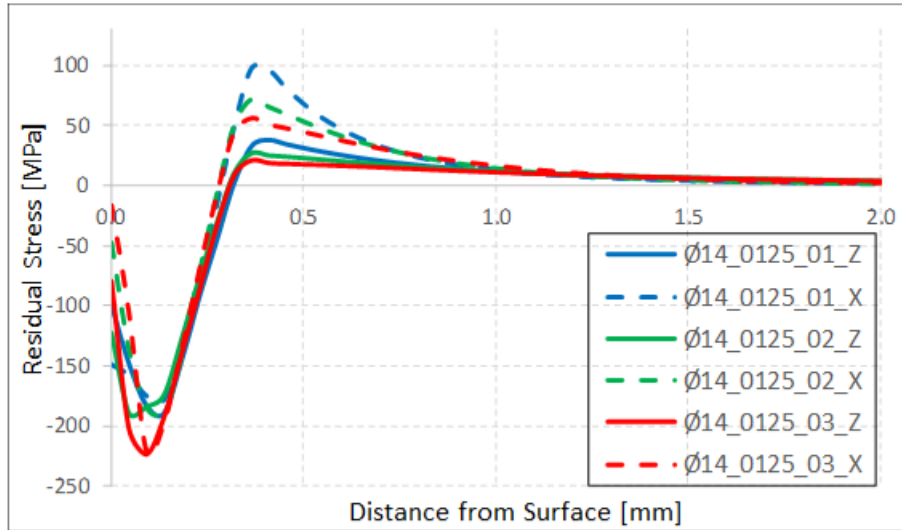


Figure 54 Residual Stress Results on Ø14 Model, σ_z , σ_x , 125 N for All Feed Parameters

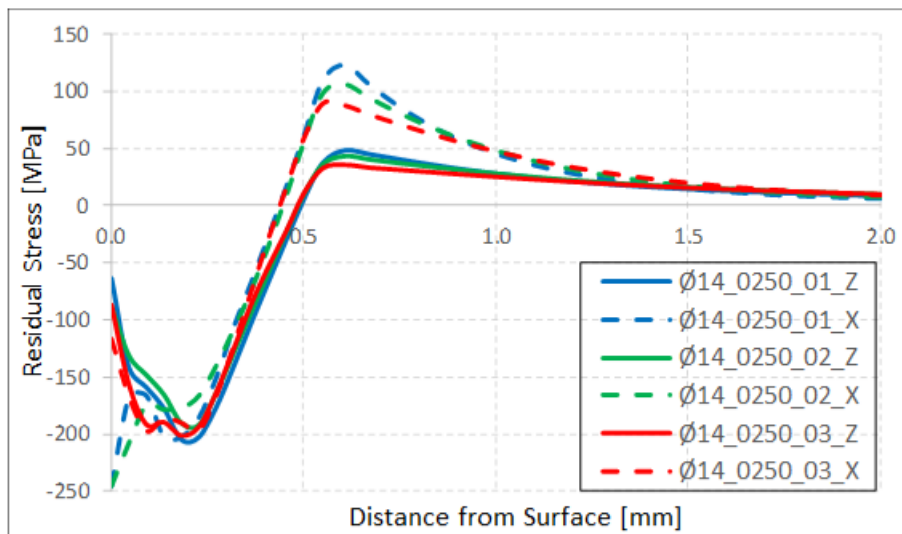


Figure 55 Residual Stress Results on Ø14 Model, σ_z , σ_x , 250 N for All Feed Parameters

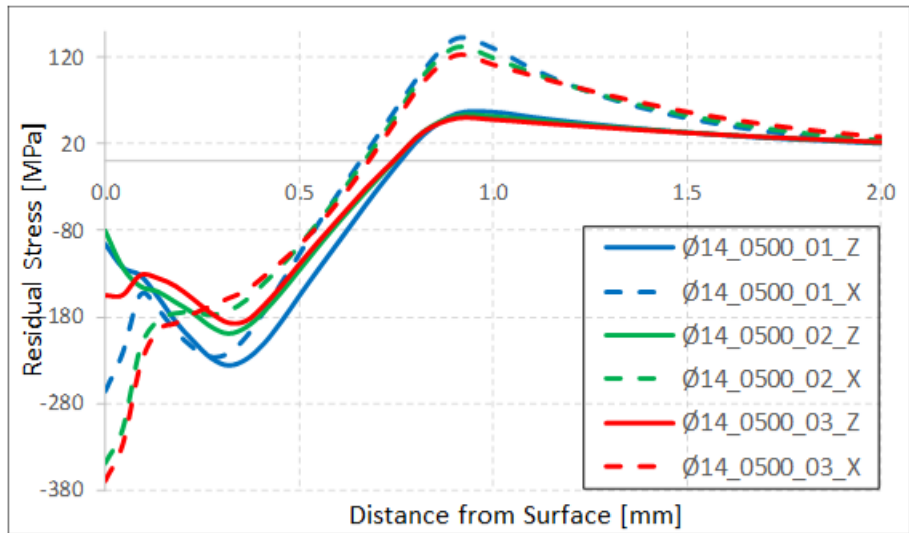


Figure 56 Residual Stress Results on Ø14 Model, σ_z , σ_x , 500 N for All Feed Parameters

On the three graphs above (Fig. 54, 55, 56); for 14 mm diameter circular geometry longitudinal rolling model, the residual stress trend was similar to the square model. Feed parameters did not have much effect on the residual stresses.

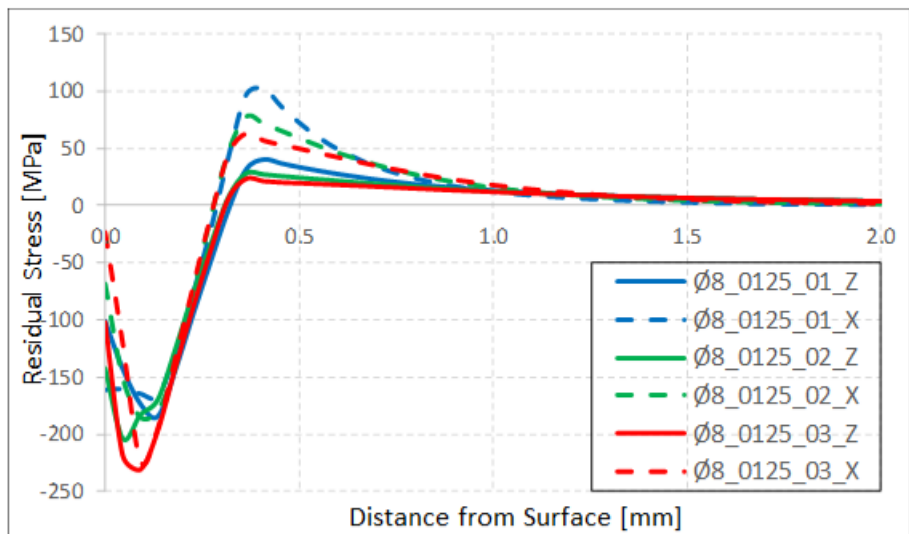


Figure 57 Residual Stress Results on Ø8 Model, σ_z , σ_x , 125 N for All Feed Parameters

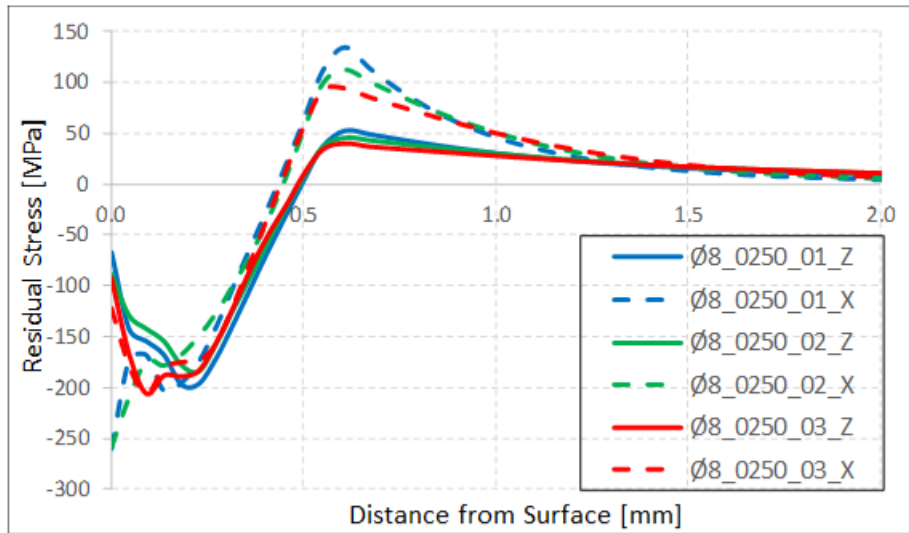


Figure 58 Residual Stress Results on Ø8 Model, σ_z , σ_x , 250 N for All Feed Parameters

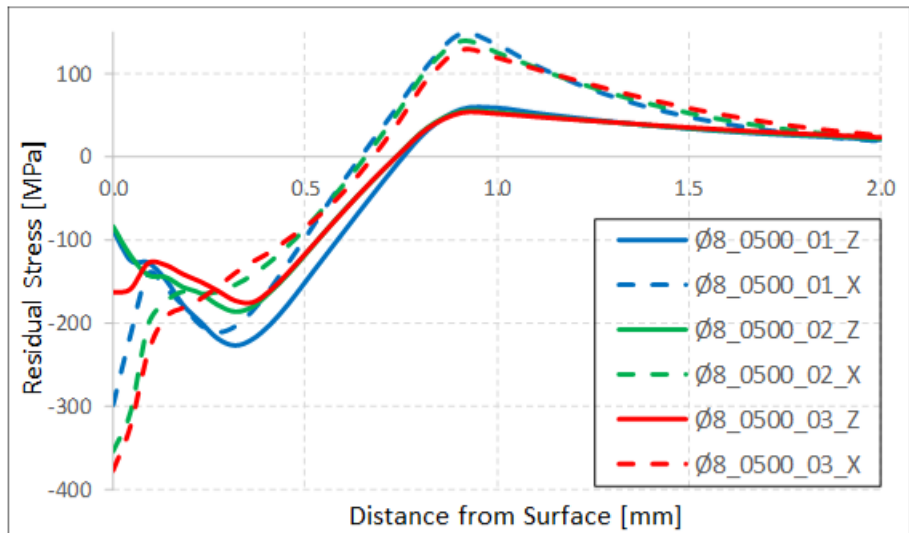


Figure 59 Residual Stress Results on Ø8 Model, σ_z , σ_x , 500 N for All Feed Parameters

On the three graphs above (Fig. 57, 58, 59); for 8 mm diameter circular geometry longitudinal rolling model, the residual stress trend was similar to the square model. Feed parameters did not have much effect on the residual stress magnitudes. The results were as expected when it was compared with the other geometry residual stress investigations.

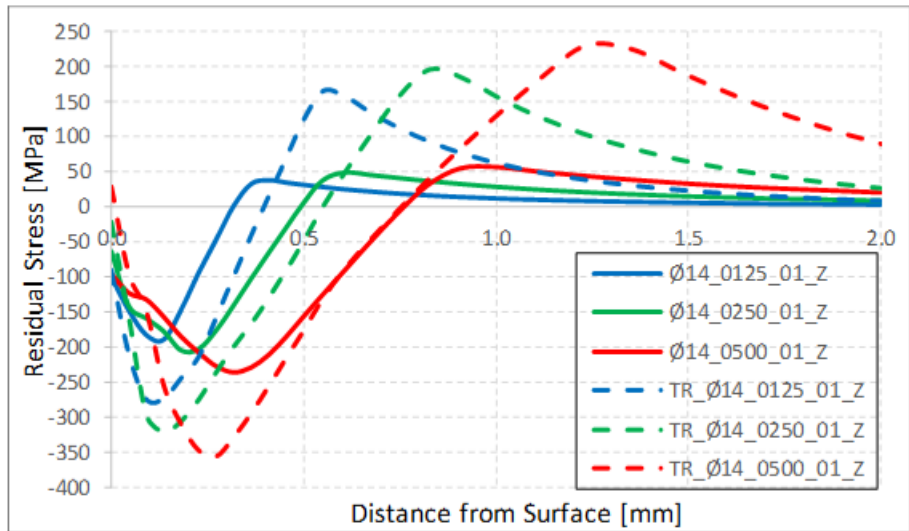


Figure 60 Residual Stress Results on Ø14 mm Longitudinal and Tangential Model, σ_z , 0.1 mm Feed for All Force Parameters

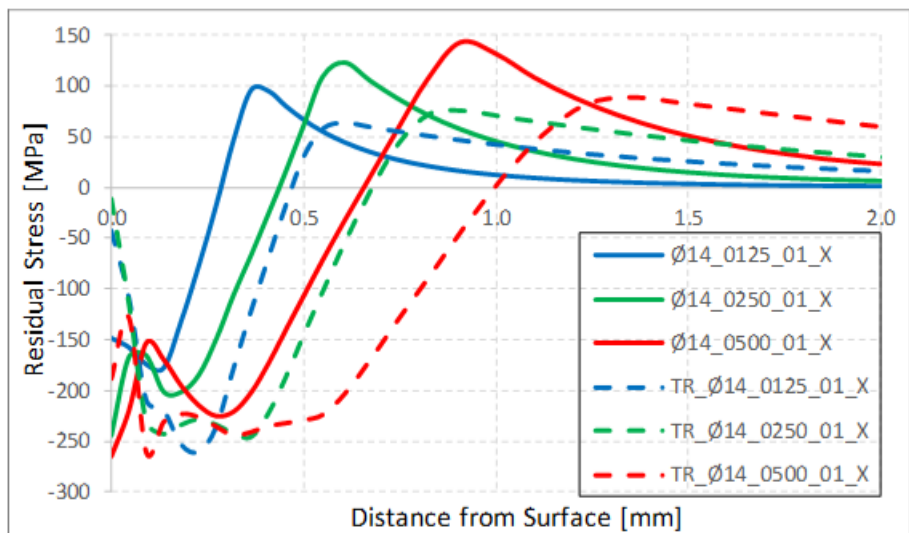


Figure 61 Residual Stress Results on Ø14 mm Longitudinal and Tangential Model, σ_x , 0.1 mm Feed for All Force Parameters

On the two graphs above (Fig. 60, 61); 14 mm diameter longitudinal rolling and 14 mm diameter tangential rolling residuals stress results were compared for the same feed parameters. 125 N, 250 N and 500 N results showed that residual stress magnitudes for tangential rolling were a little bit higher than longitudinal rolling results on the same depth for both direction of compressive residual stresses. But the stress level difference was much higher for σ_x results than σ_z stress results.

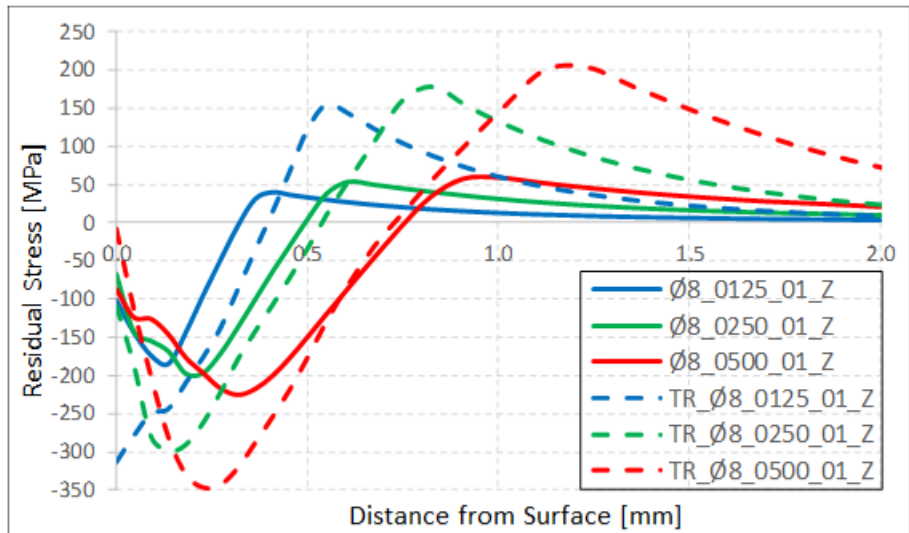


Figure 62 Residual Stress Results on Ø8 mm Longitudinal and Tangential Model, σ_z , 0.1 mm Feed for All Force Parameters

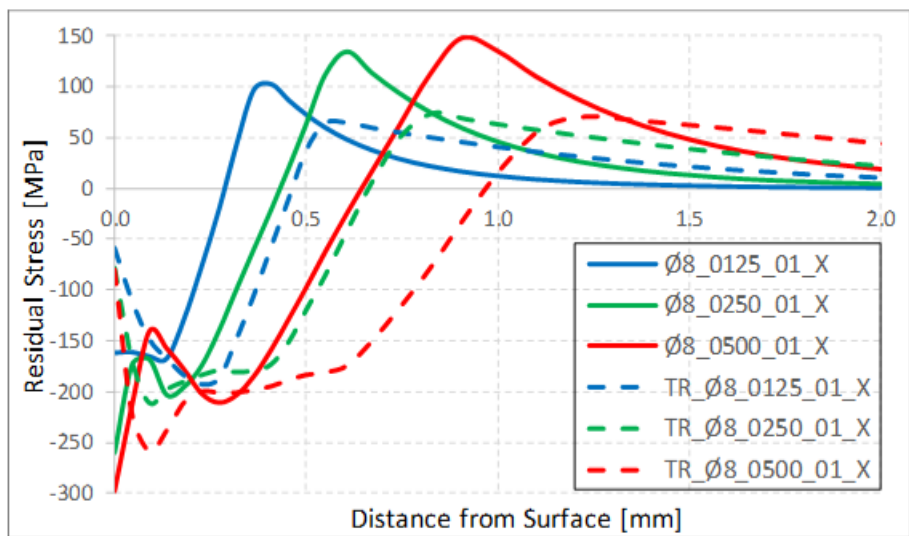


Figure 63 Residual Stress Results on Ø8 mm Longitudinal and Tangential Model, σ_x , 0.1 mm Feed for All Force Parameters

On the two graphs above (Fig. 62, 63); 8 mm diameter longitudinal rolling and 8 mm diameter tangential rolling residuals stress results were compared for the same feed parameters. 125 N, 250 N and 500 N results showed that residual stress magnitudes for tangential rolling were a little bit higher than for longitudinal rolling results on the same depth for both direction of compressive residual stresses. Results showed the same trend with 14 mm diameter model geometry results. Also, for tangential rolling, 14 mm diameter

model and 8 mm diameter residual stress results were very close to each other for both stress direction.

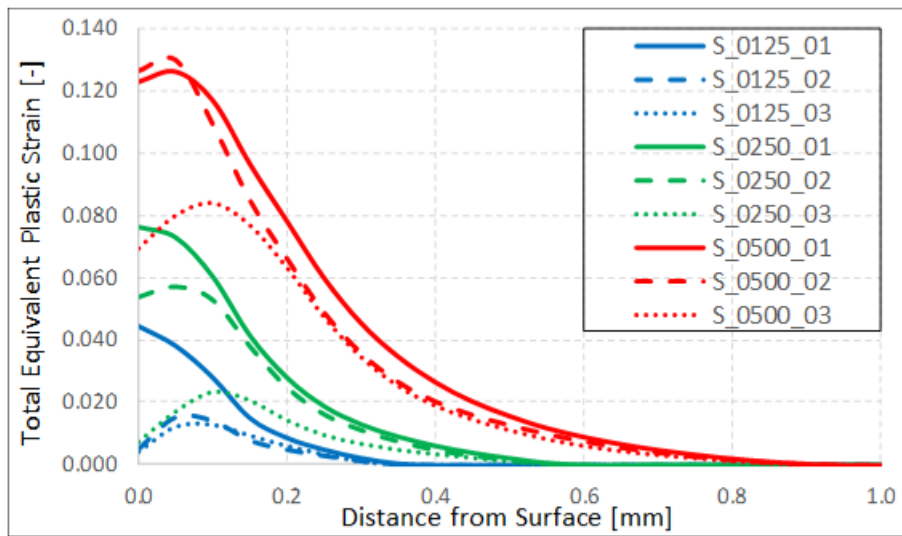


Figure 64 Total Equivalent Plastic Strain Results on Square Model for All Feed and Force Parameters

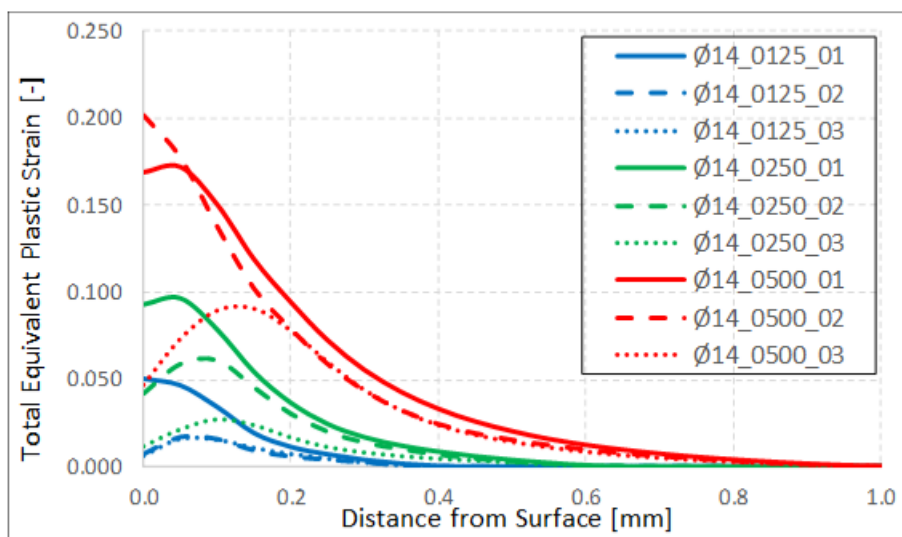


Figure 65 Total Equivalent Plastic Strain Results on Ø14 mm Model for All Feed and Force Parameters

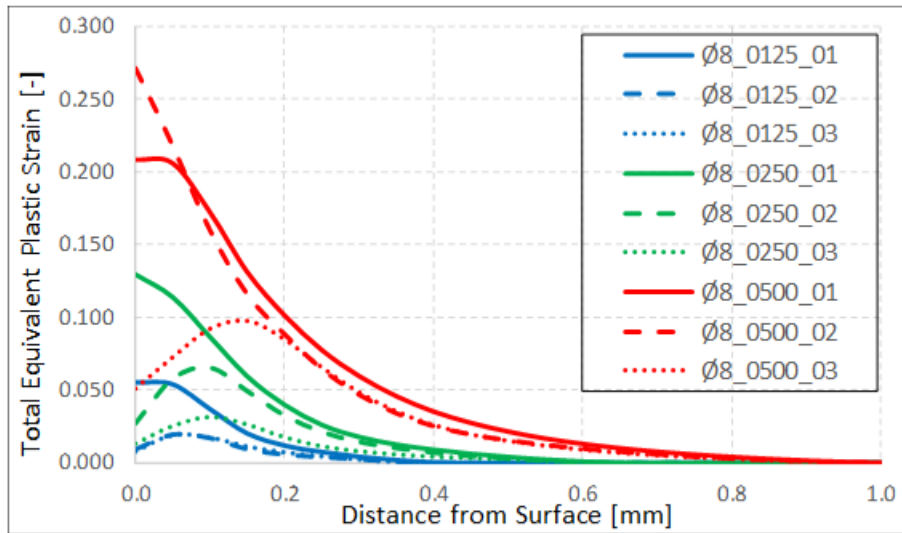


Figure 66 Total Equivalent Plastic Strain Results on Ø8 mm Model for All Feed and Force Parameters

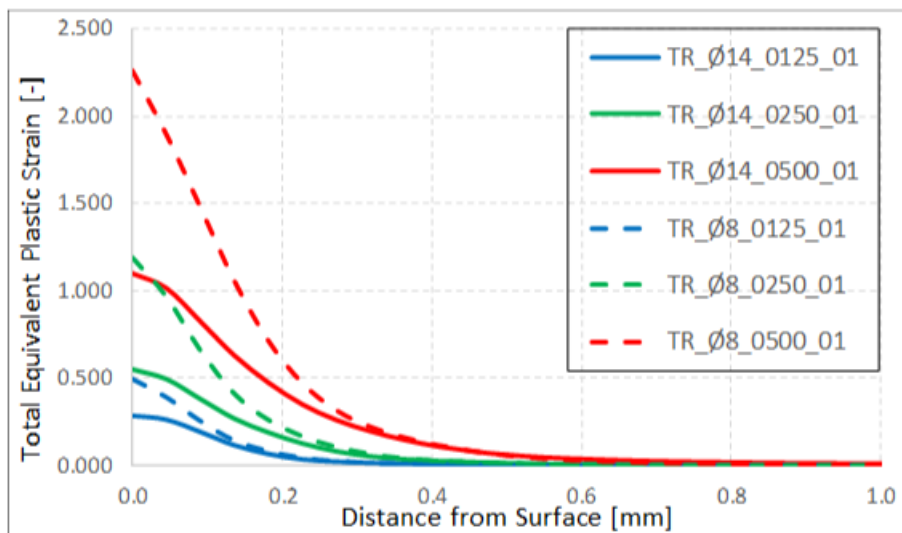


Figure 67 Total Equivalent Plastic Strain Results on Ø8 mm and Ø14 mm Model for 0.1mm Feed and Force Parameters

All geometry total equivalent plastic strain results were plotted on the above graphs (Fig. 64, 65, 66, 67). The smallest strain values were on the square model, the biggest plastic strain values were on the 8 mm diameter longitudinal rolling models. Through the depth, all the total equivalent plastic strain values approached to zero, which was expected.

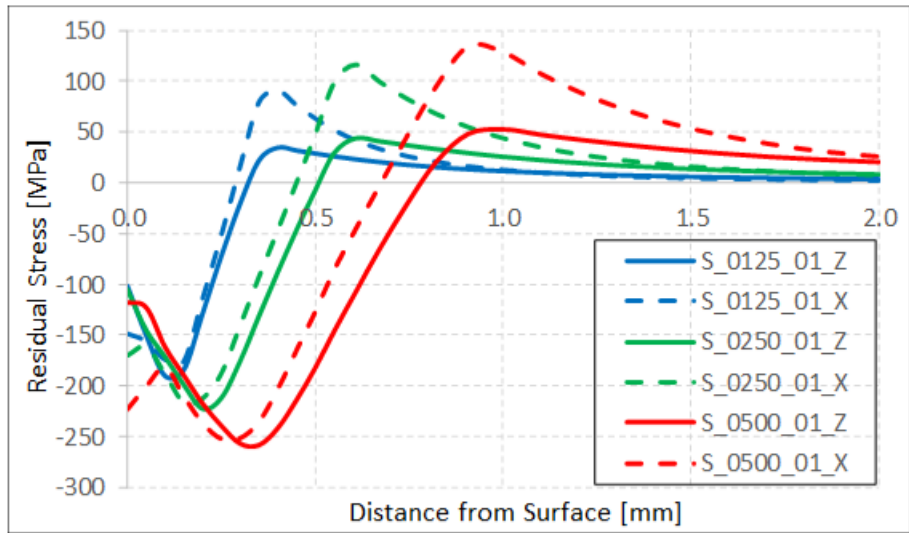


Figure 68 Square Model, 125 N, 250 N, 500 N, 0.1 mm Feed Parameter, σ_z , σ_x

On the graph above (Fig. 68); the results were taken from symmetry axis from surface to 2 mm depth and at the end of the 5th rolling operation for square model at 0.1 mm feed parameter. All the force parameters were applied to the model. As can see from the graph label, blue lines show 125 N, green lines show 250 N, red lines show 500 N applications. Straight lines show σ_z , dashed lines show σ_x results. As can be seen from the graph, all results started with compressive residual stress and made peaks in the depth range of 0-0.5 mm and turned into tensile residual stresses and made peaks again at different depths. σ_z and σ_x results followed each other in trend. It was also obvious that the more force was applied, the more residual stress results obtained. For tensile residual stresses, 125 N results made peak at 0.4 mm, 250 N results made peak at 0.6 mm and 500 N results made peak at 0.9 mm depth. At depth 2 mm, all the residual stress values converge through zero.

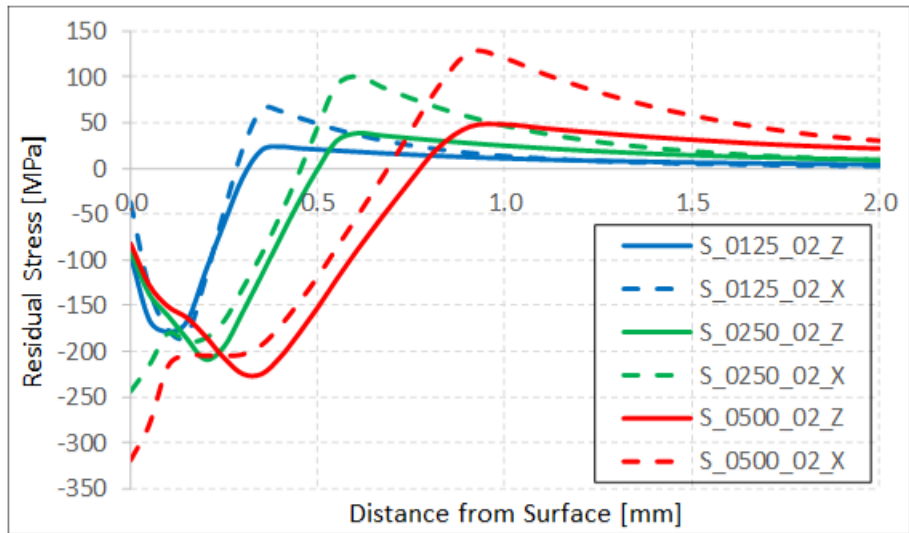


Figure 69 Square Model, 125 N, 250 N, 500 N, 0.2 mm Feed Parameter, σ_z , σ_x

On the graph above (Fig. 69); 0.2 mm feed results were analyzed. These results were similar with 0.1 mm feed parameter. Initial compressive residual stress magnitudes were higher except 125 N results. Their peak depths were unchanged for both stress directions, but peak stresses were just a little bit lower.

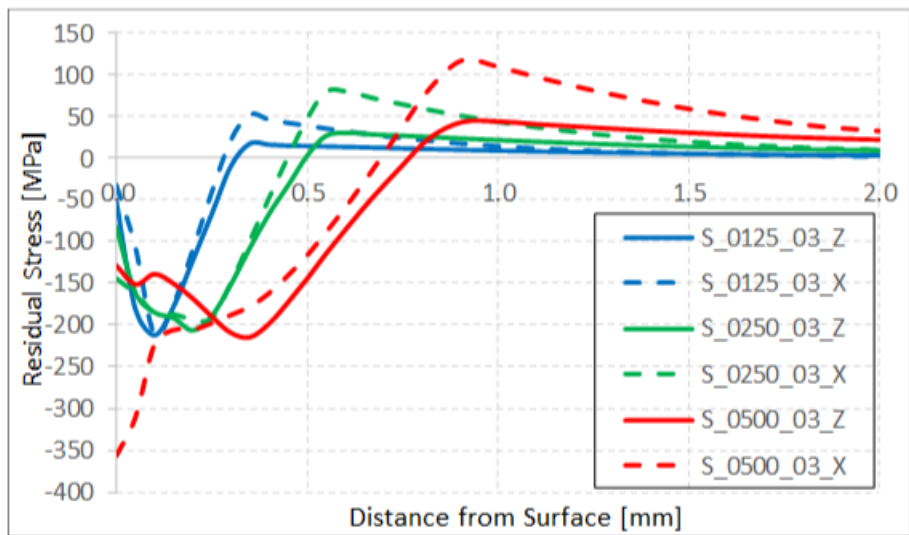


Figure 70 Square Model, 125 N, 250 N, 500 N, 0.3 mm Feed Parameter, σ_z , σ_x

On the graph above (Fig. 70); 0.3 mm feed results were analyzed. These results were similar with 0.2 mm feed parameter. Initial compressive residual stresses were higher except 125 N results. Tensile compressive stresses highly decreased compared to other feed parameters. σ_x compressive residual stresses were the highest for 500 N at the surface of material.

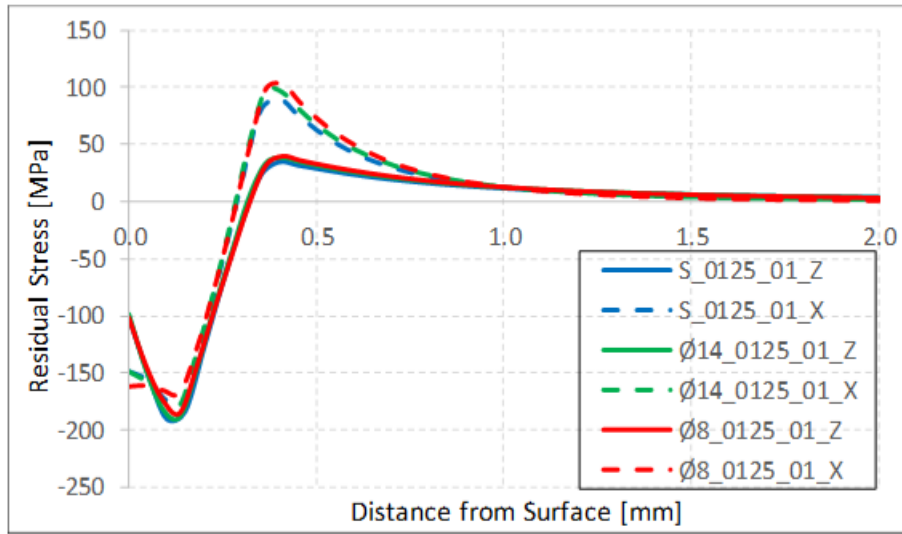


Figure 71 Square, Ø14 mm, Ø8 mm Model, 125 N, 0.1 mm Feed Parameter, σ_z , σ_x

This graph (Fig. 71) was created to show geometry change effect on residual stresses for the same load and feed parameters. These results showed that geometry change did not affect the residual stresses and their values were almost the same for 125 N load. They reached 0 MPa at 1.5 mm depth through the depth of 2 mm.

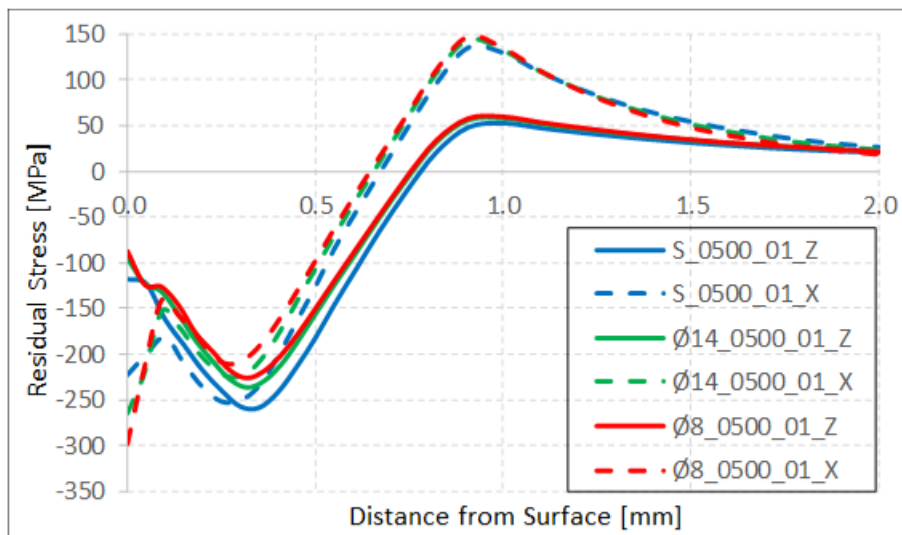


Figure 72 Square, Ø14 mm, Ø8 mm Model, 500 N, 0.1 mm Feed Parameter, σ_z , σ_x

On the graph above (Fig. 72), 500 N load were applied for all geometries at 0.1 mm feed. These results showed that due to force increase, depth and magnitude of residual stresses increased. σ_z magnitudes did not change much but σ_x magnitudes increased at the surface.

It was obvious that the effect of geometry change on the residual stress magnitudes can be negligible.

6. SUMMARY AND OUTLOOK

All the results were taken from the analysis program Marc Mentat. Analyses were done implicitly. Firstly; prismatic geometry, secondly; 14 mm diameter cylindrical and thirdly; 8 mm diameter cylindrical geometry were rolled. 5 rolling operations were applied in the longitudinal direction to the materials starting from left hand to right hand side on x-y plane. 5 rolling operations were applied, because residual stresses reached a saturation level. In all analyses, 0.1 mm, 0.2 mm and 0.3 mm feed parameters were used.

It was desired that; a saturation level should be obtained for each feed parameters. This saturation of residual stresses was investigated for 0.2 mm feed parameter. Total rolling operation on the material was 10 mm for each roller, and roller speed was 10 mm/s. 10 mm rolling was applied in order to reduce calculation time. 10 mm/s speed was used in order to let residual stresses occurs properly on the surface of the material. Total feed length was 0.4 mm for 0.1 mm feed parameter, 0.8 mm for 0.2 feed parameter and 1.2 mm for 0.3 mm feed parameter. For all feed parameters; 125 N, 250 N and 500 N force parameters were used. So, for one geometry, 9 analyses were run. In addition to that, deep rolling application area was fine meshed and minimum 0.25 mm mesh size was used according to convergence analyses. Although the number of elements in the analyses model were decreased, i.e. geometry was simplified, one analysis had taken 3-4 days to finish in a laptop computer. When they were run on work station, the analyses had taken 2-3 days to finish. Run time of 8 mm diameter cylindrical geometry model was the shortest, prismatic geometry was moderate and the 14 mm diameter cylindrical geometry was the longest according to their number of elements. Their run time was a little bit higher but in order to investigate residual stresses in the rolling direction and transverse direction, analyses should be 3-dimensional. For accuracy of the results and to prevent the penetration of mesh elements, quadratic elements were used. Also, tangential rolling was applied to the cylindrical geometries which was another conventional rolling operation. These geometries were also simplified. Only one feed parameter 0.1 mm was used. Residual stress results were taken from 4 mm width and 1 mm depth in the middle section on x-y plane. Because saturation was achieved on that section in rolling direction, and the main aim was to

investigate residual stresses in rolling and transverse direction. According to residual stress distribution results, depth of residual stresses was about 1-2 mm.

For prismatic model which is conventional, principles stresses on middle plane was a little bit higher for small force parameters. Feed parameters did not affect the residual stresses very much for low forces. While the force is increasing, depth and magnitude residual stresses increase logically. Also, for cylindrical geometry residual stresses increased compared to prismatic geometry. For 500 N load, compressive residual stresses were higher than the yield point. Transverse direction compressive residual stresses were higher than the longitudinal direction until the depth of 0.2 mm. But after that depth, compressive stresses in longitudinal direction were higher. For all forces, compressive stresses were changing to tensile stresses. Occurrence of compressive residual stresses on prismatic parts and cylindrical parts were almost the same for the same force. Which could mean, the same fatigue life increase may be achieved for industrial parts. In the tangential rolling, rolling direction and longitudinal rolling operation transverse direction correspond to the same direction of stresses. So, if compressive residual stresses were compared within the same diameter cylindrical geometries; tangential rolling compressive residual stresses were higher. The situation was the same for other direction. Total equivalent plastic strain results started from plastic deformation values, greater than 0.002, and approached to zero through the depth of 1 mm. Feed parameters affected the strain results. As the feed and force magnitudes increased, the highest strain results were obtained. These results were also expected. Although the compressive residual stress distribution was as desired for deep rolling area, some tensile residual stress areas occurred.

Consequently; small feed parameters are not recommended since it results high strain hardening with a limited effect residual stresses that are under the yield stress. So, according to results 0.2 mm feed parameter can be used. In addition, a higher magnitude of rolling force is also not recommended. Because high forces increase the depth of residual stresses and high depth of residual stresses are not recommended for fatigue applications.

For further studies, samples of analyzed geometries will be produced, and deep rolling will be applied to that samples. Residual stress measurement will be made by hole drilling method. The process will be validated by fatigue tests, and the increase of service life will be investigated. As a final step, a real industrial part will be deep rolled, and fatigue life increase will be determined. This will prove efficiency of the deep rolling process and lead

to a proof that the deep rolling can be used in the industry very effectively compared to other surface treatment methods.

7. APPENDIX

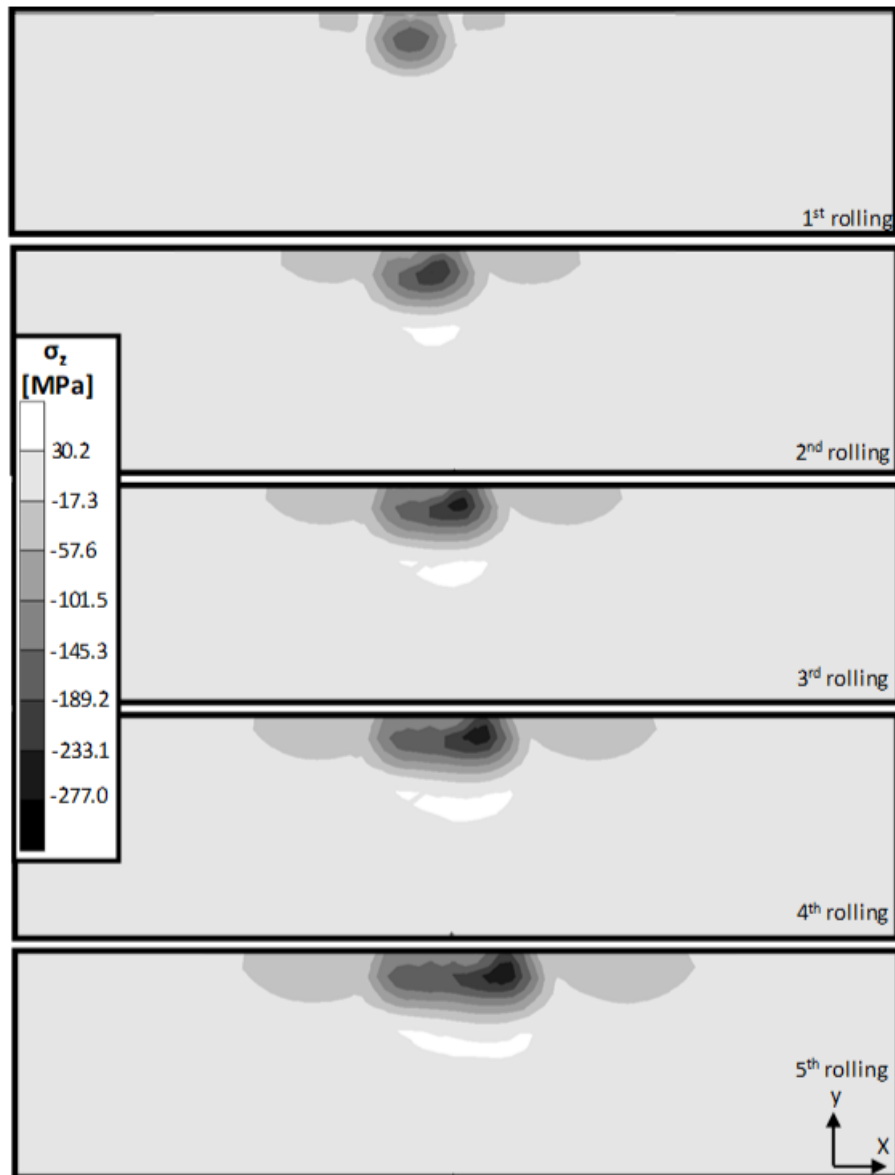


Figure 73 Residual Stress Distribution on Square Model, σ_z , 125 N, 0.1 mm Feed
Parameter

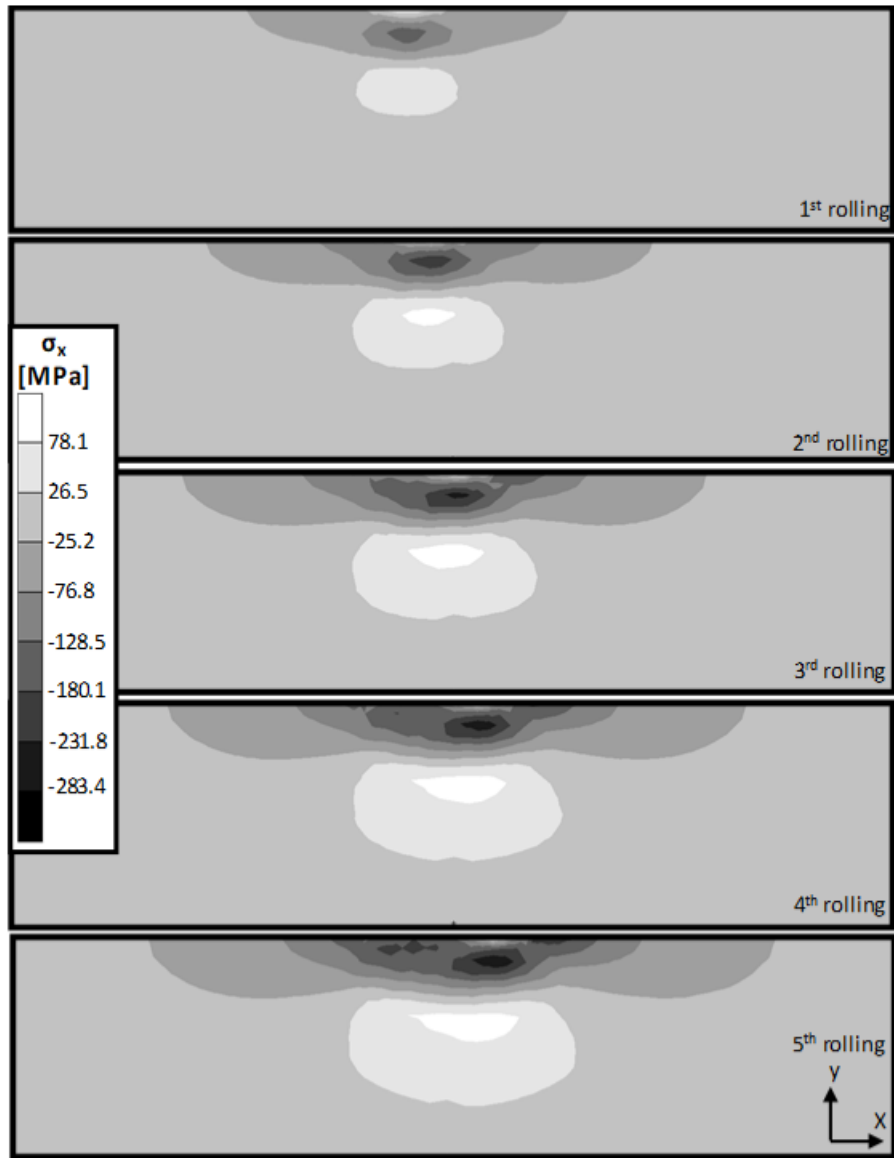


Figure 74 Residual Stress Distribution on Square Model, σ_x , 125 N, 0.1 mm Feed
Parameter

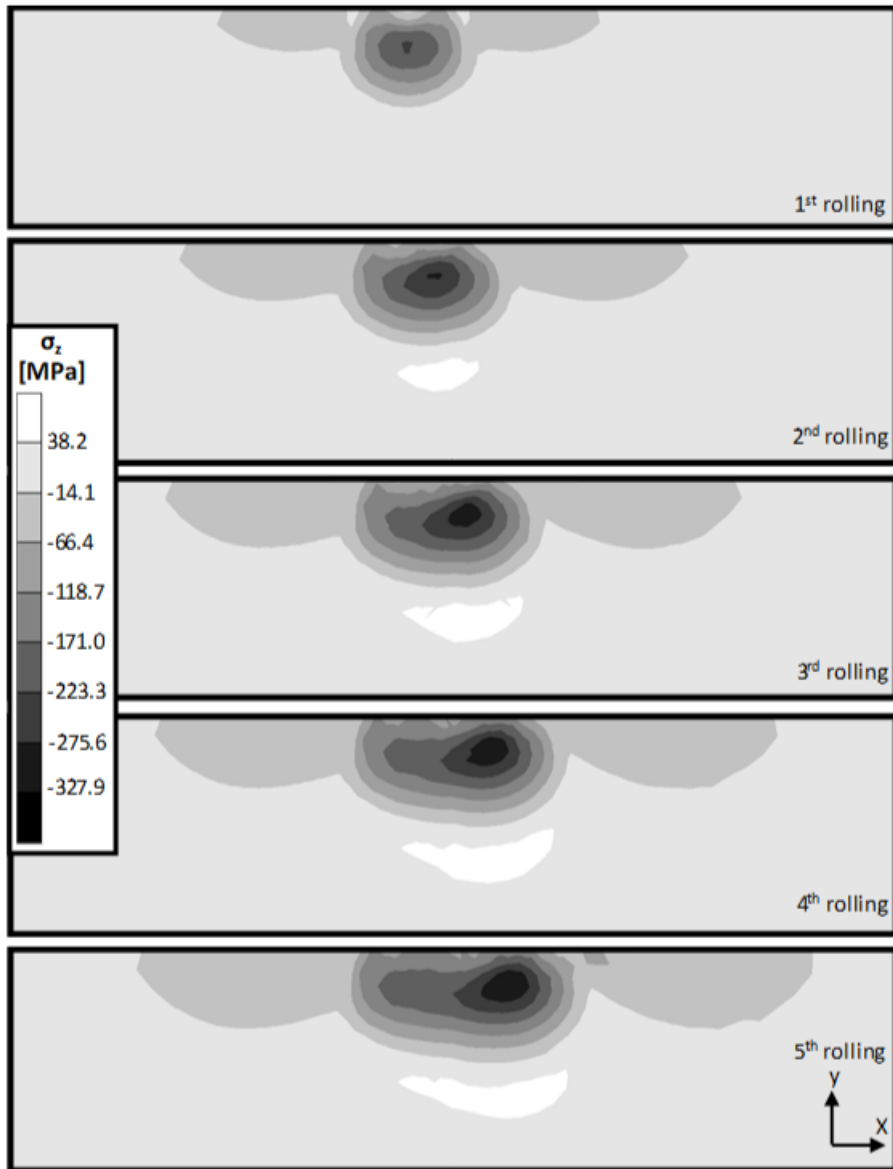


Figure 75 Residual Stress Distribution on Square Model, σ_z , 250 N, 0.1 mm Feed
Parameter

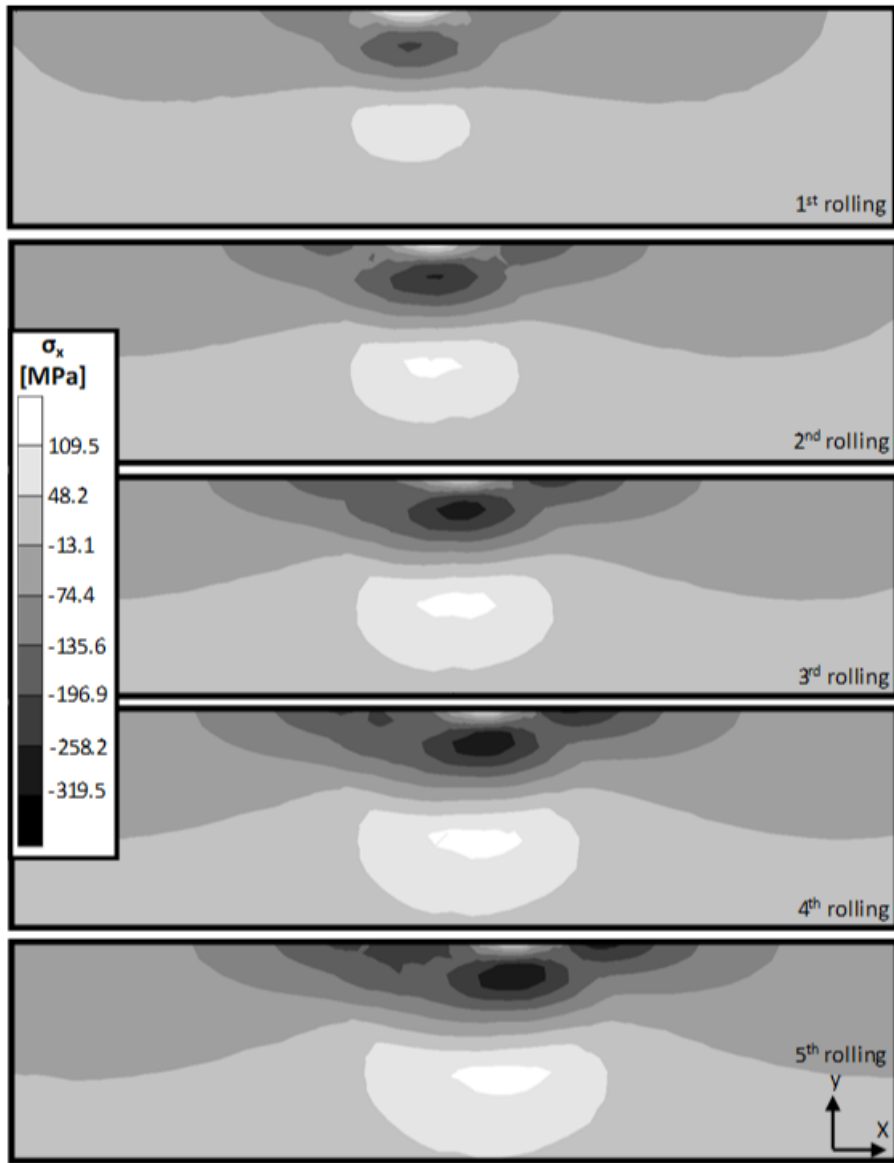


Figure 76 Residual Stress Distribution on Square Model, σ_x , 250 N, 0.1 mm Feed
Parameter

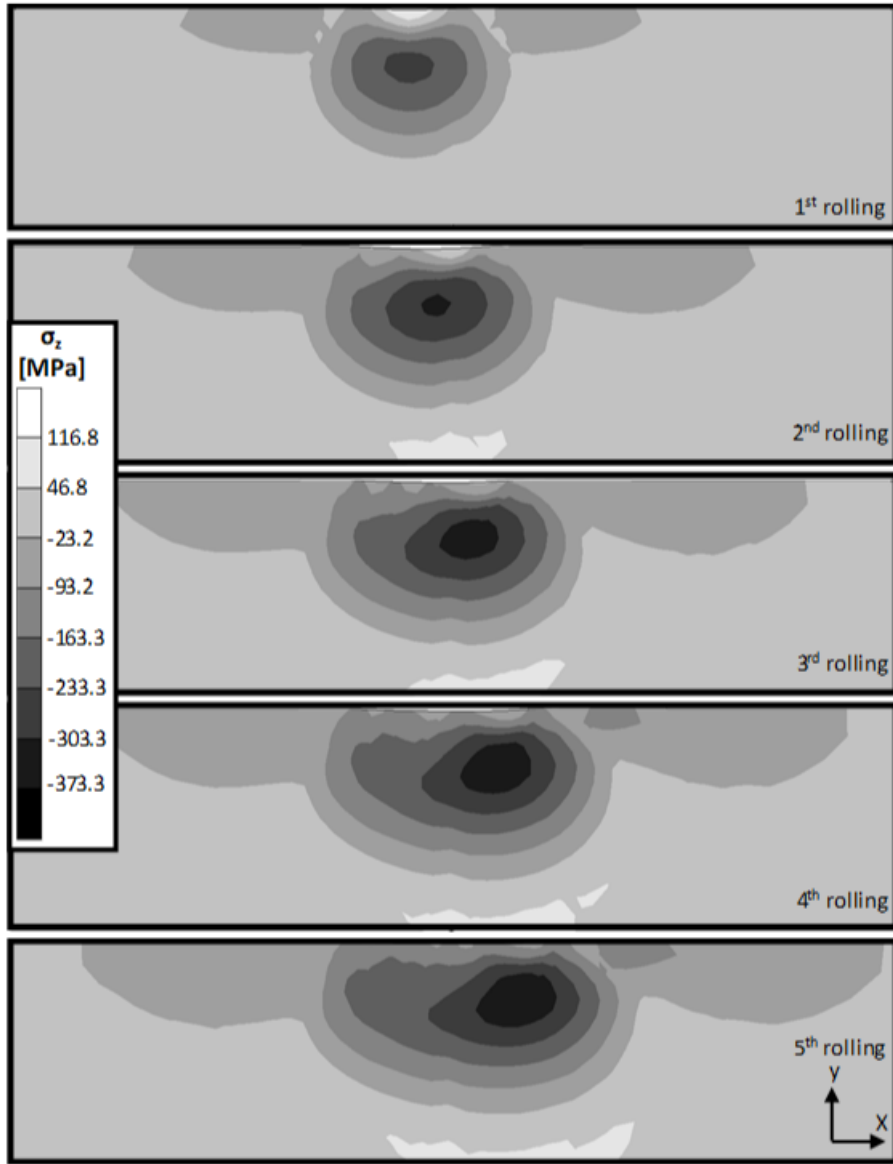


Figure 77 Residual Stress Distribution on Square Model, σ_z , 500 N, 0.1mm Feed Parameter

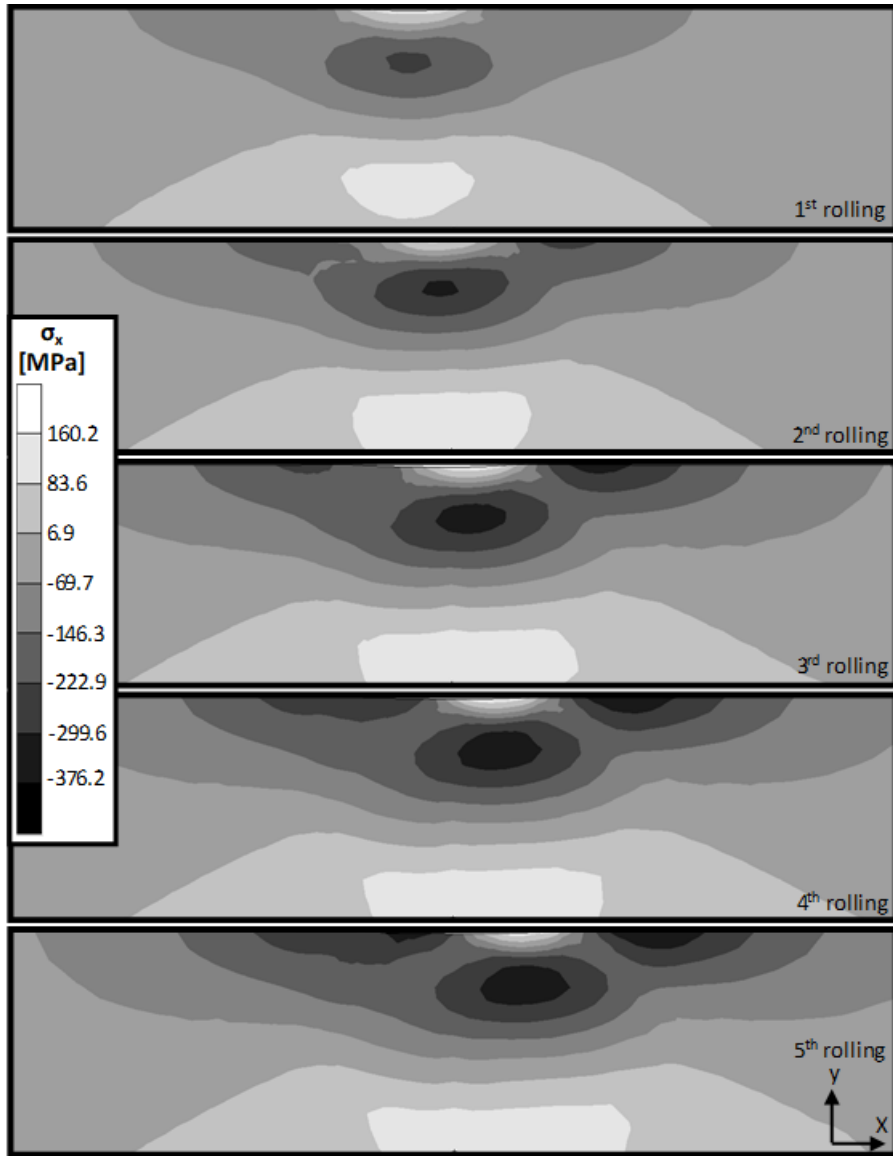


Figure 78 Residual Stress Distribution on Square Model, σ_x , 500 N, 0.1 mm Feed
Parameter

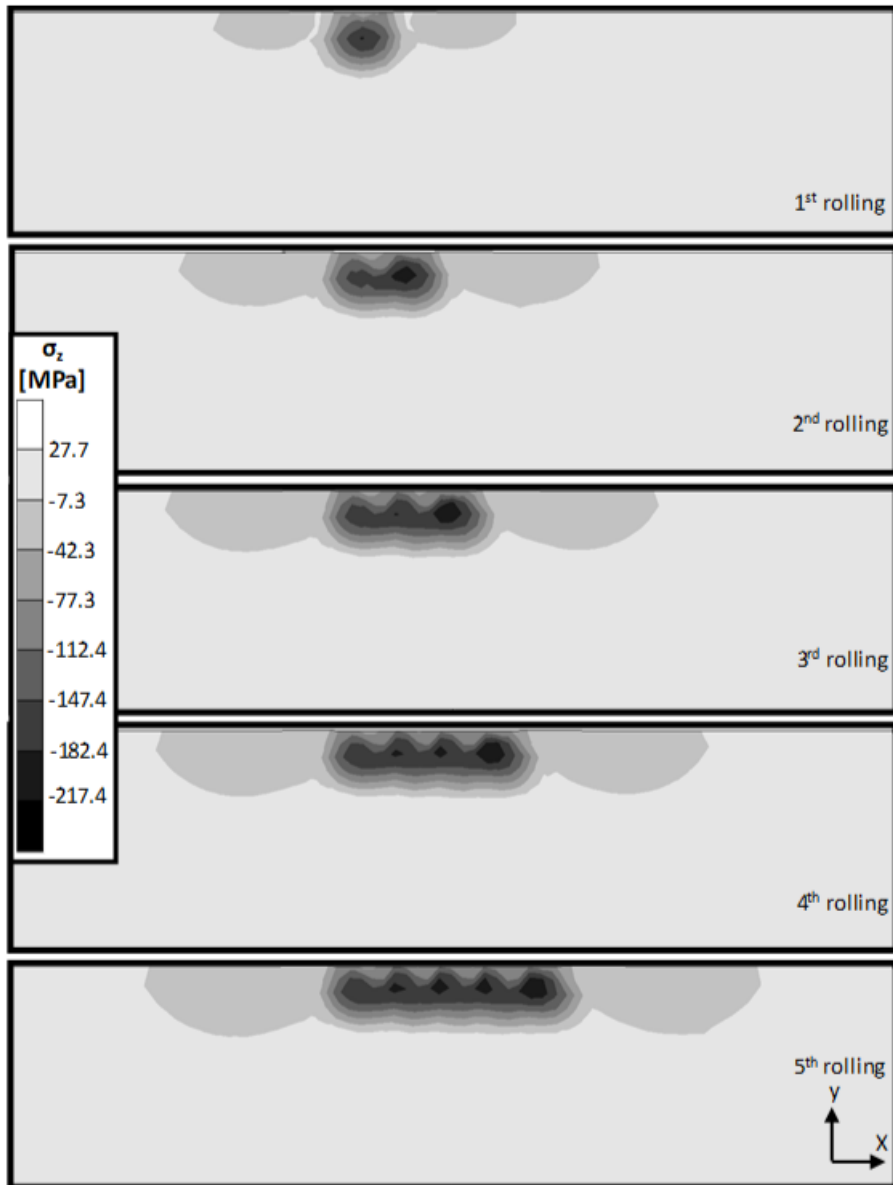


Figure 79 Residual Stress Distribution on Square Model, σ_z , 125 N, 0.2 mm Feed
Parameter

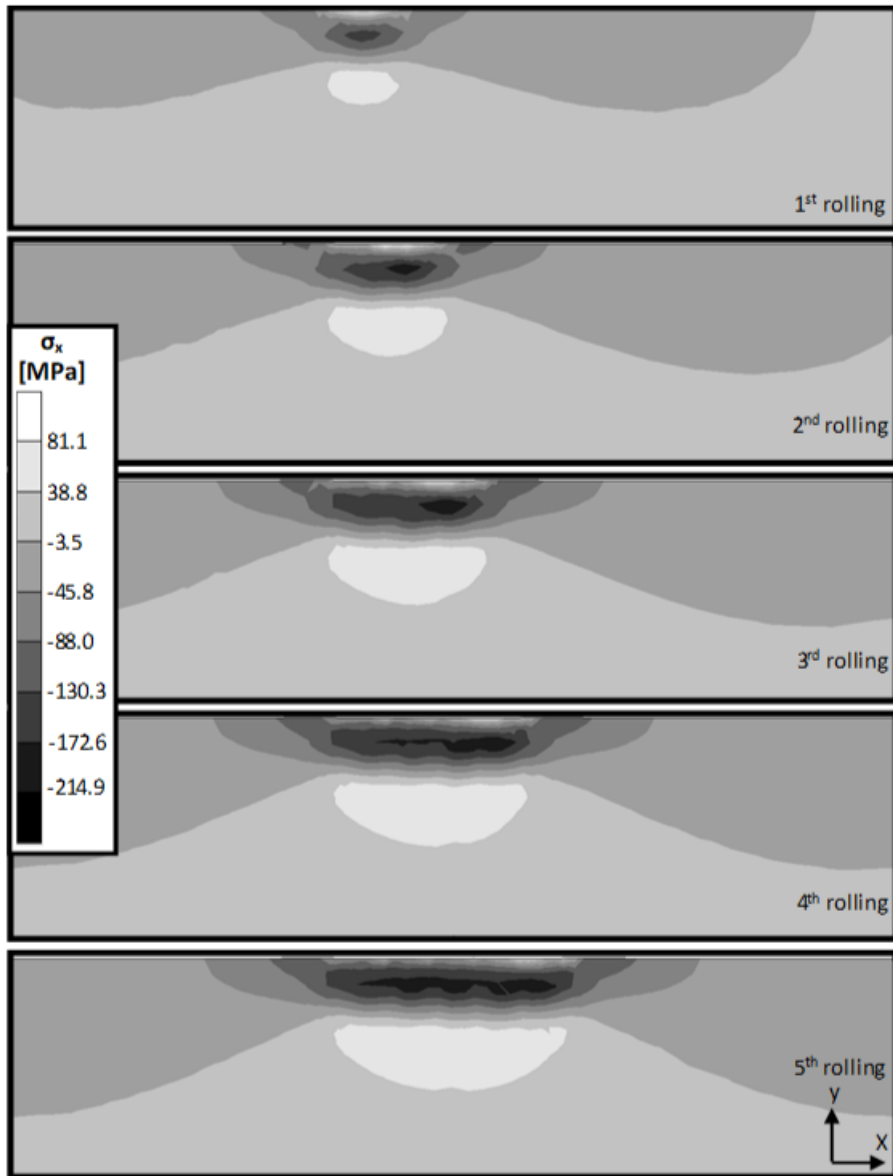


Figure 80 Residual Stress Distribution on Square Model, σ_x , 125 N, 0.2 mm Feed
Parameter

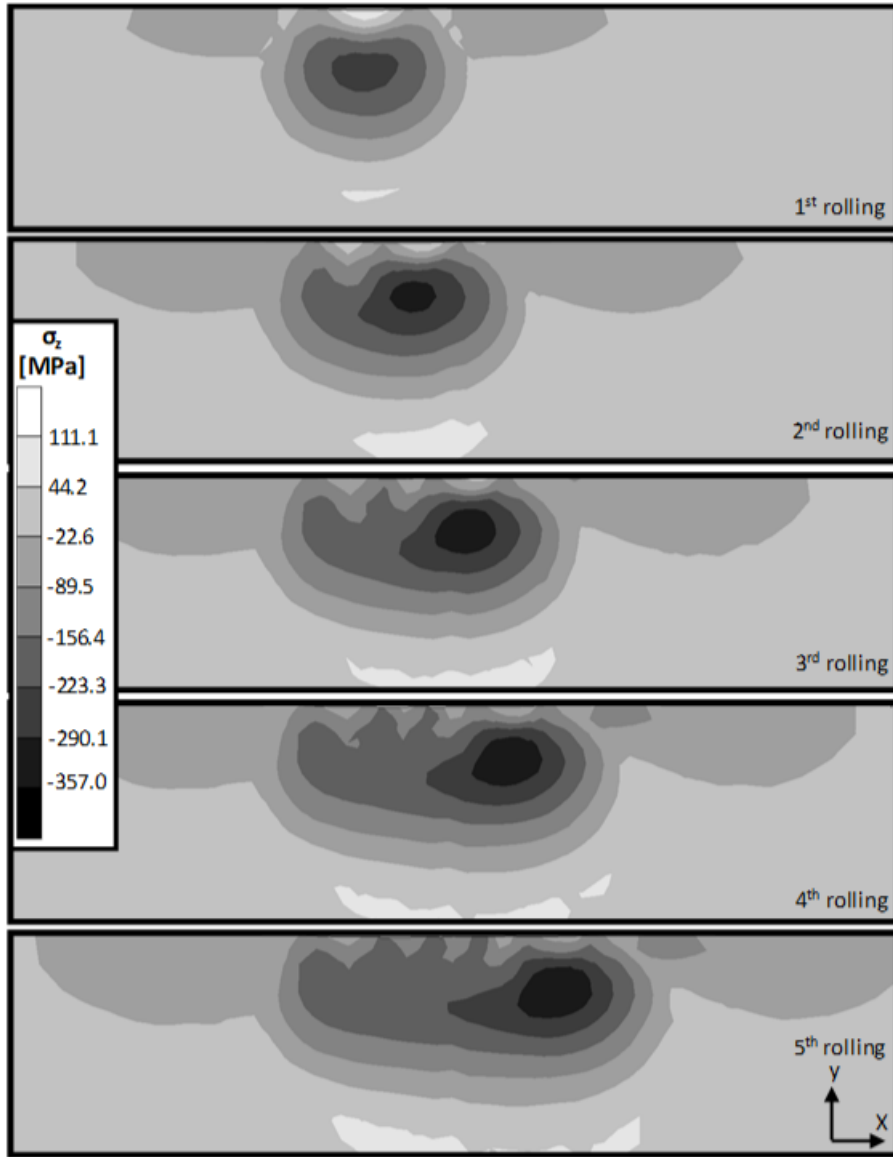


Figure 81 Residual Stress Distribution on Square Model, σ_z , 500 N, 0.2 mm Feed
Parameter

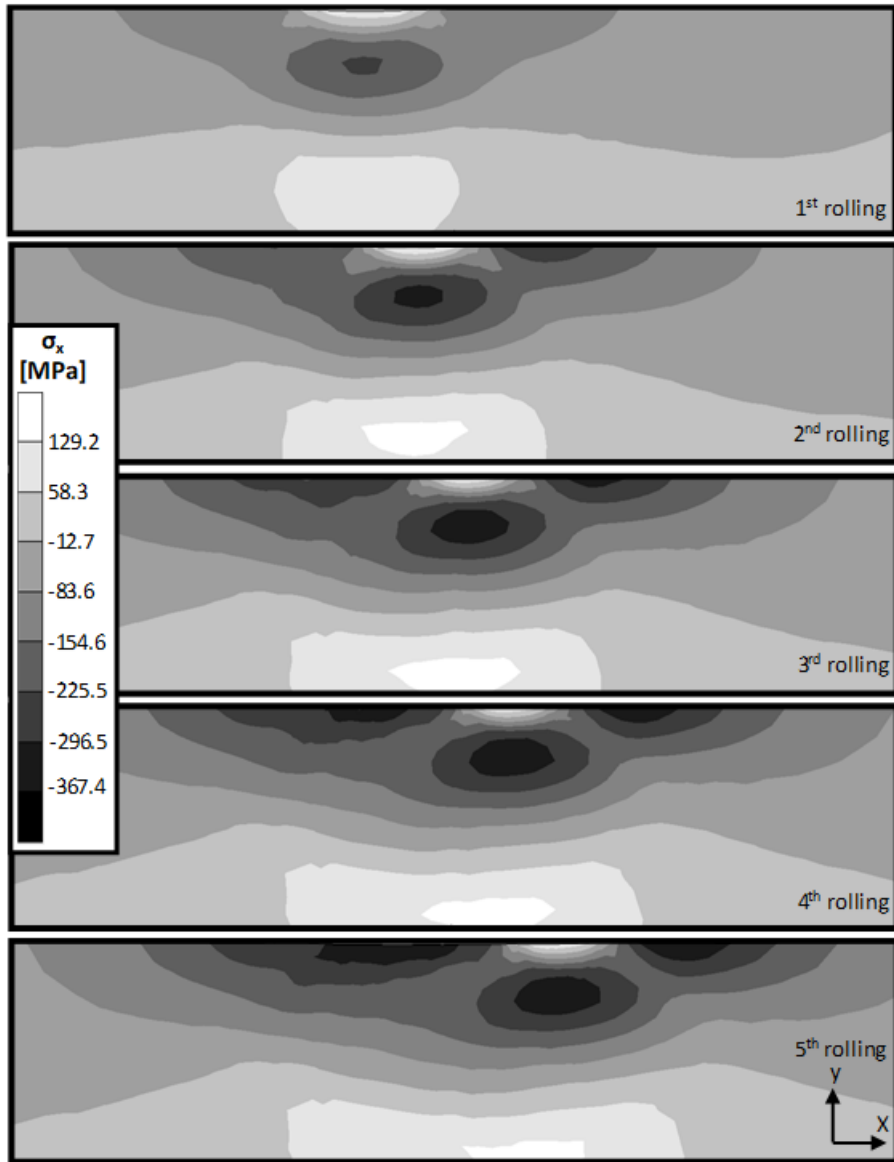


Figure 82 Residual Stress Distribution on Square Model, σ_x , 500 N, 0.2 mm Feed
Parameter

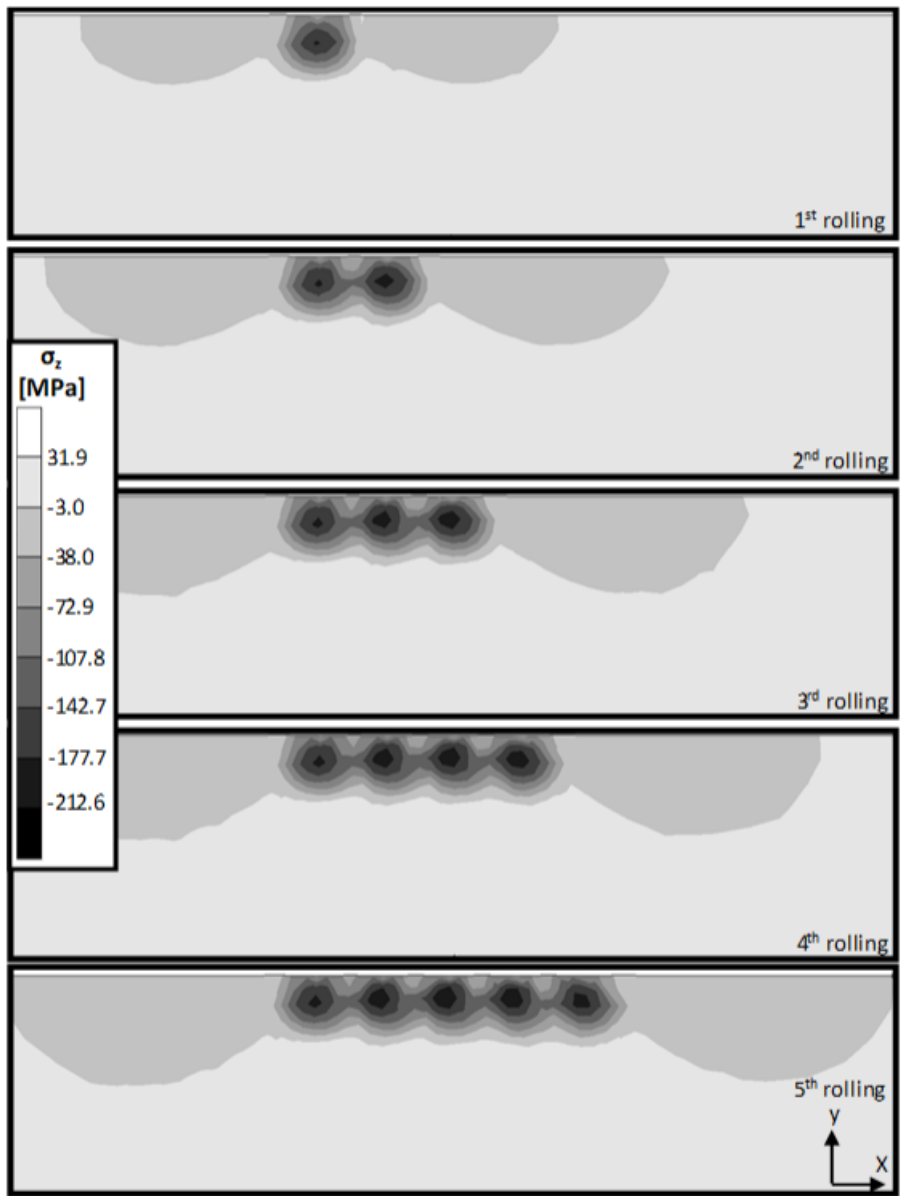


Figure 83 Residual Stress Distribution on Square Model, σ_z , 125 N, 0.3 mm Feed
Parameter

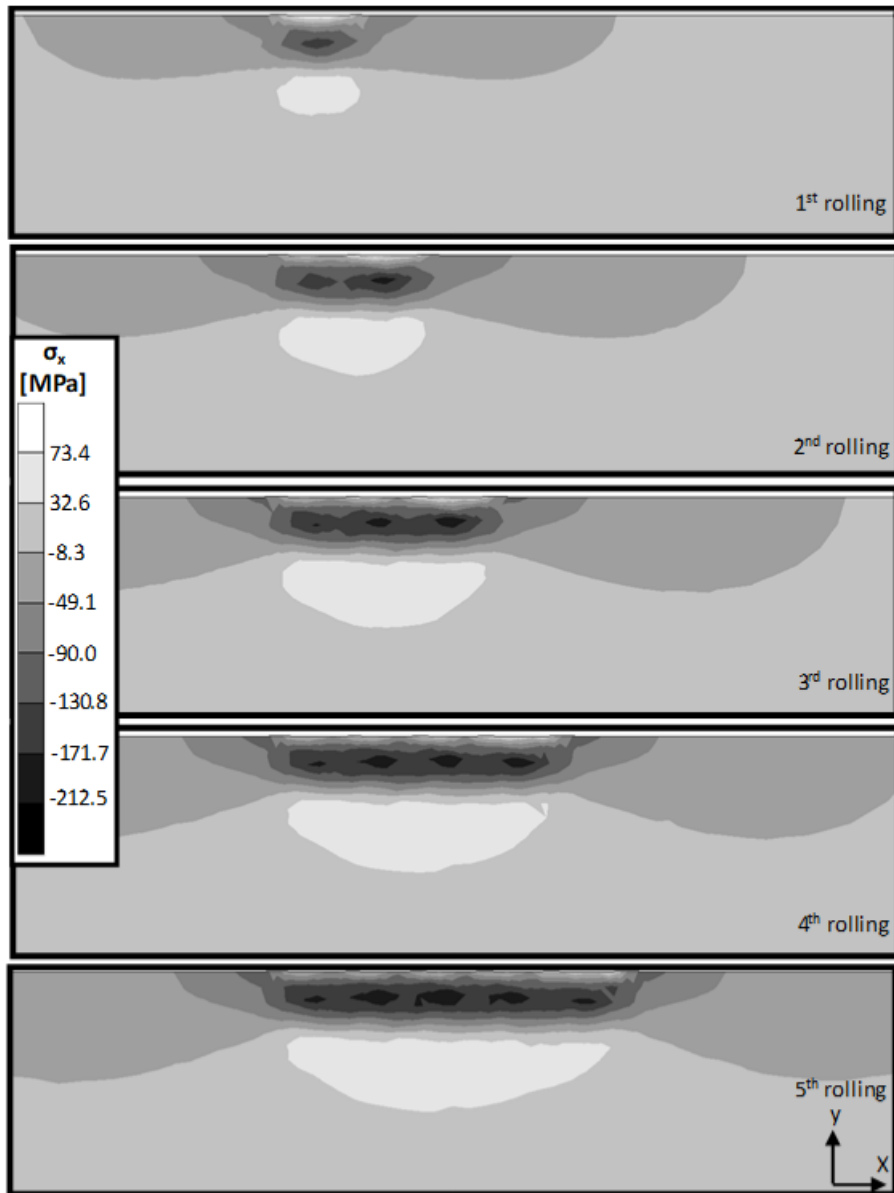


Figure 84 Residual Stress Distribution on Square Model, σ_x , 125 N, 0.3 mm Feed
Parameter

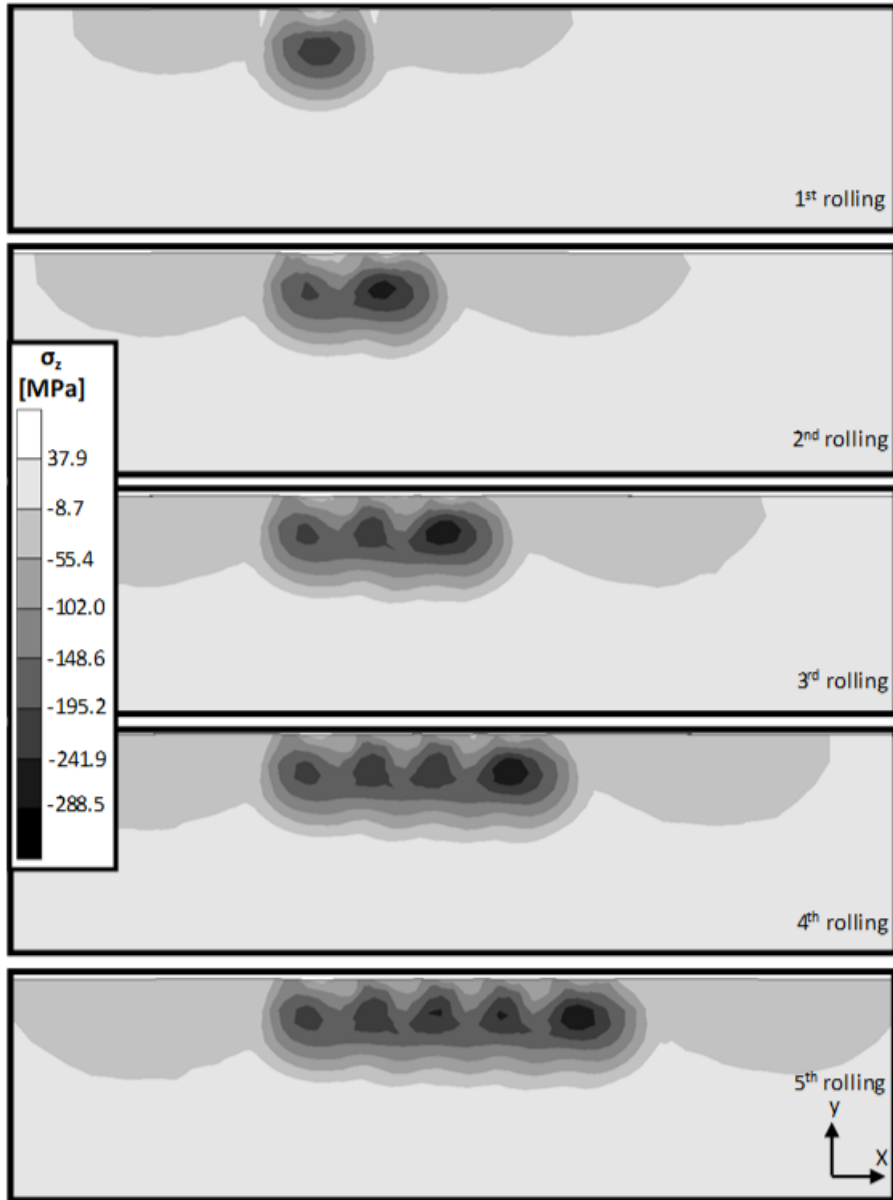


Figure 85 Residual Stress Distribution on Square Model, σ_z , 250 N, 0.3 mm Feed
Parameter

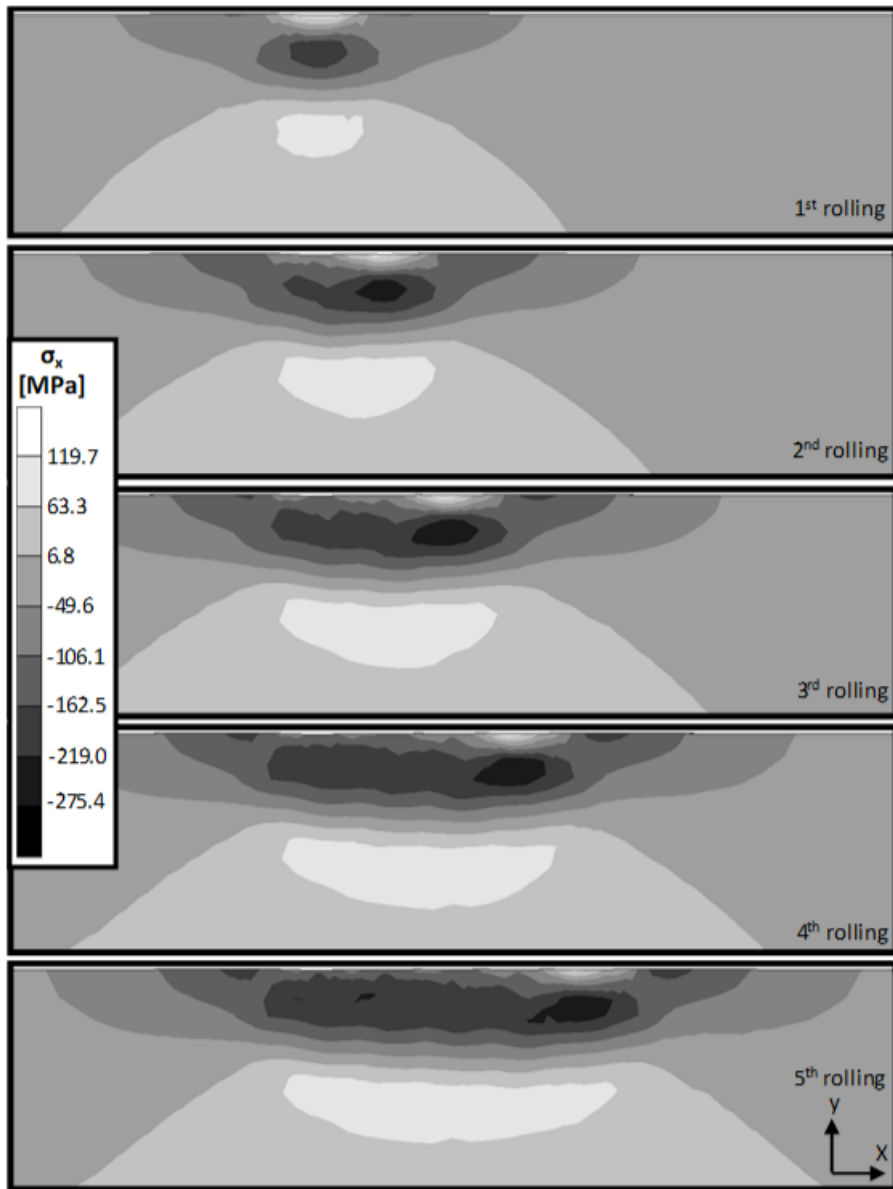


Figure 86 Residual Stress Distribution on Square Model, σ_x , 250 N, 0.3 mm Feed
Parameter

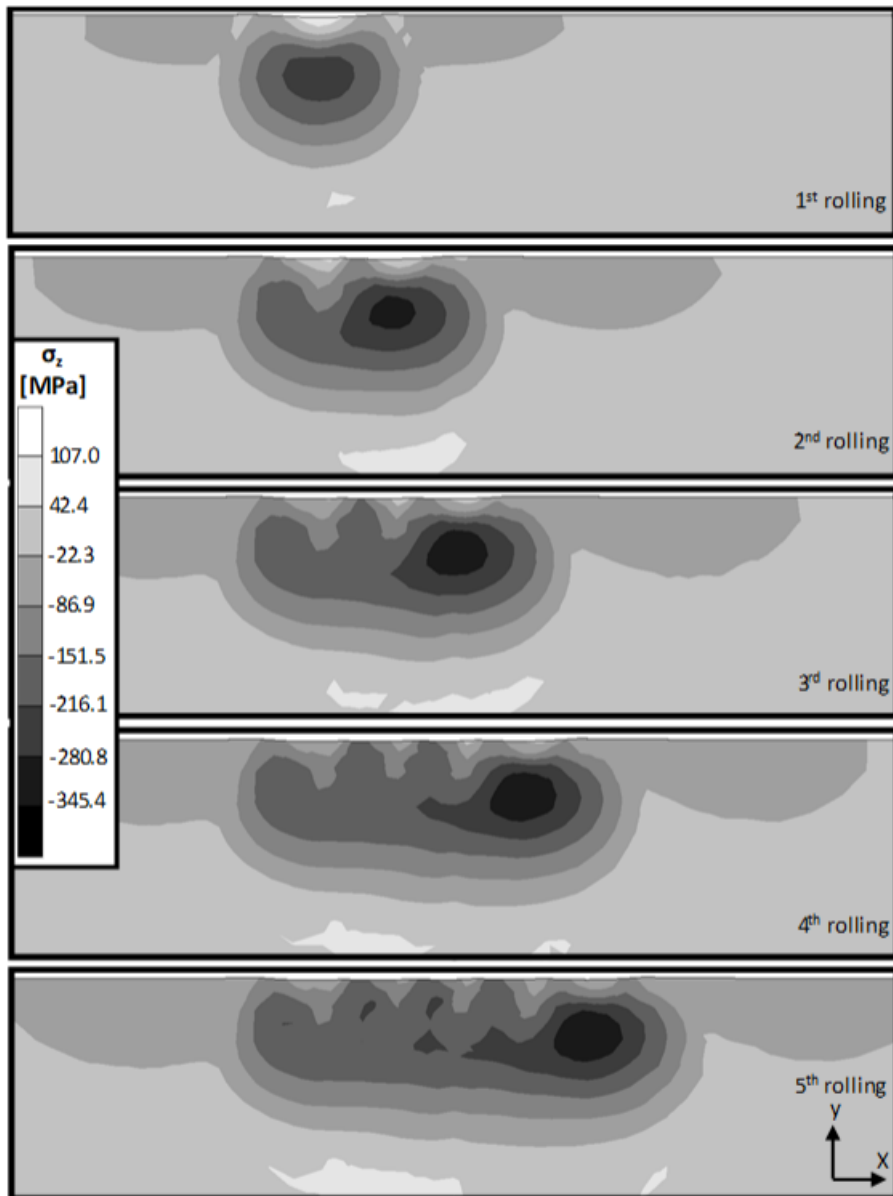


Figure 87 Residual Stress Distribution on Square Model, σ_z , 500 N, 0.3 mm Feed
Parameter

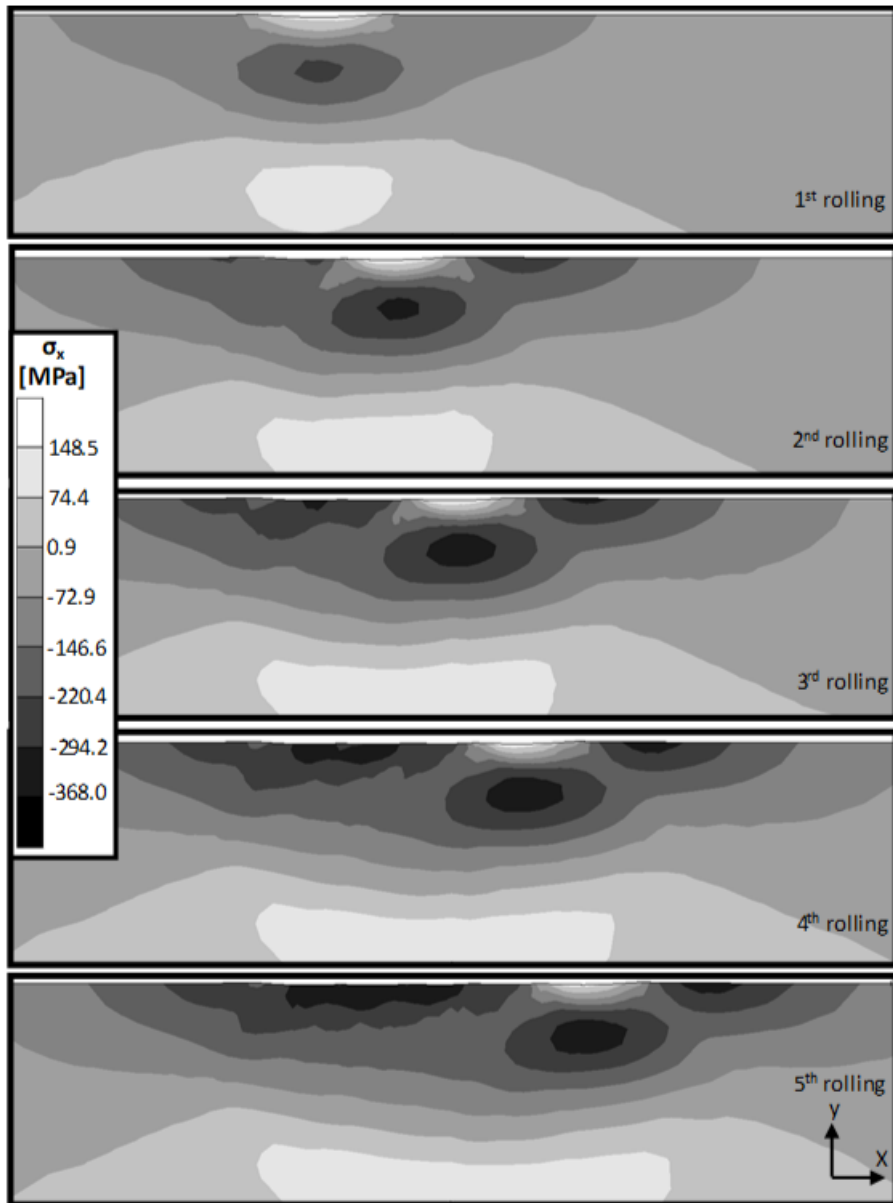


Figure 88 Residual Stress Distribution on Square Model, σ_x , 500 N, 0.3 mm Feed
Parameter

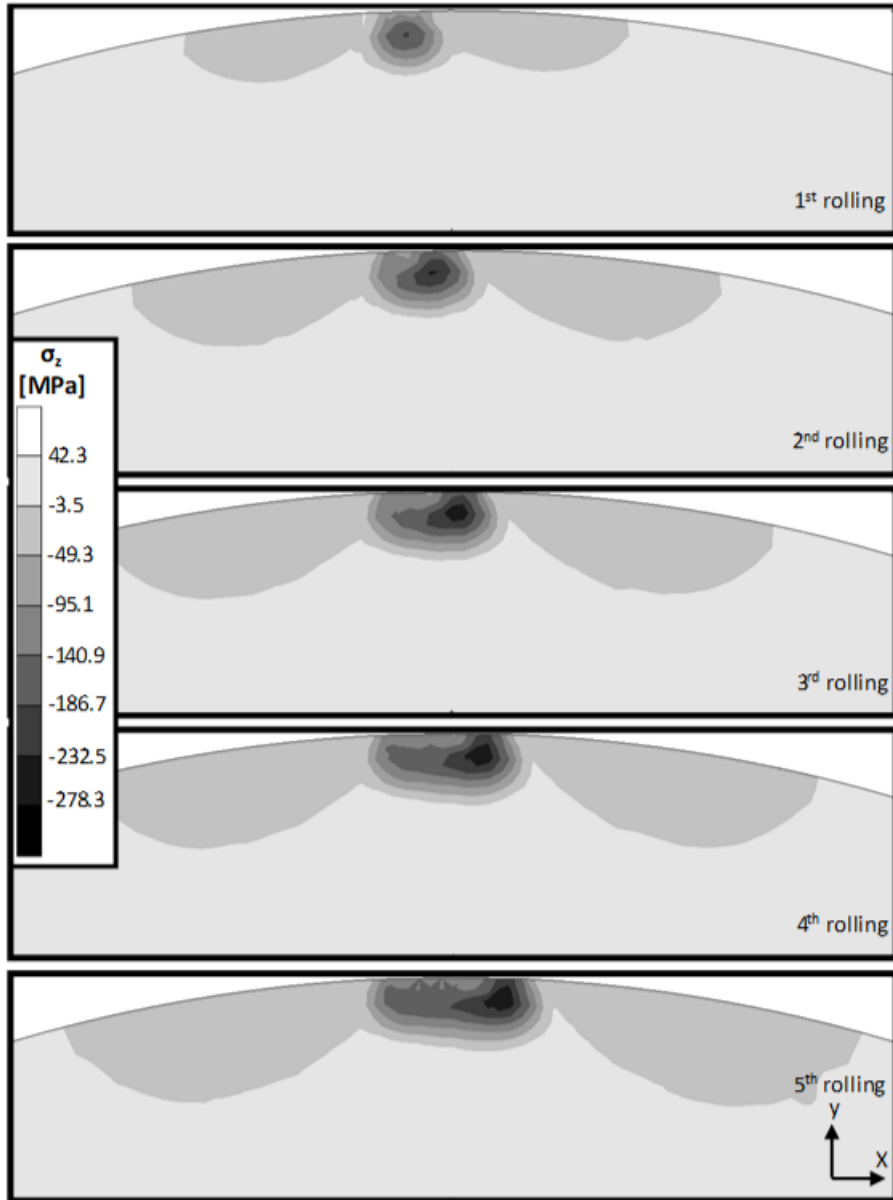


Figure 89 Residual Stress Distribution on $\text{Ø}14$ Model, σ_z , 125 N, 0.1 mm Feed Parameter

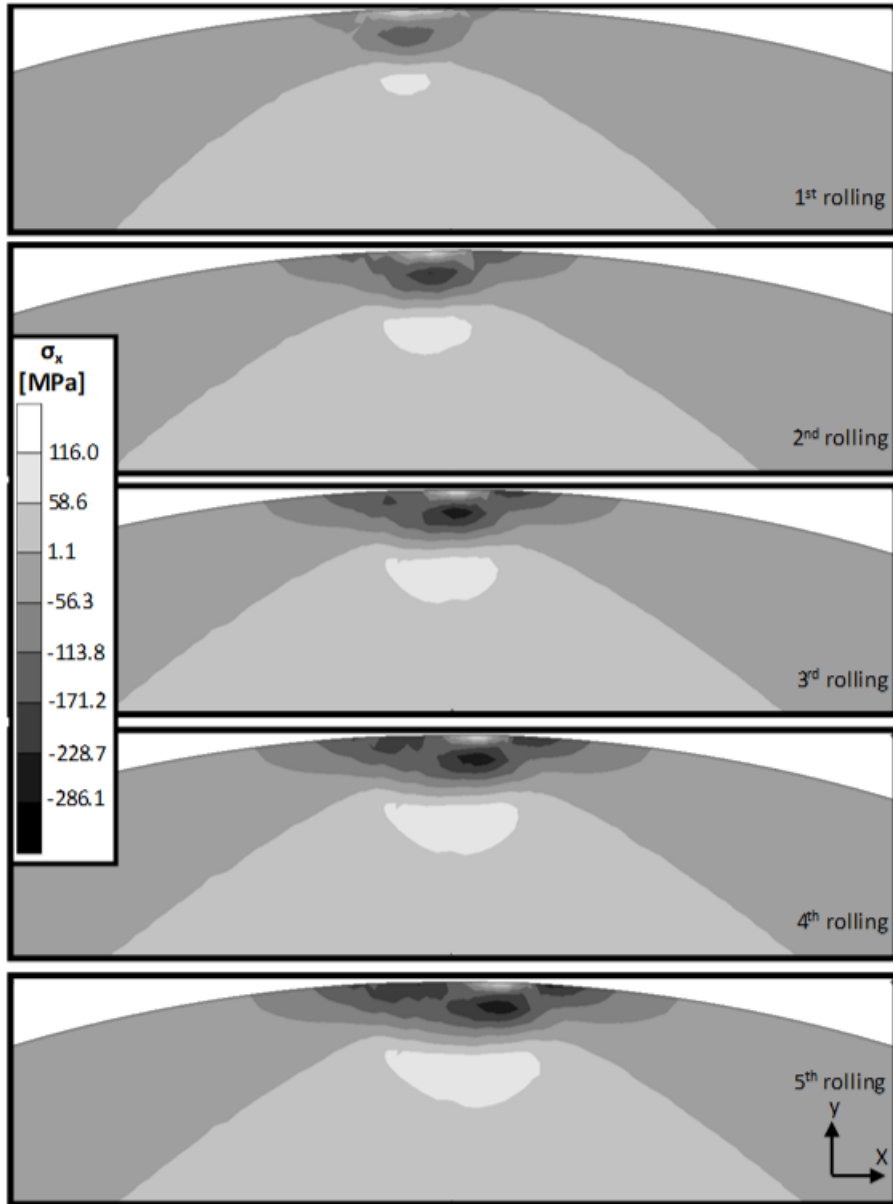


Figure 90 Residual Stress Distribution on $\text{Ø}14$ Model, σ_x , 125 N, 0.1 mm Feed Parameter

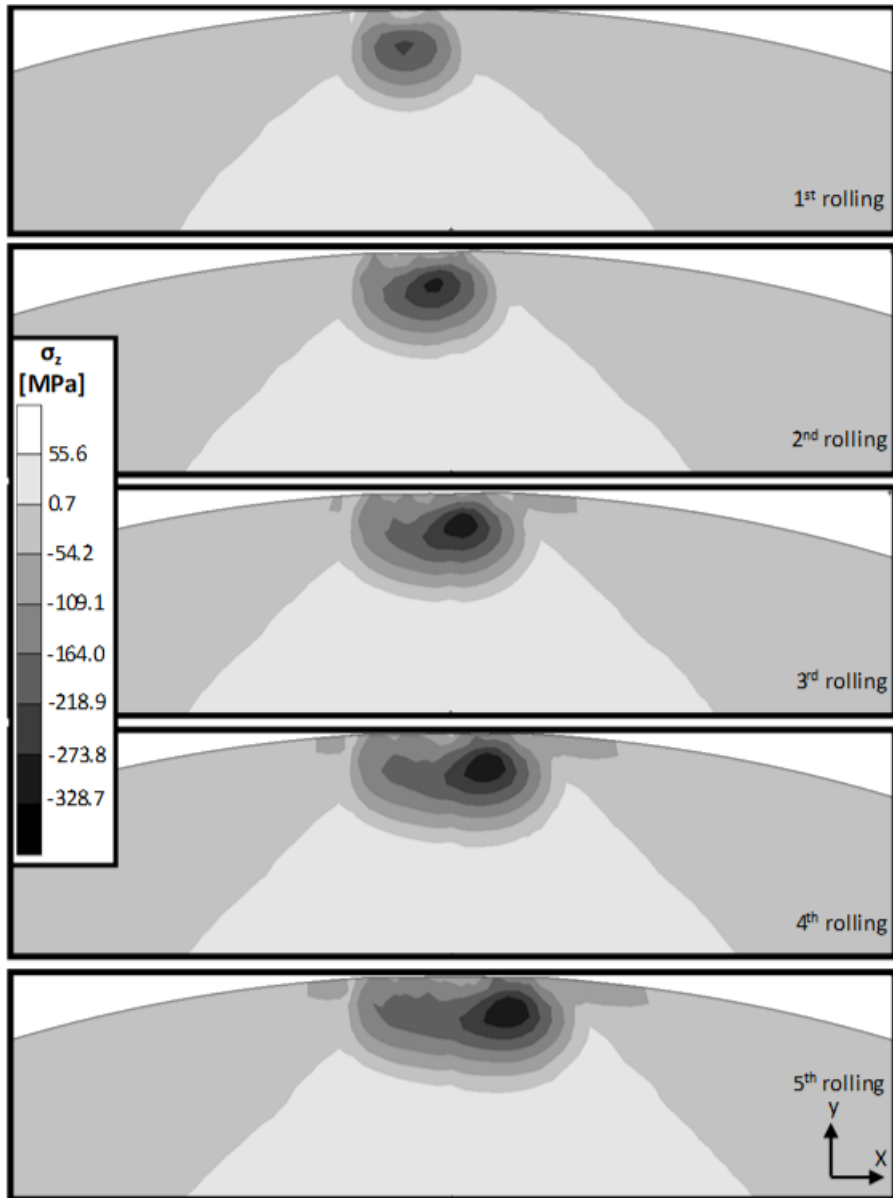


Figure 91 Residual Stress Distribution on $\text{Ø}14$ Model, σ_z , 250 N, 0.1 mm Feed Parameter

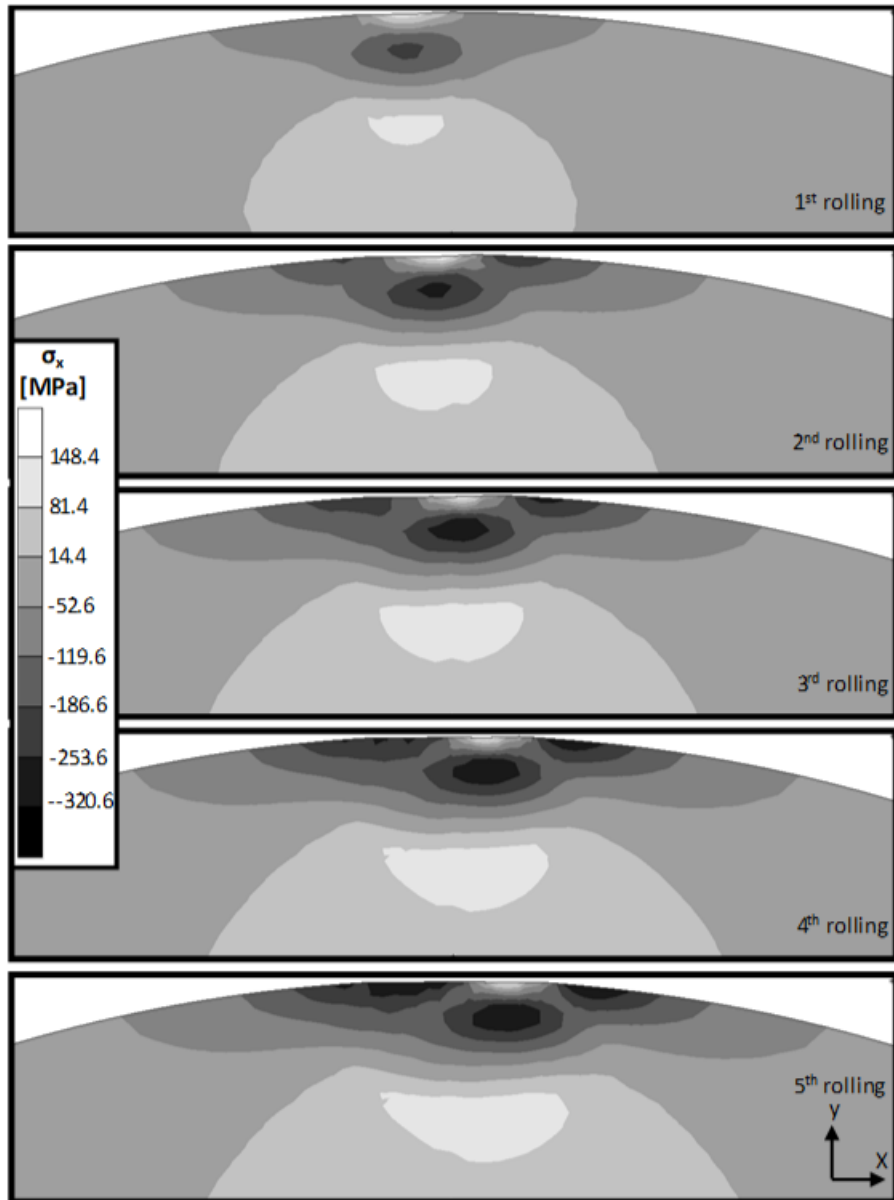


Figure 92 Residual Stress Distribution on $\text{Ø}14$ Model, σ_x , 250 N, 0.1 mm Feed Parameter

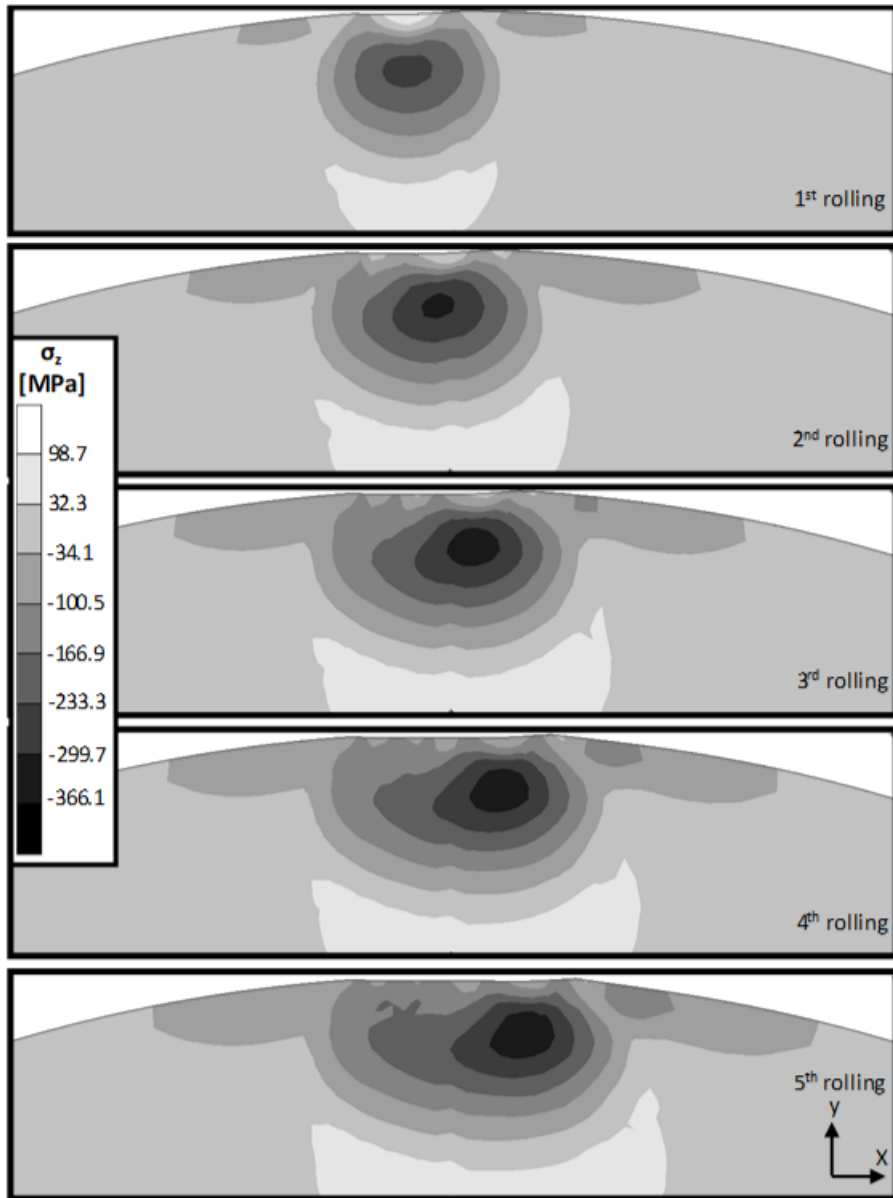


Figure 93 Residual Stress Distribution on Ø14 Model, σ_z , 500 N, 0.1 mm Feed Parameter

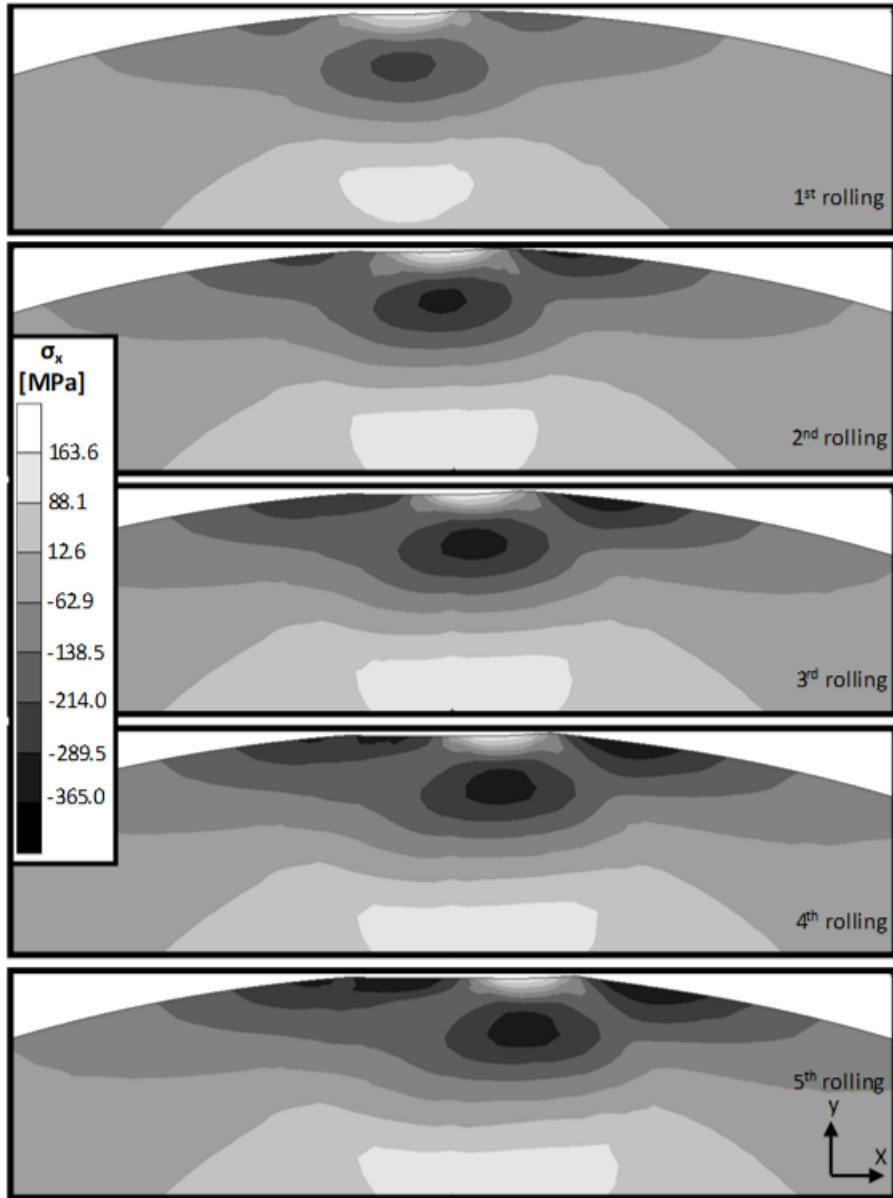


Figure 94 Residual Stress Distribution on $\text{Ø}14$ Model, σ_x , 500 N, 0.1 mm Feed Parameter

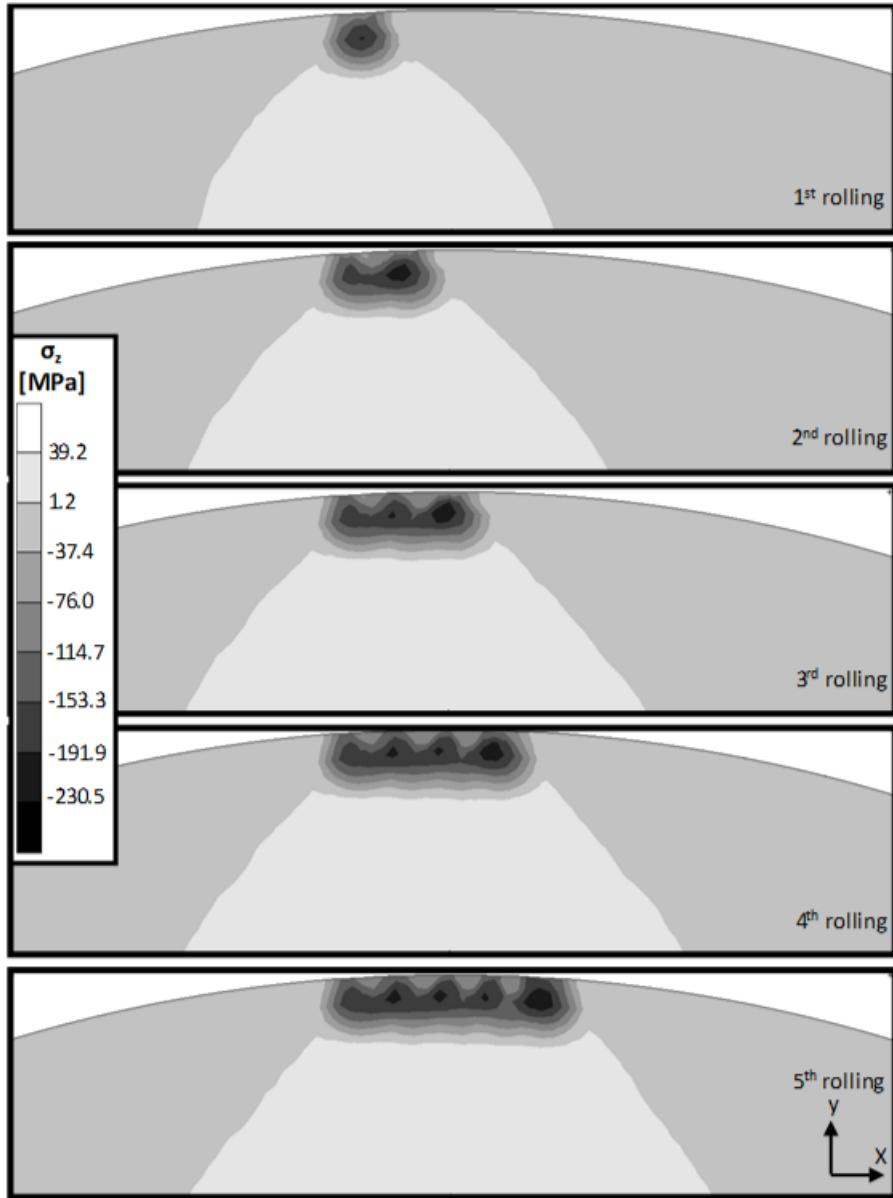


Figure 95 Residual Stress Distribution on $\text{Ø}14$ Model, σ_z , 125 N, 0.2 mm Feed Parameter

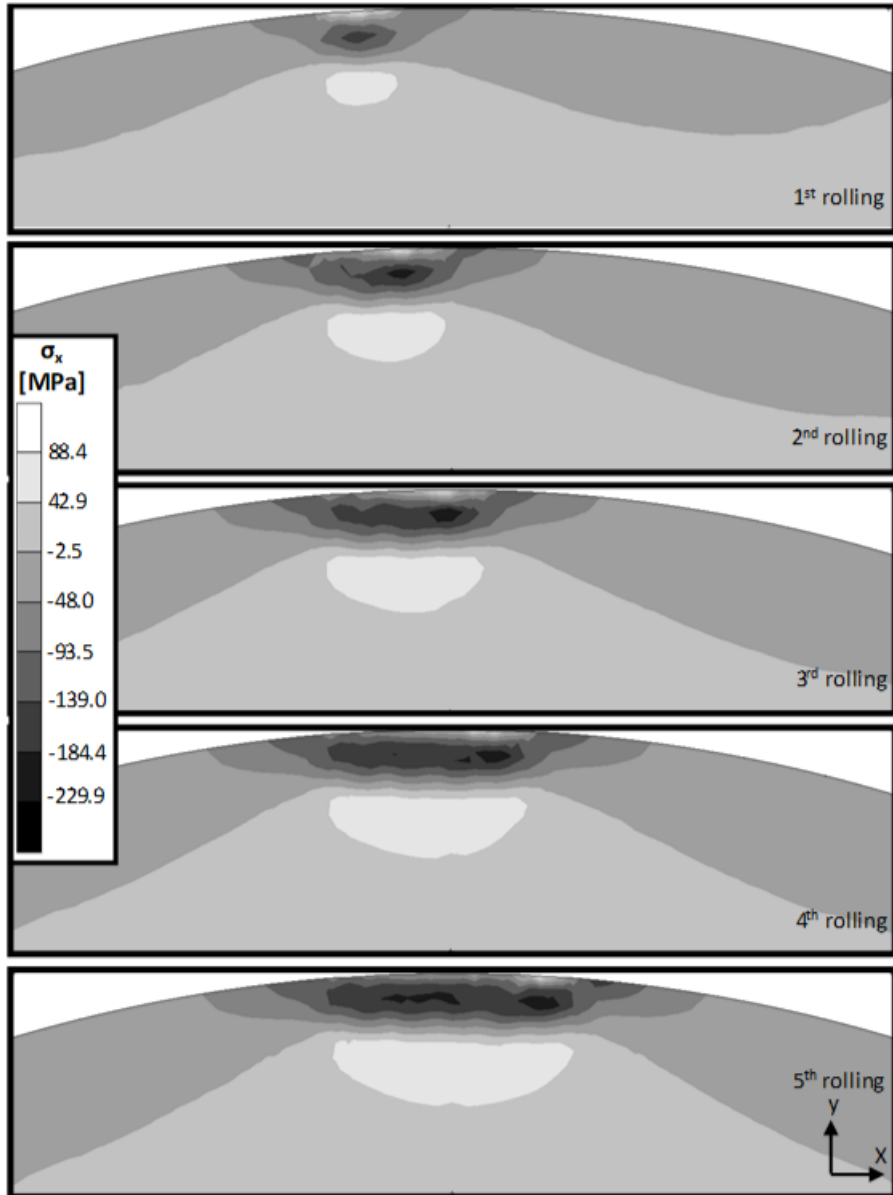


Figure 96 Residual Stress Distribution on $\text{Ø}14$ Model, σ_x , 125 N, 0.2 mm Feed Parameter

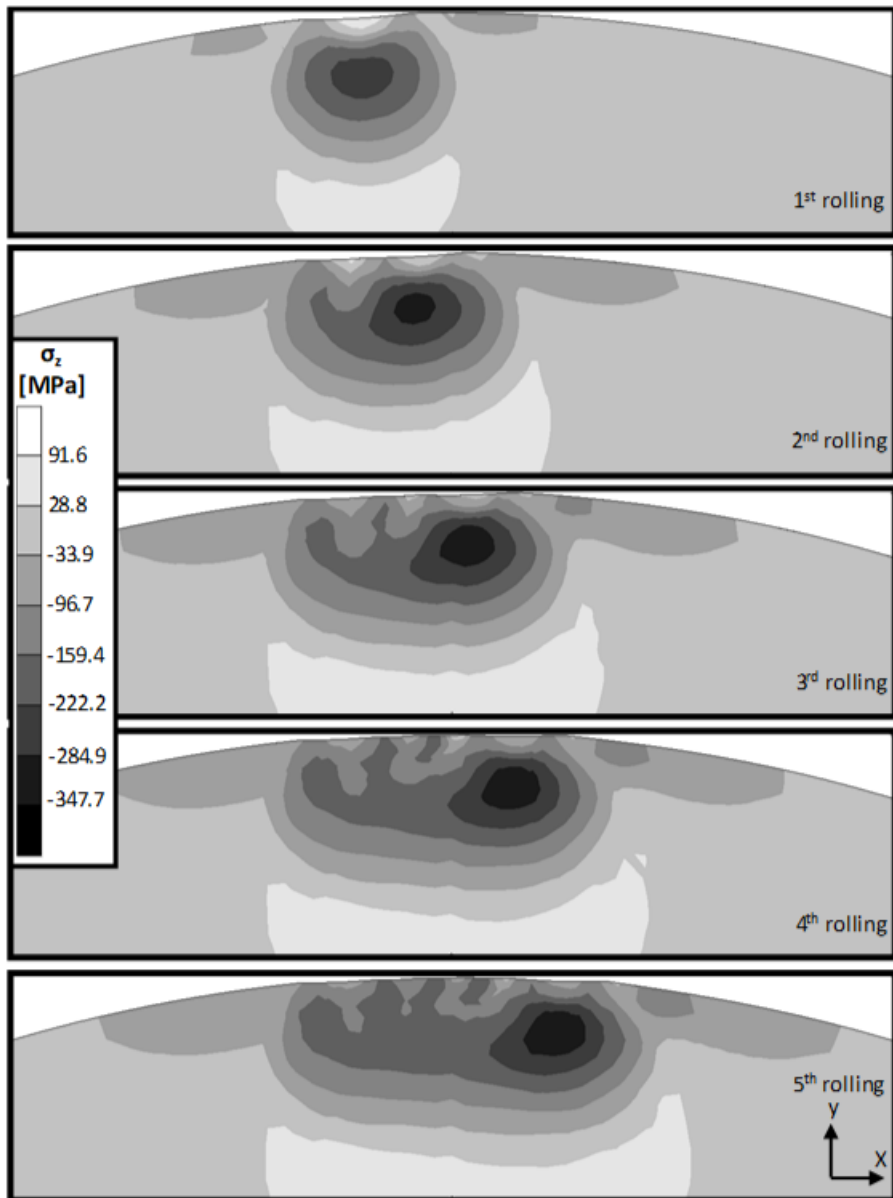


Figure 97 Residual Stress Distribution on $\text{Ø}14$ Model, σ_z , 500 N, 0.2 mm Feed Parameter

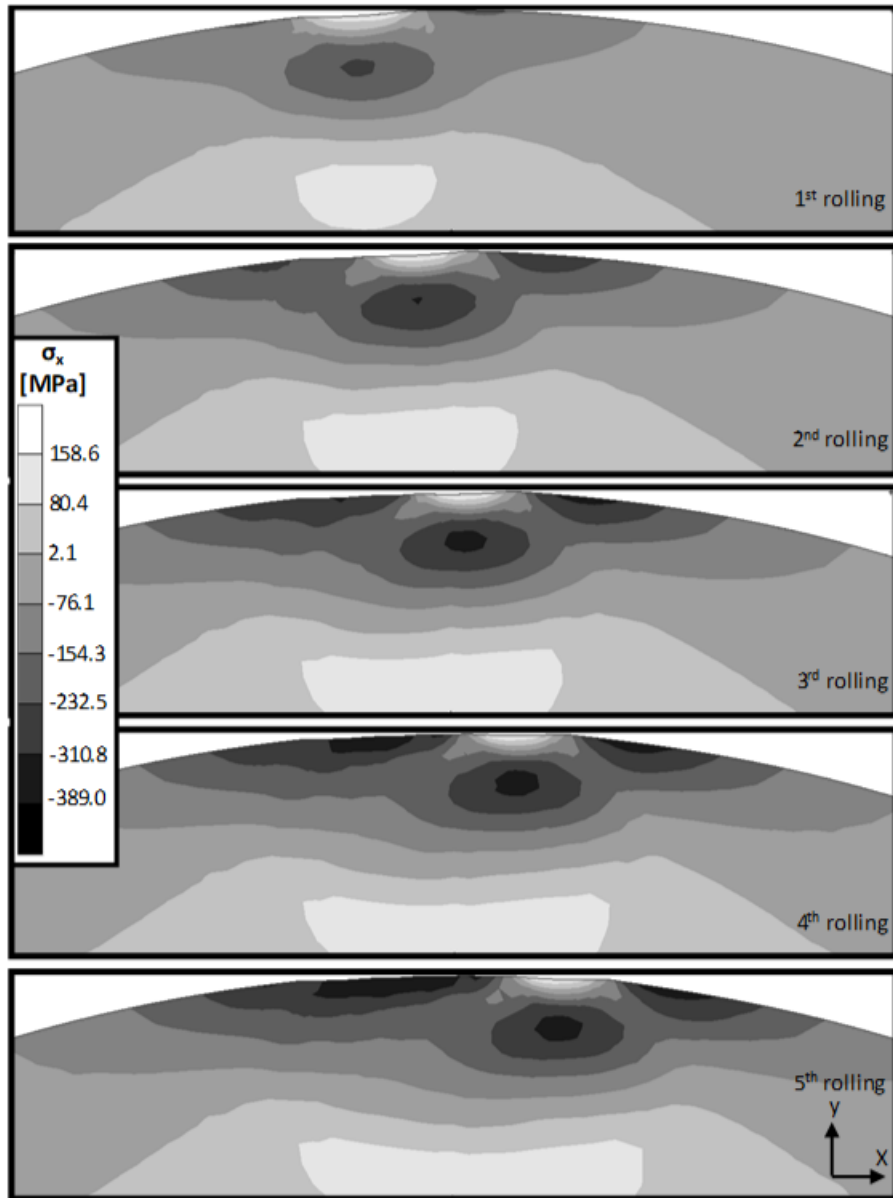


Figure 98 Residual Stress Distribution on $\text{Ø}14$ Model, σ_x , 500 N, 0.2 mm Feed Parameter

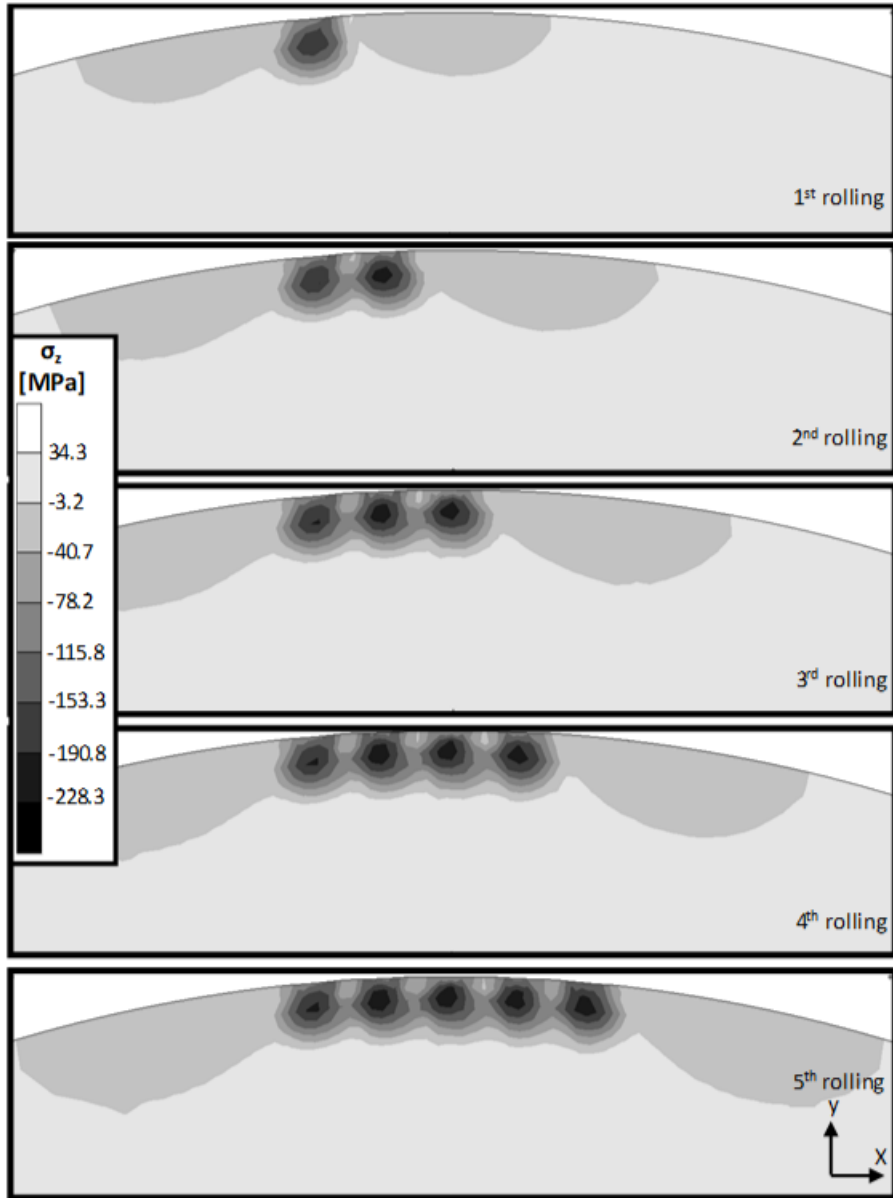


Figure 99 Residual Stress Distribution on $\text{Ø}14$ Model, σ_z , 125 N, 0.3 mm Feed Parameter

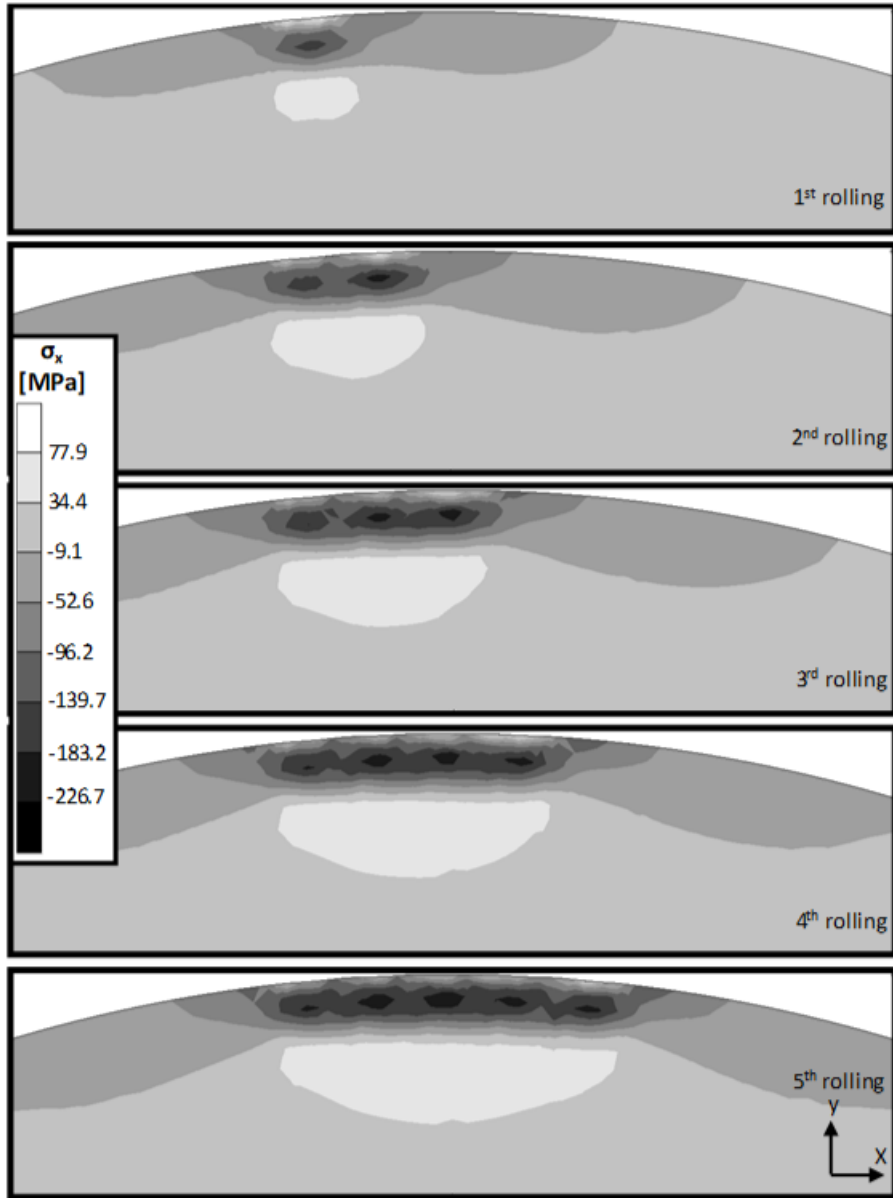


Figure 100 Residual Stress Distribution on $\text{Ø}14$ Model, σ_x , 125 N, 0.3 mm Feed Parameter

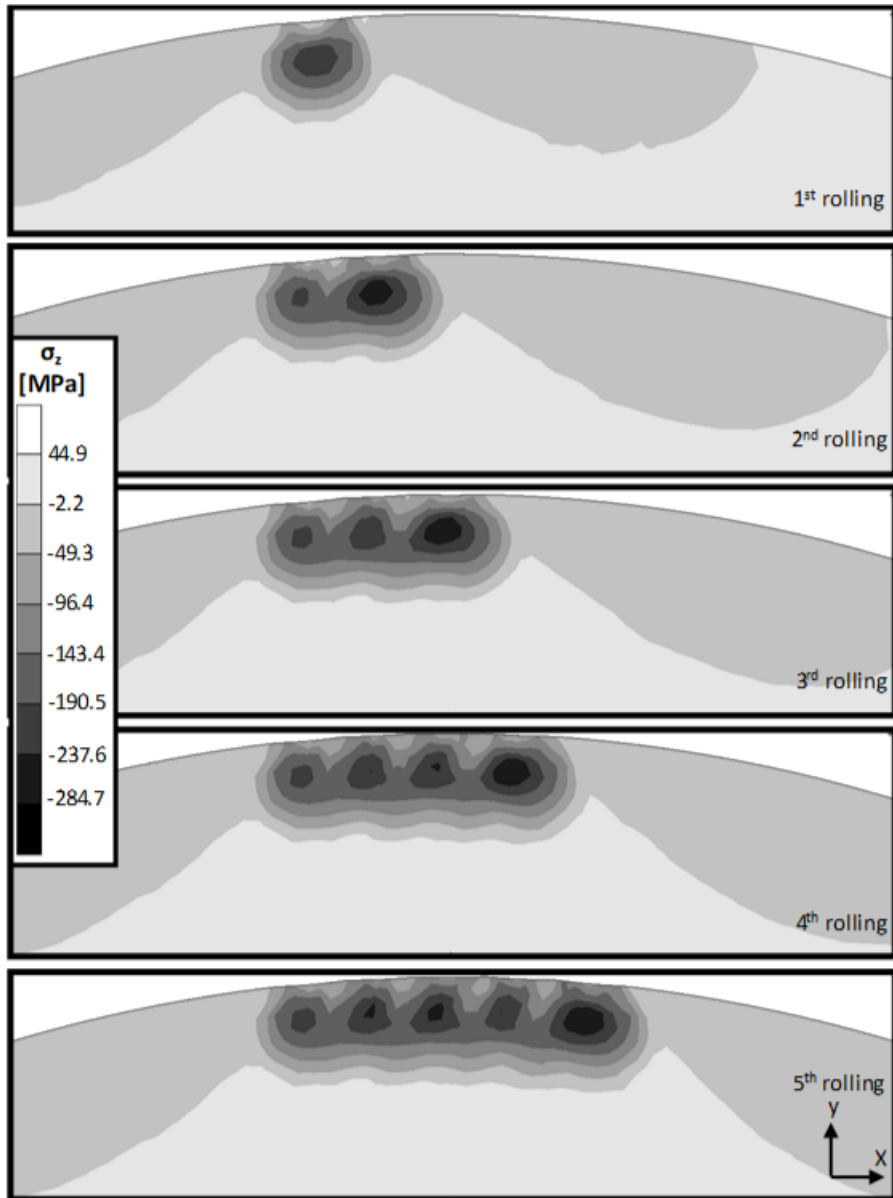


Figure 101 Residual Stress Distribution on $\text{Ø}14$ Model, σ_z , 250 N, 0.3 mm Feed Parameter

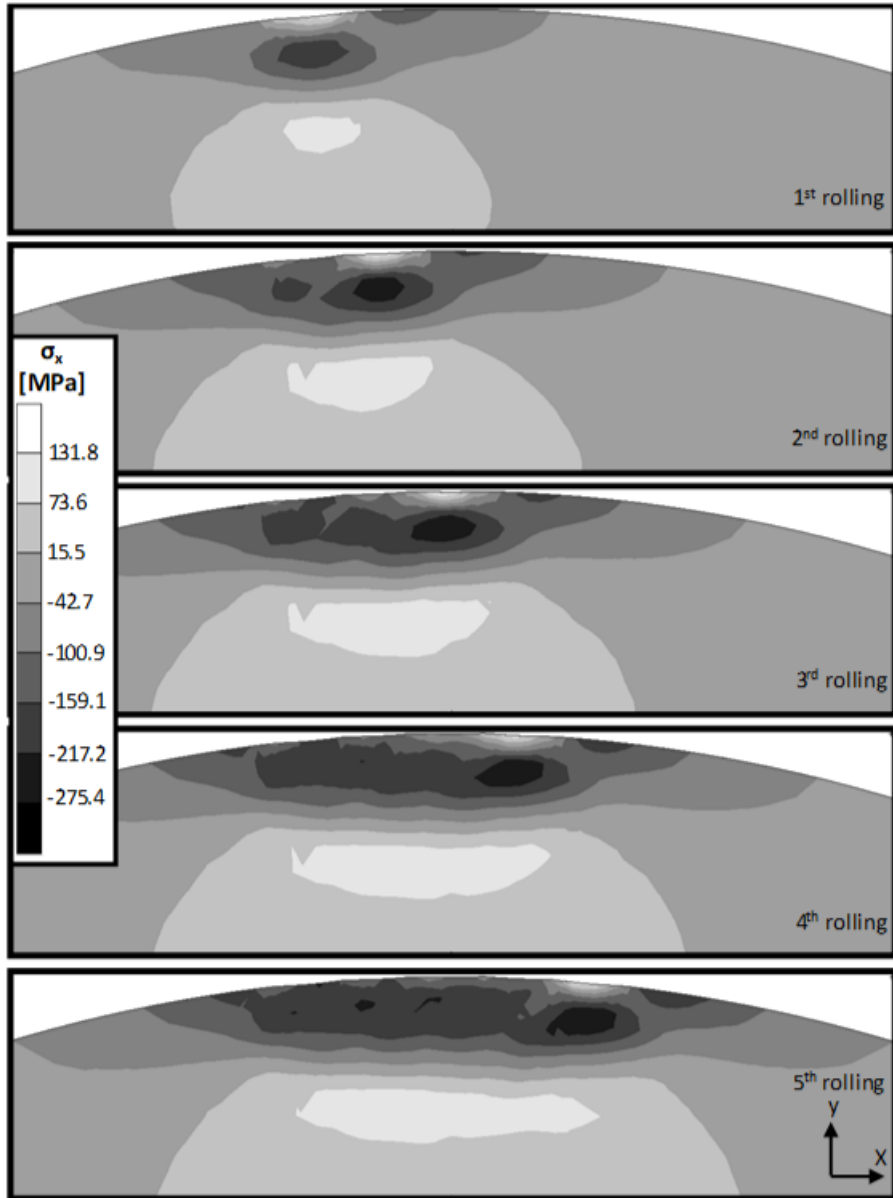


Figure 102 Residual Stress Distribution on Ø14 Model, σ_x , 250 N, 0.3 mm Feed Parameter

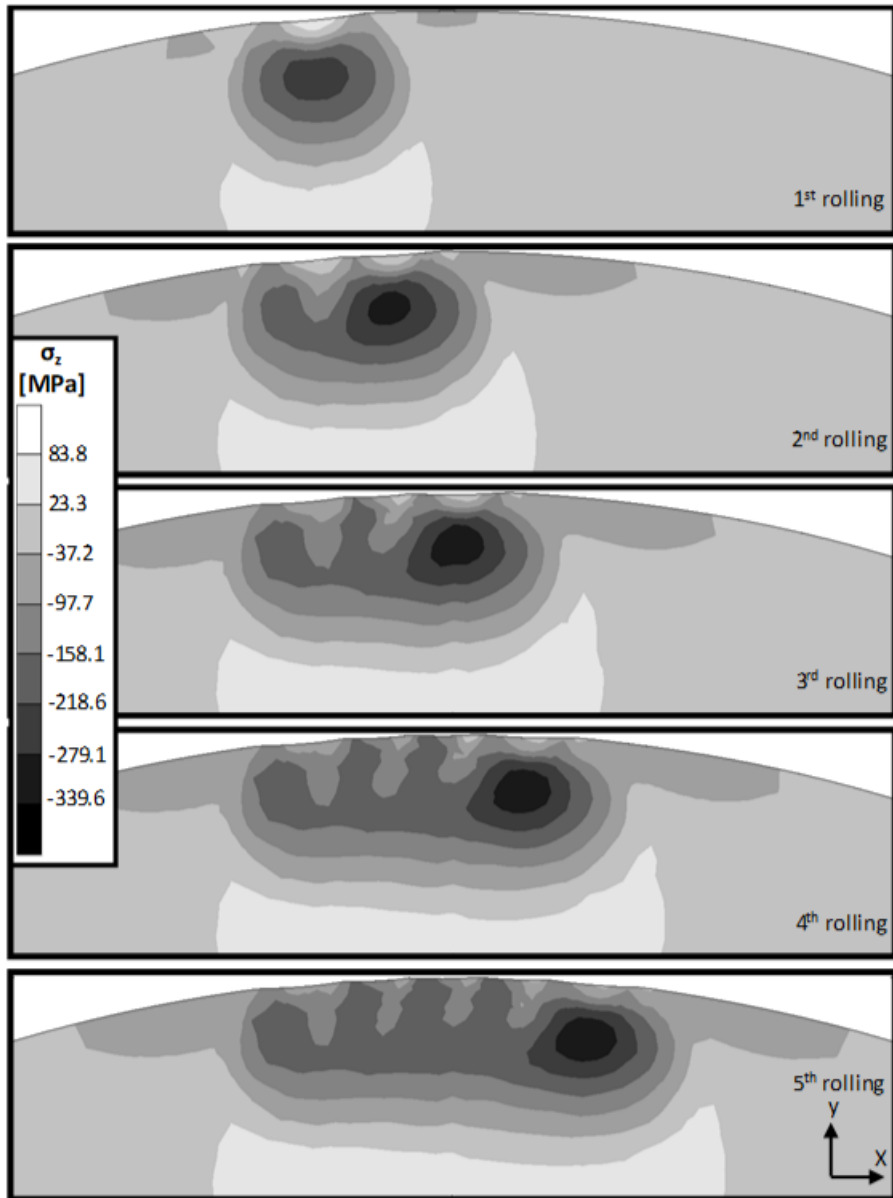


Figure 103 Residual Stress Distribution on $\text{Ø}14$ Model, σ_z , 500 N, 0.3 mm Feed Parameter

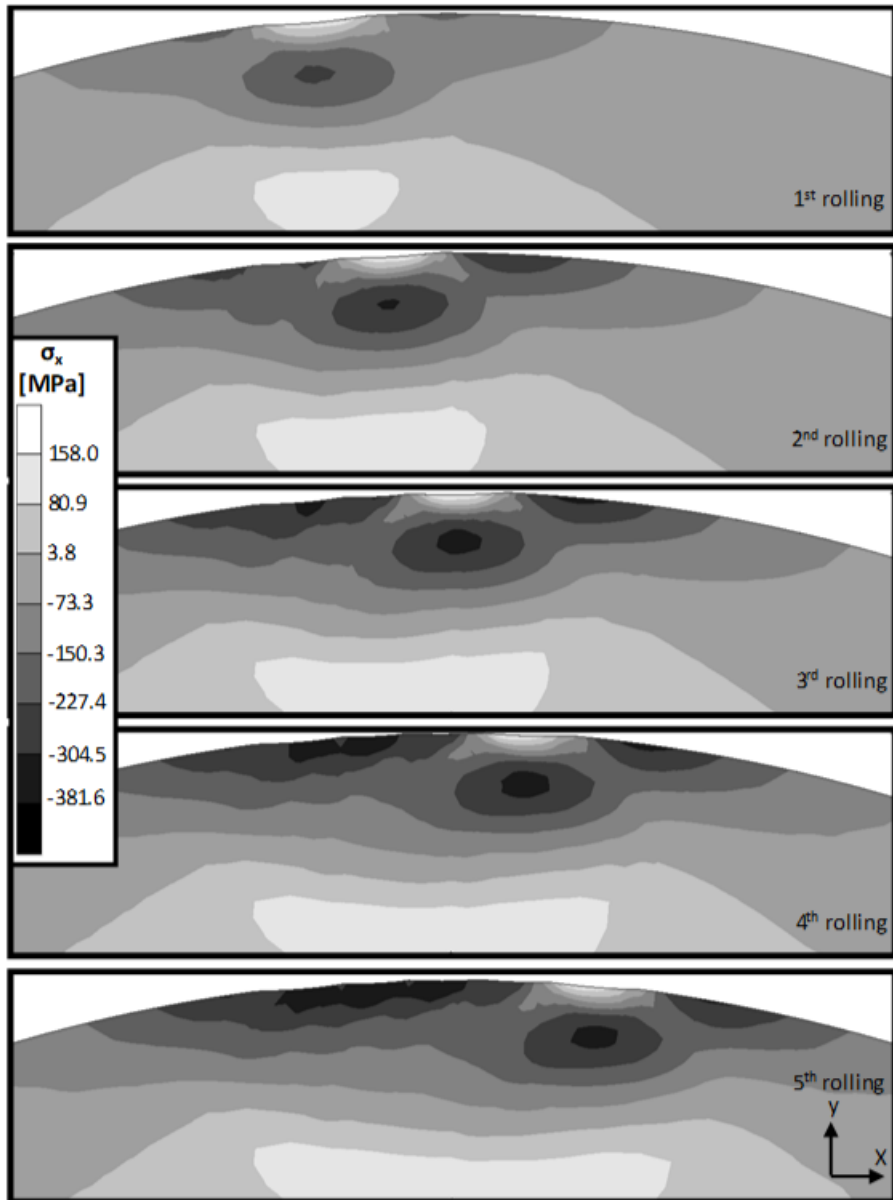


Figure 104 Residual Stress Distribution on $\text{Ø}14$ Model, σ_x , 500 N, 0.3 mm Feed Parameter

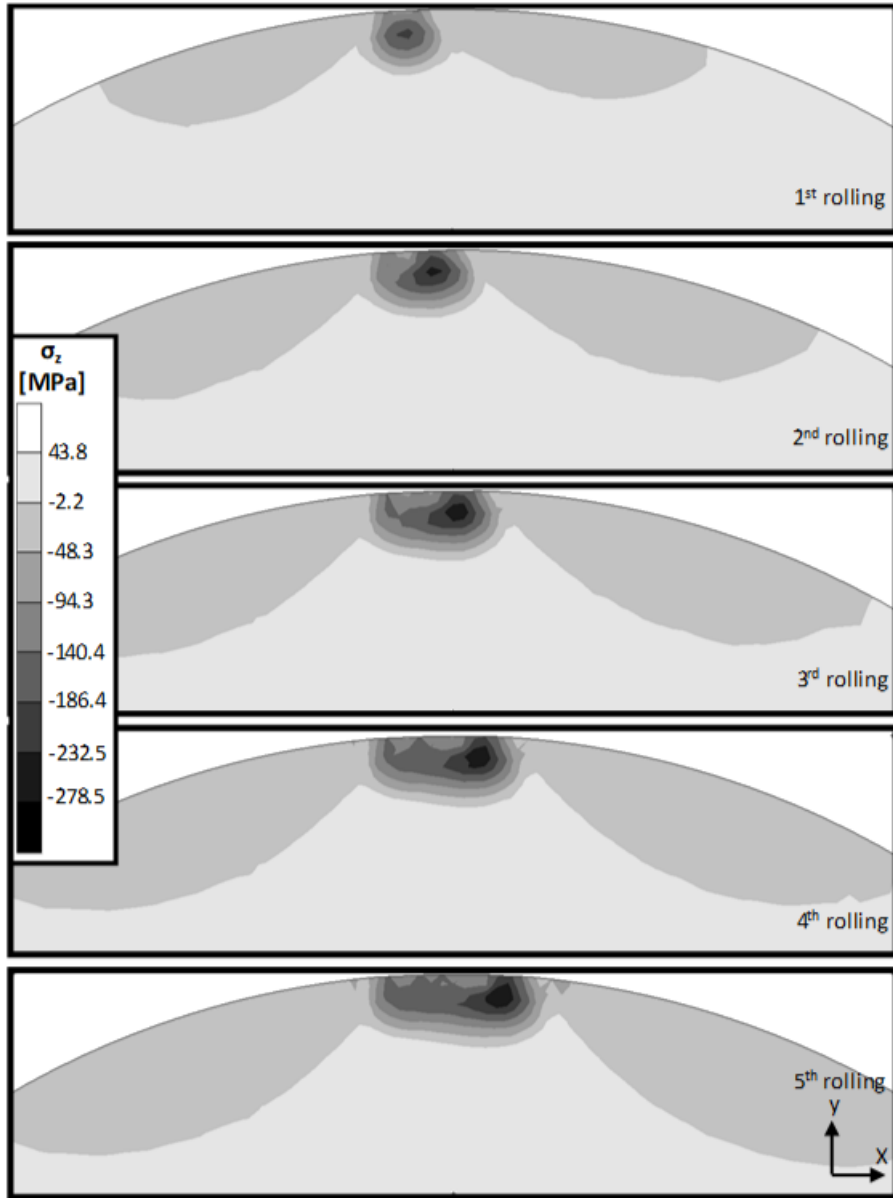


Figure 105 Residual Stress Distribution on $\text{Ø}8$ Model, σ_z , 125 N, 0.1 mm Feed Parameter

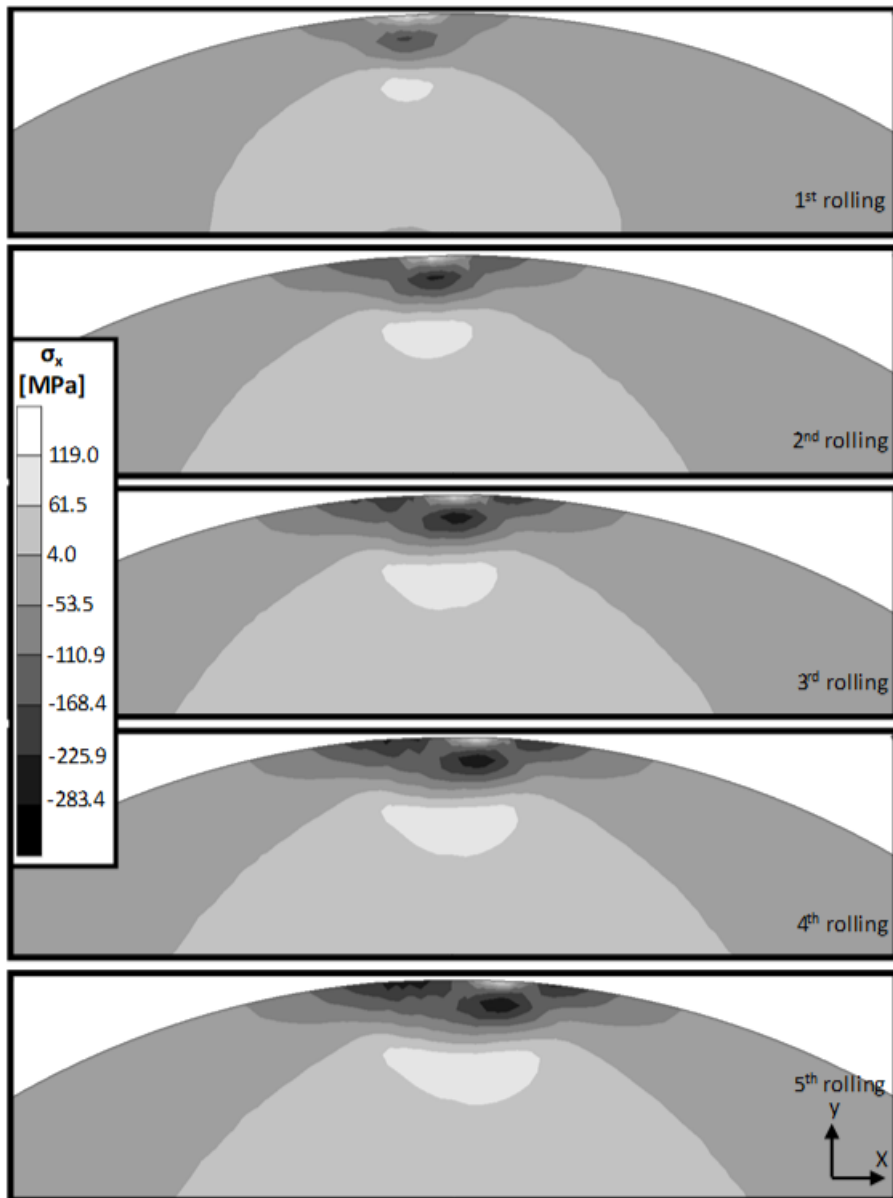


Figure 106 Residual Stress Distribution on Ø8 Model, σ_x , 125 N, 0.1 mm Feed Parameter

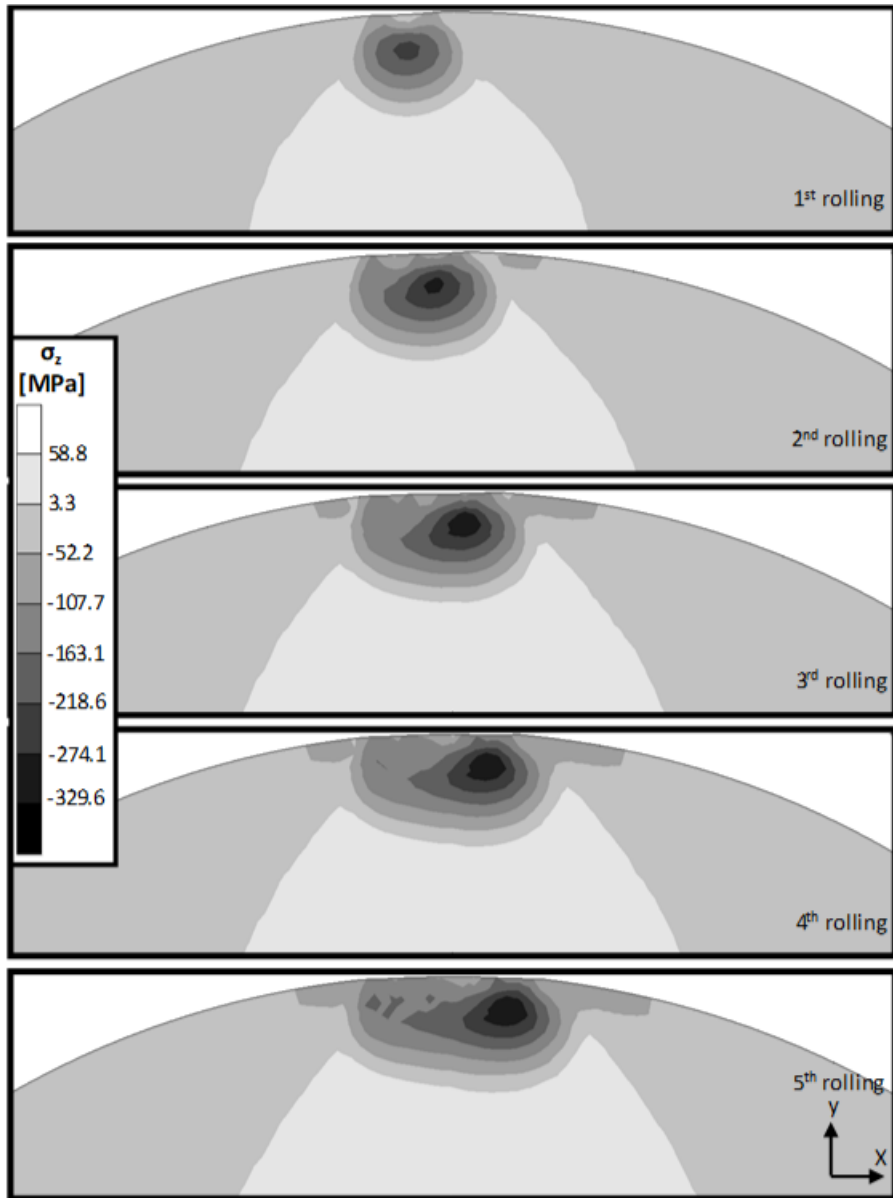


Figure 107 Residual Stress Distribution on Ø8 Model, σ_z , 250 N, 0.1 mm Feed Parameter

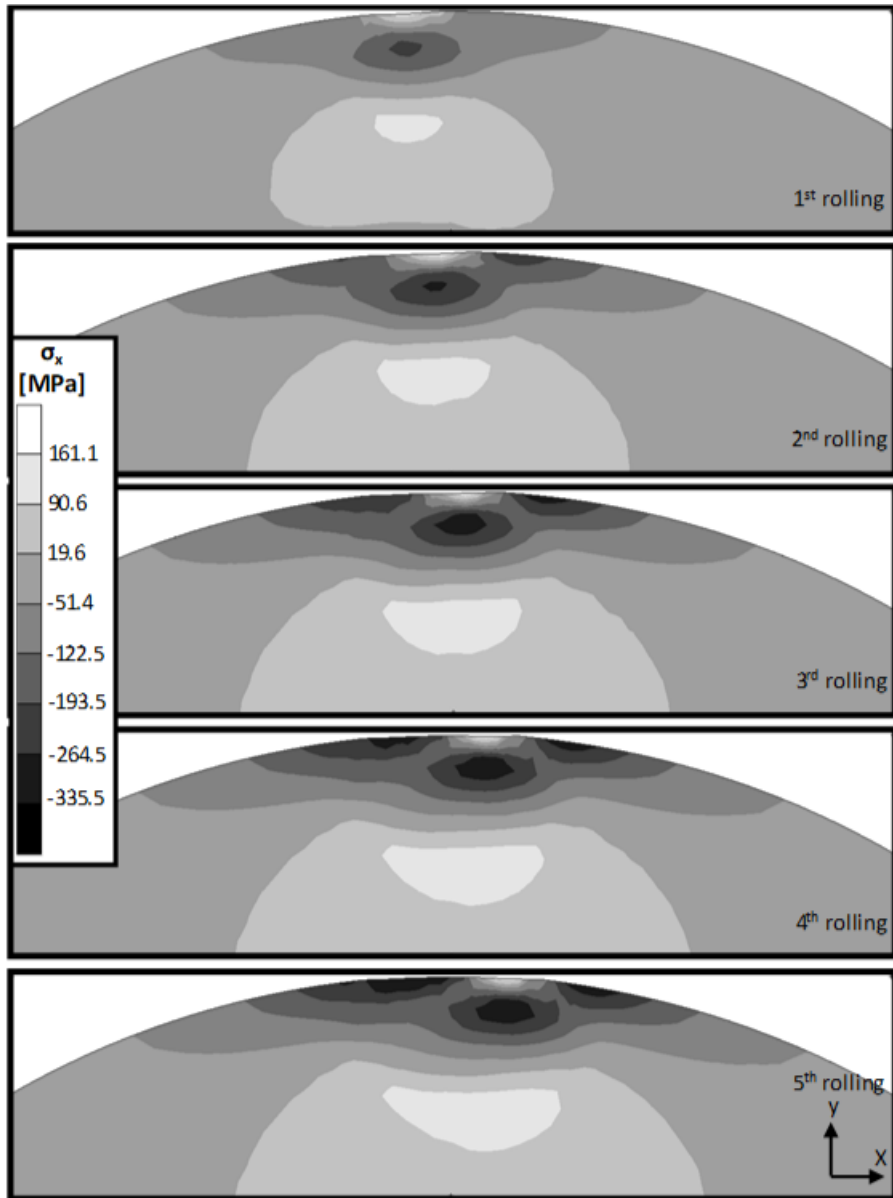


Figure 108 Residual Stress Distribution on Ø8 Model, σ_x , 250 N, 0.1 mm Feed Parameter

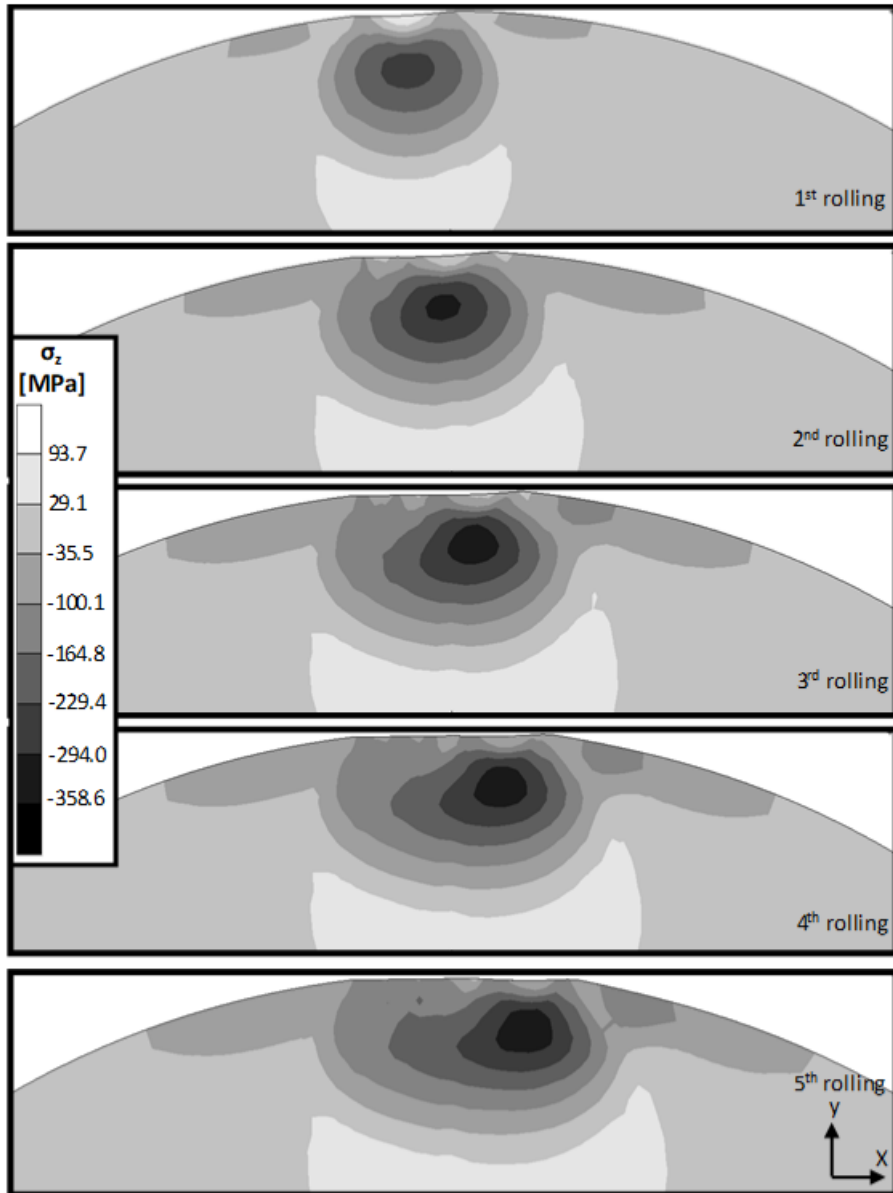


Figure 109 Residual Stress Distribution on Ø8 Model, σ_z , 500 N, 0.1 mm Feed Parameter

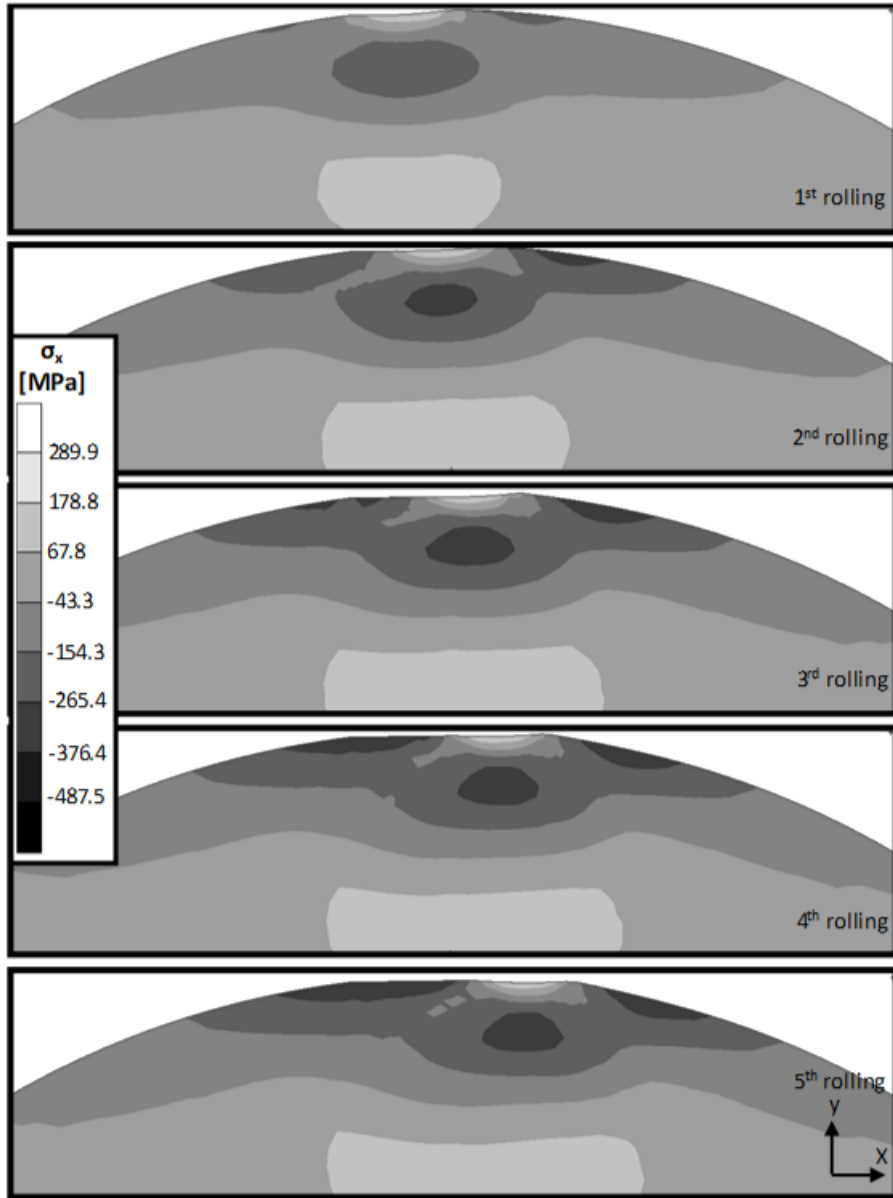


Figure 110 Residual Stress Distribution on Ø8 Model, σ_x , 500 N, 0.1 mm Feed Parameter

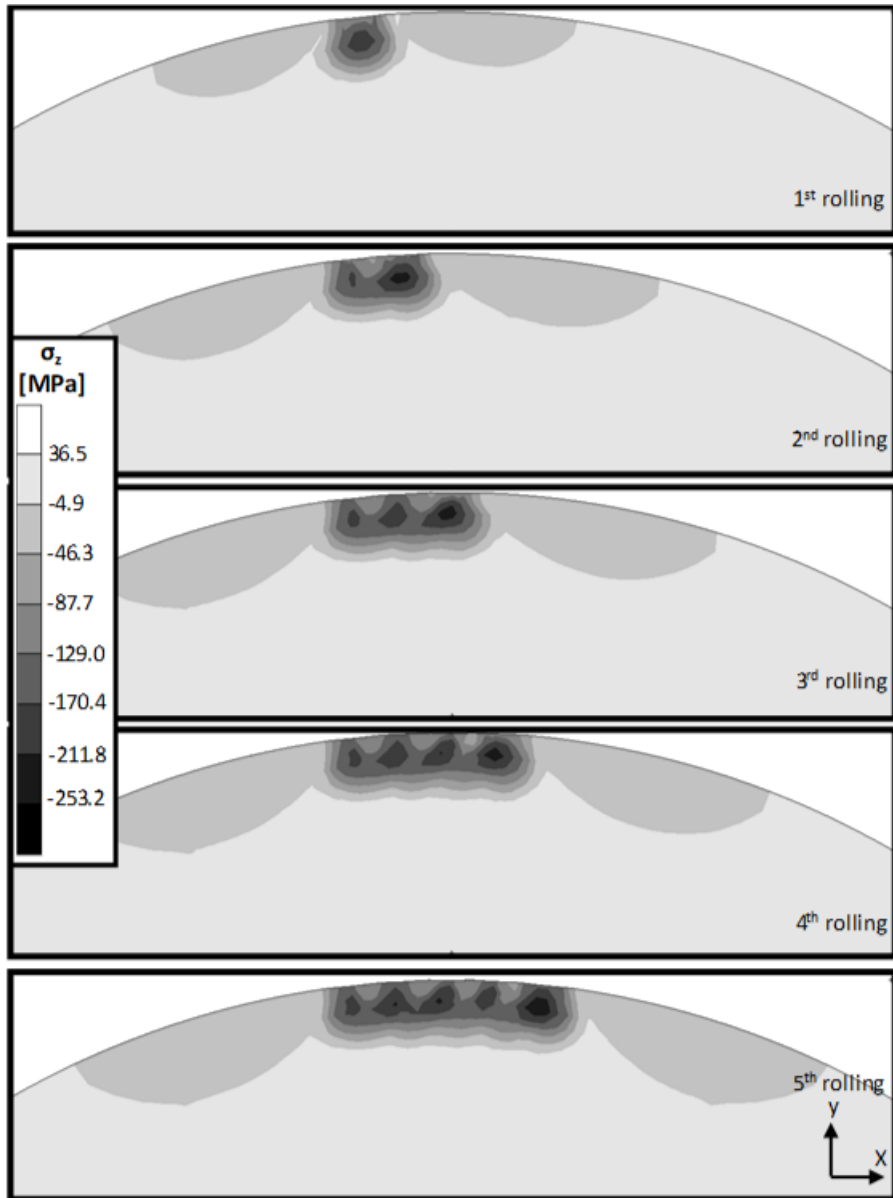


Figure 111 Residual Stress Distribution on Ø8 Model, σ_z , 125 N, 0.2 mm Feed Parameter

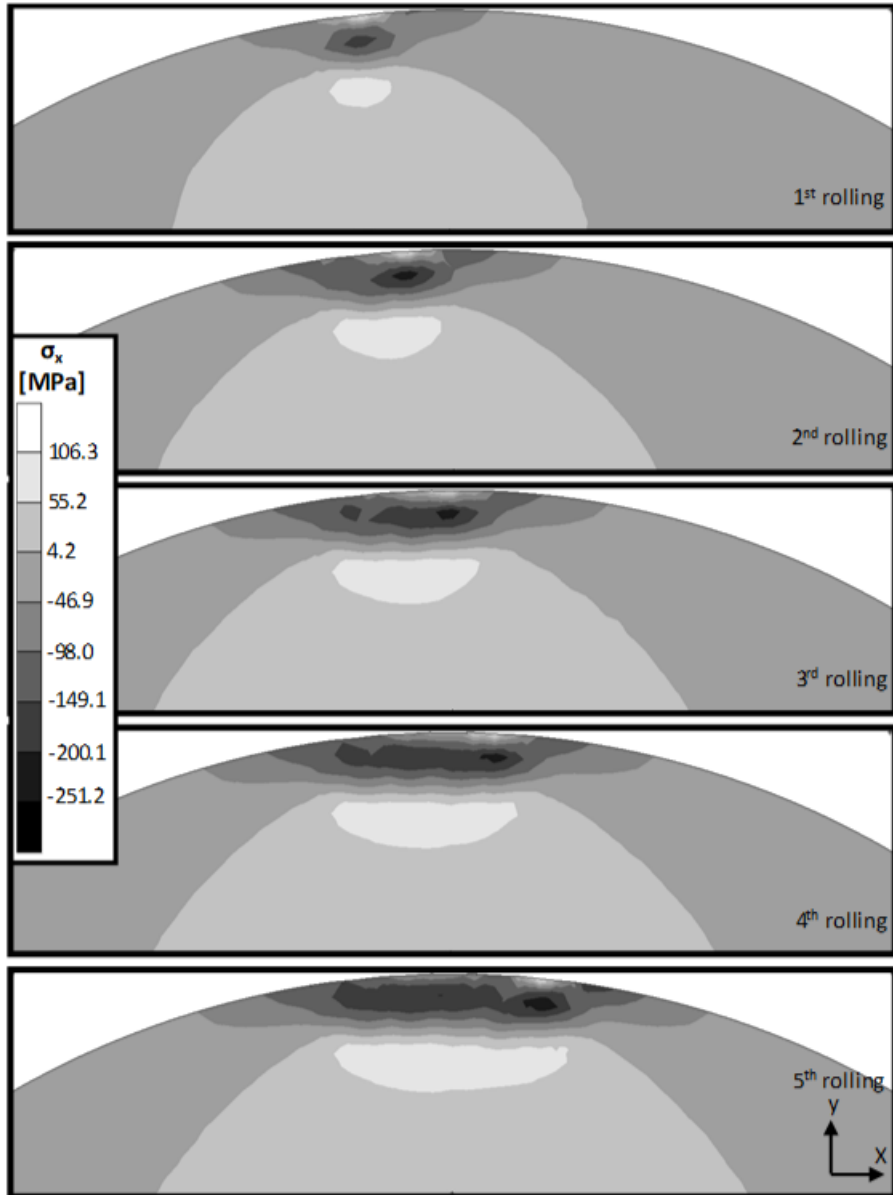


Figure 112 Residual Stress Distribution on Ø8 Model, σ_x , 125 N, 0.2 mm Feed Parameter

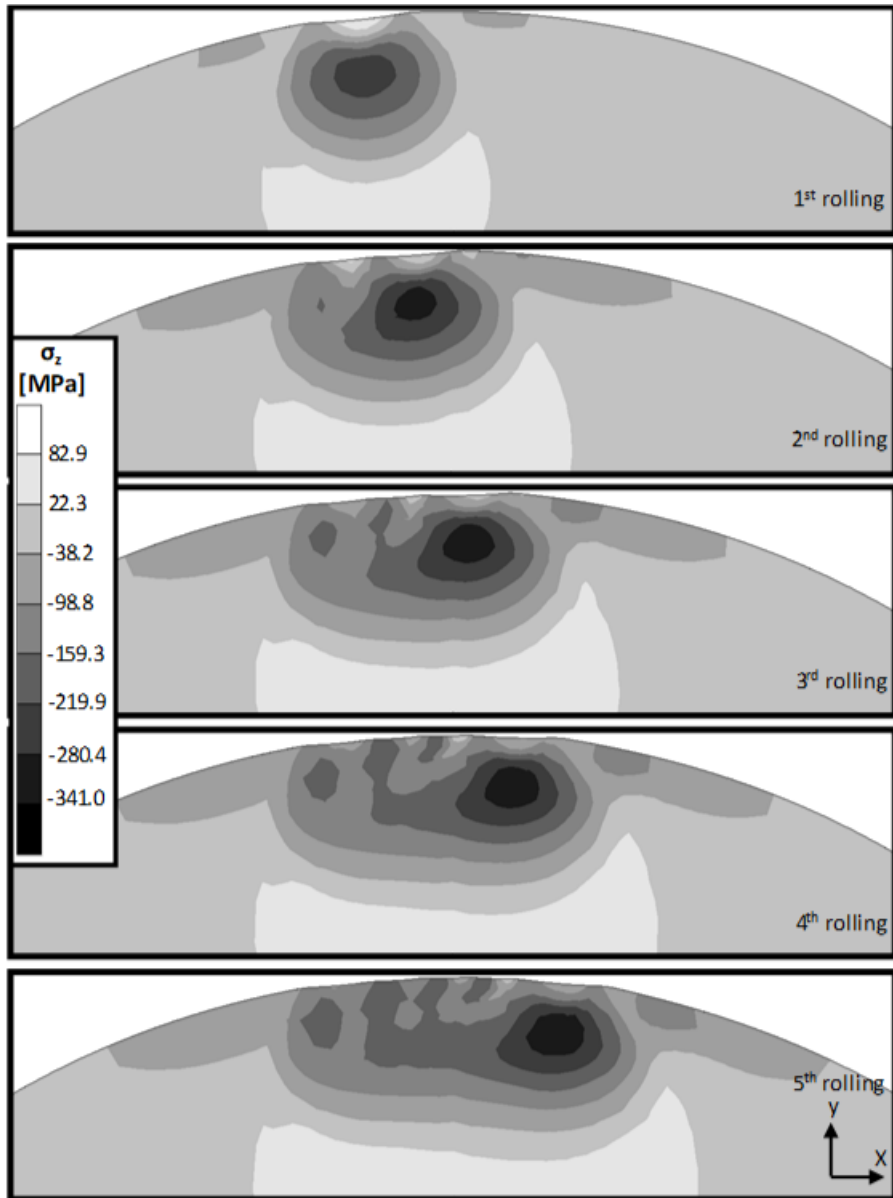


Figure 113 Residual Stress Distribution on Ø8 Model, σ_z , 500 N, 0.2 mm Feed Parameter

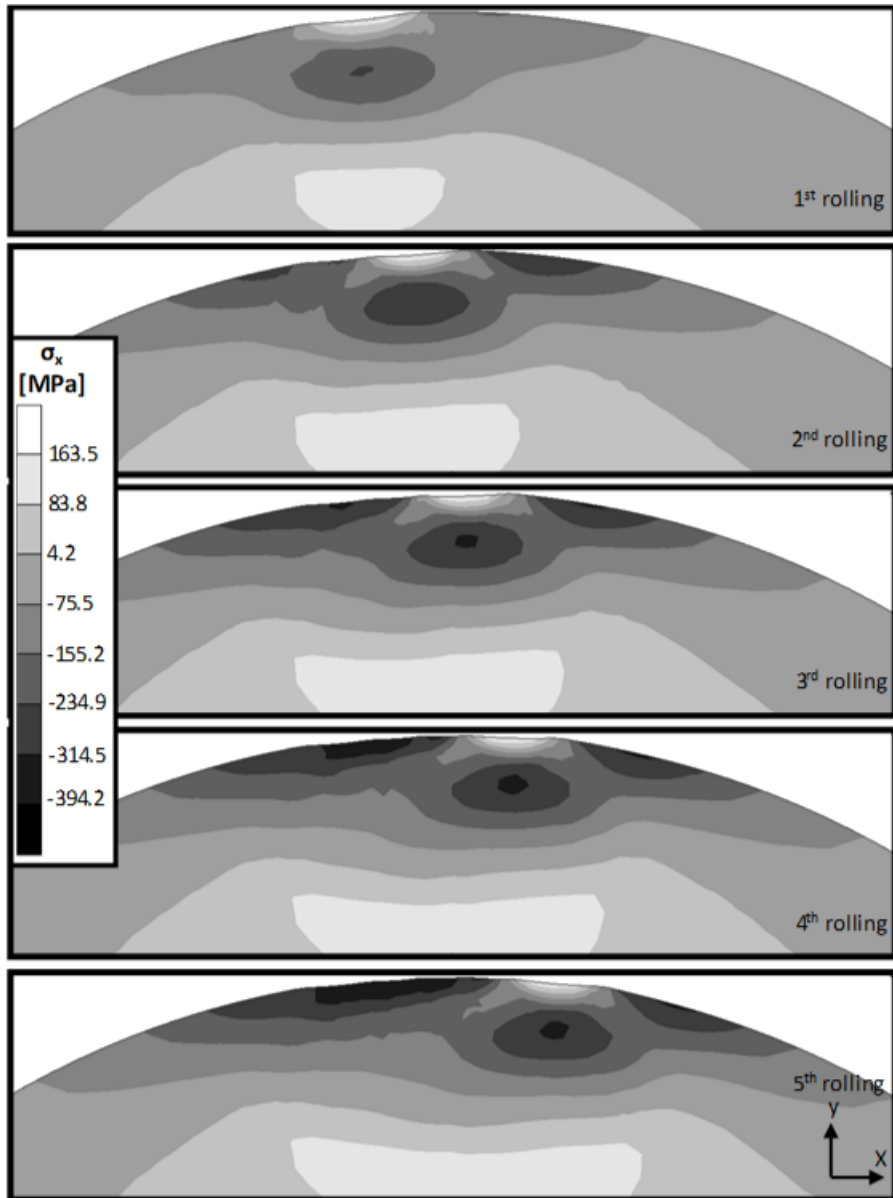


Figure 114 Residual Stress Distribution on Ø8 Model, σ_x , 500 N, 0.2 mm Feed Parameter

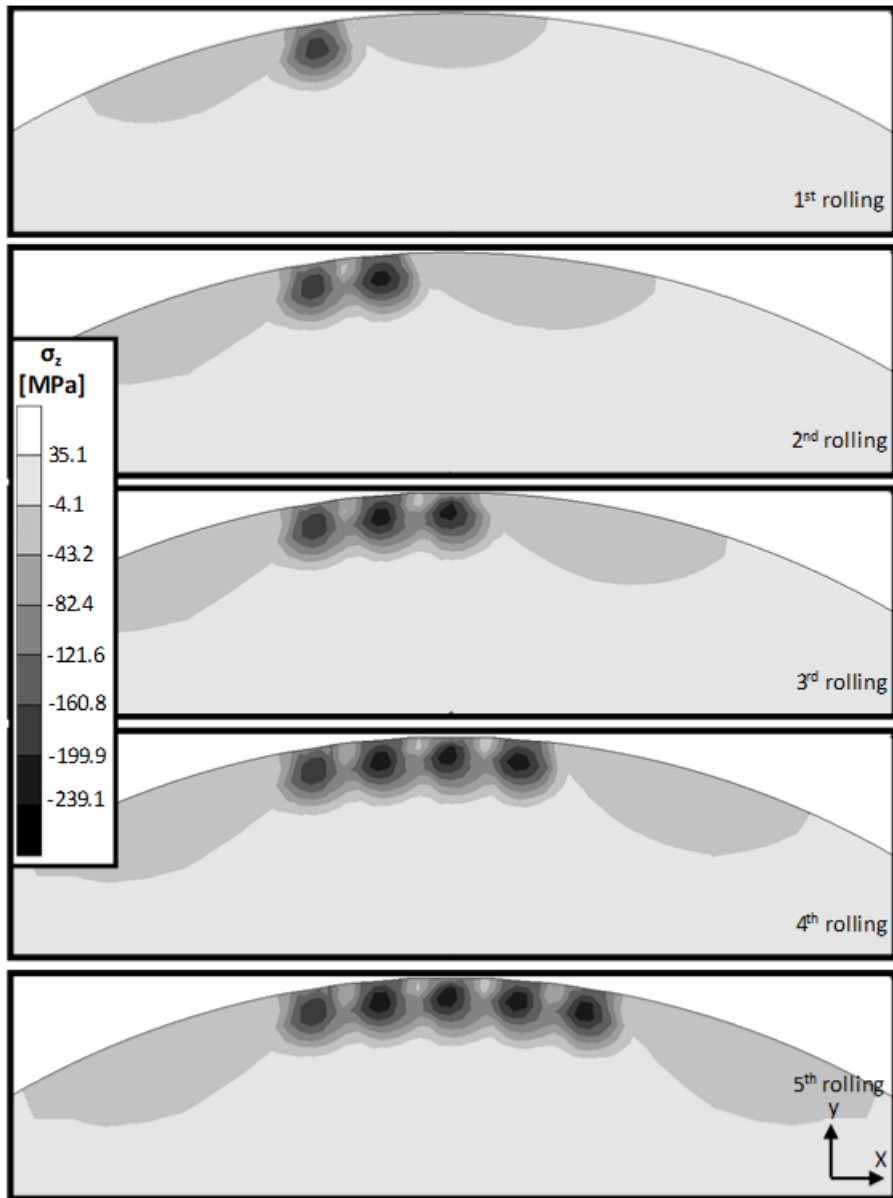


Figure 115 Residual Stress Distribution on Ø8 Model, σ_z , 125 N, 0.3 mm Feed Parameter

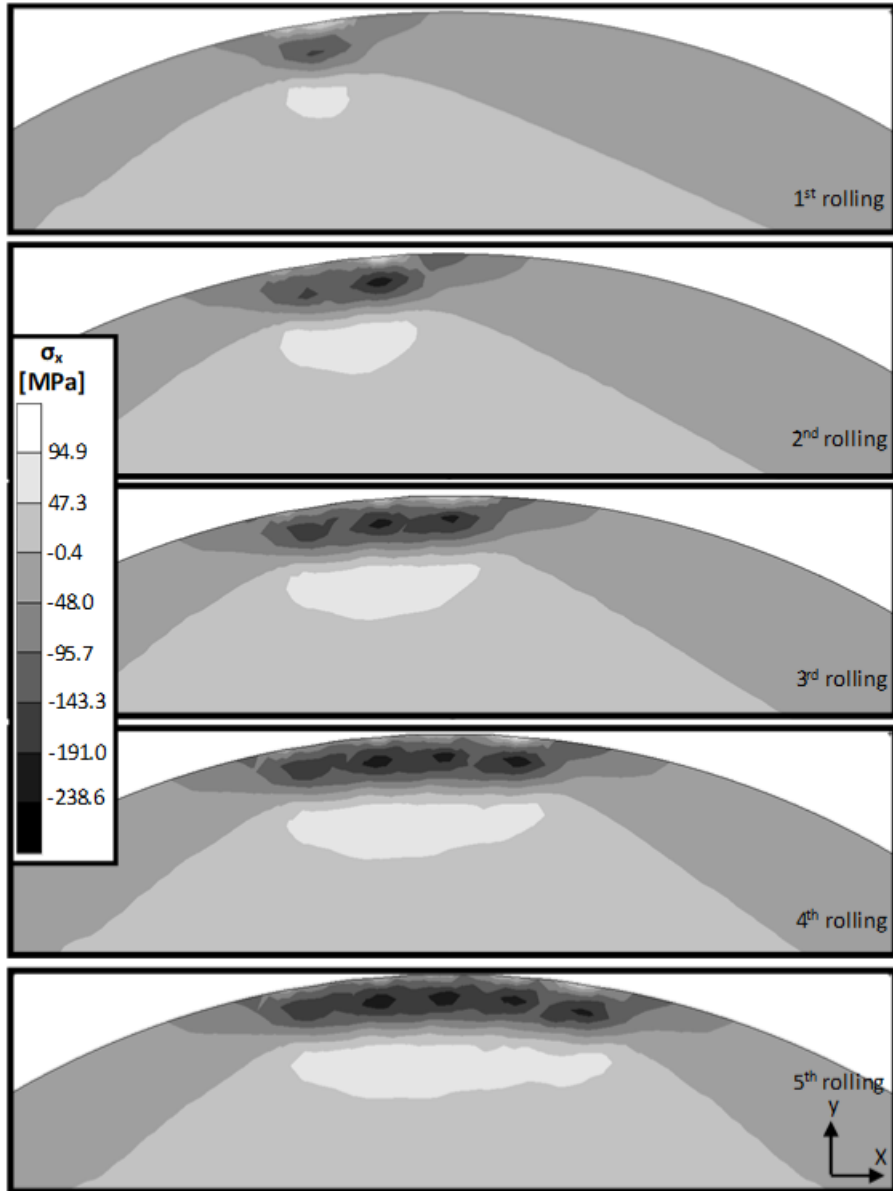


Figure 116 Residual Stress Distribution on Ø8 Model, σ_x , 125 N, 0.3 mm Feed Parameter

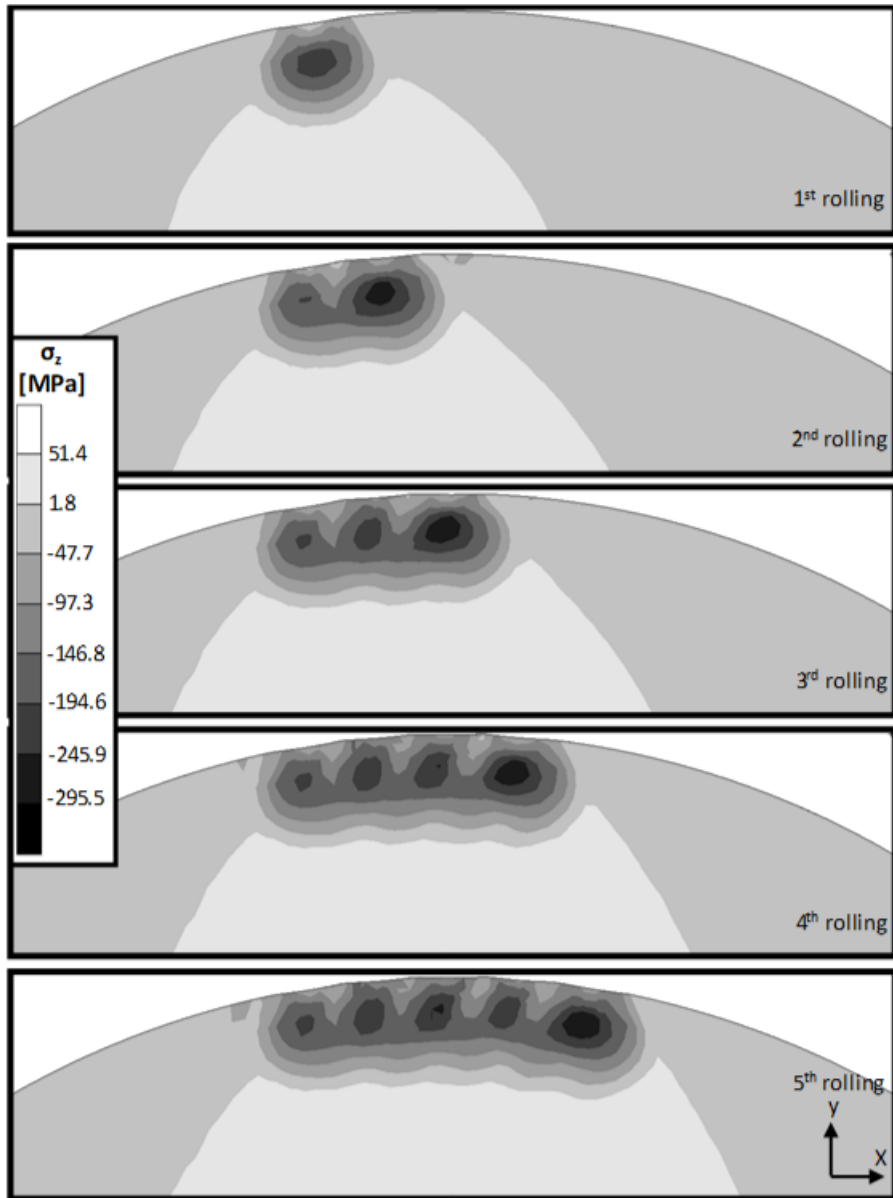


Figure 117 Residual Stress Distribution on Ø8 Model, σ_z , 250 N, 0.3 mm Feed Parameter

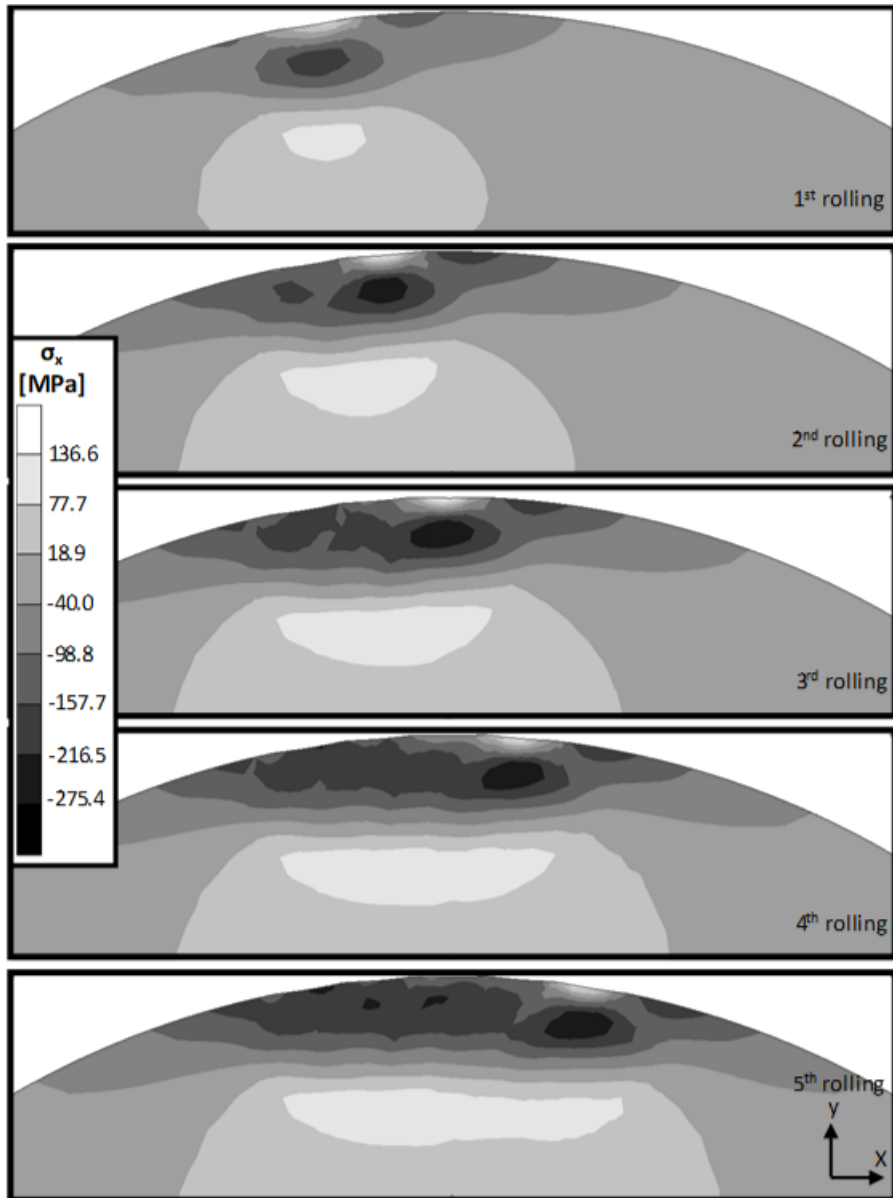


Figure 118 Residual Stress Distribution on Ø8 Model, σ_x , 250 N, 0.3 mm Feed Parameter

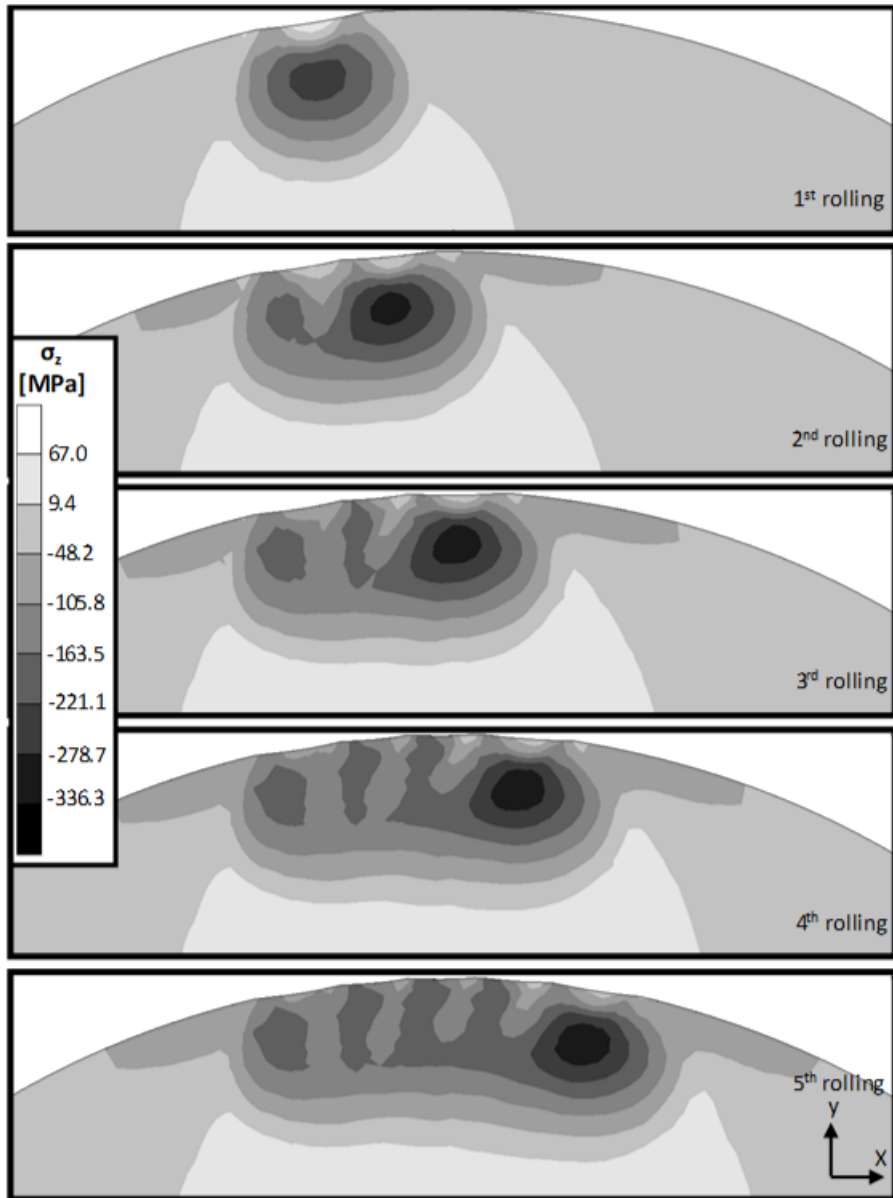


Figure 119 Residual Stress Distribution on Ø8 Model, σ_z , 500 N, 0.3 mm Feed Parameter

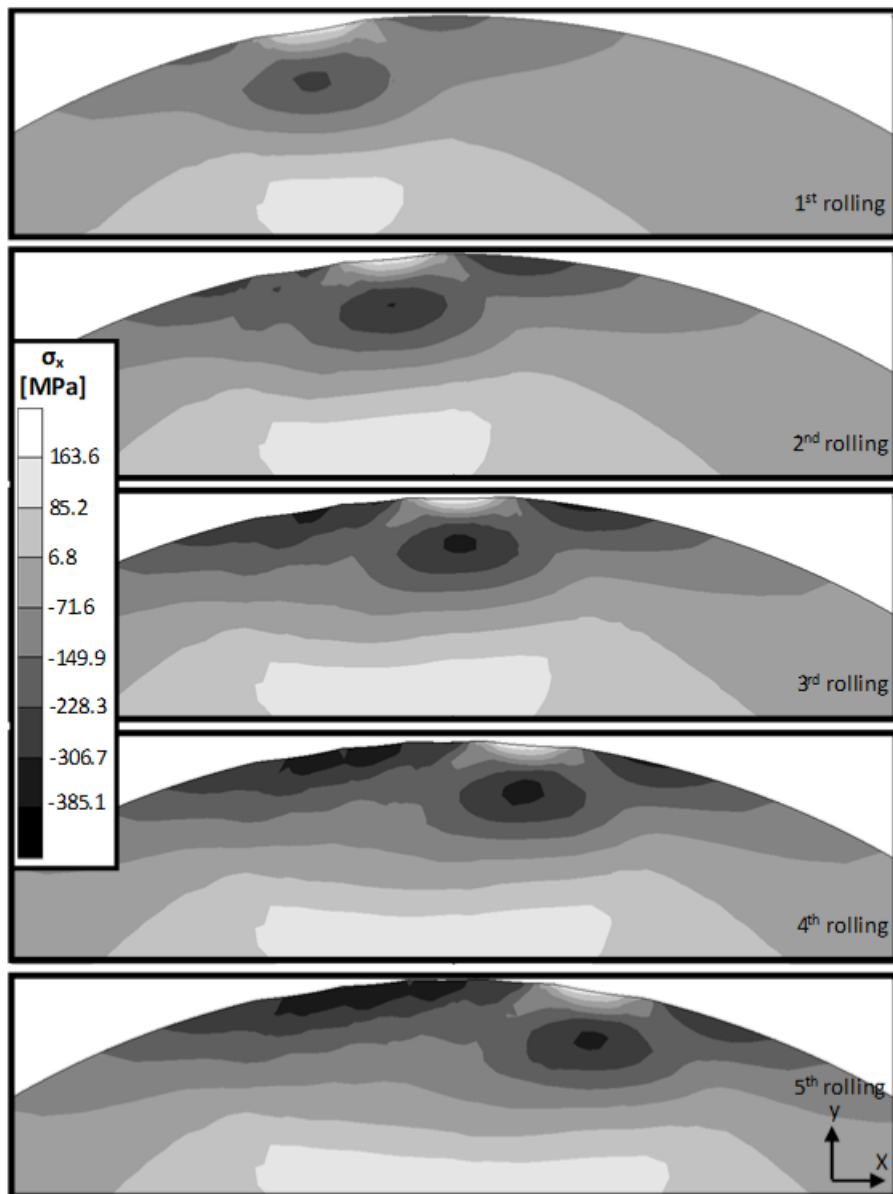


Figure 120 Residual Stress Distribution on Ø8 Model, σ_x , 500 N, 0.3 mm Feed Parameter

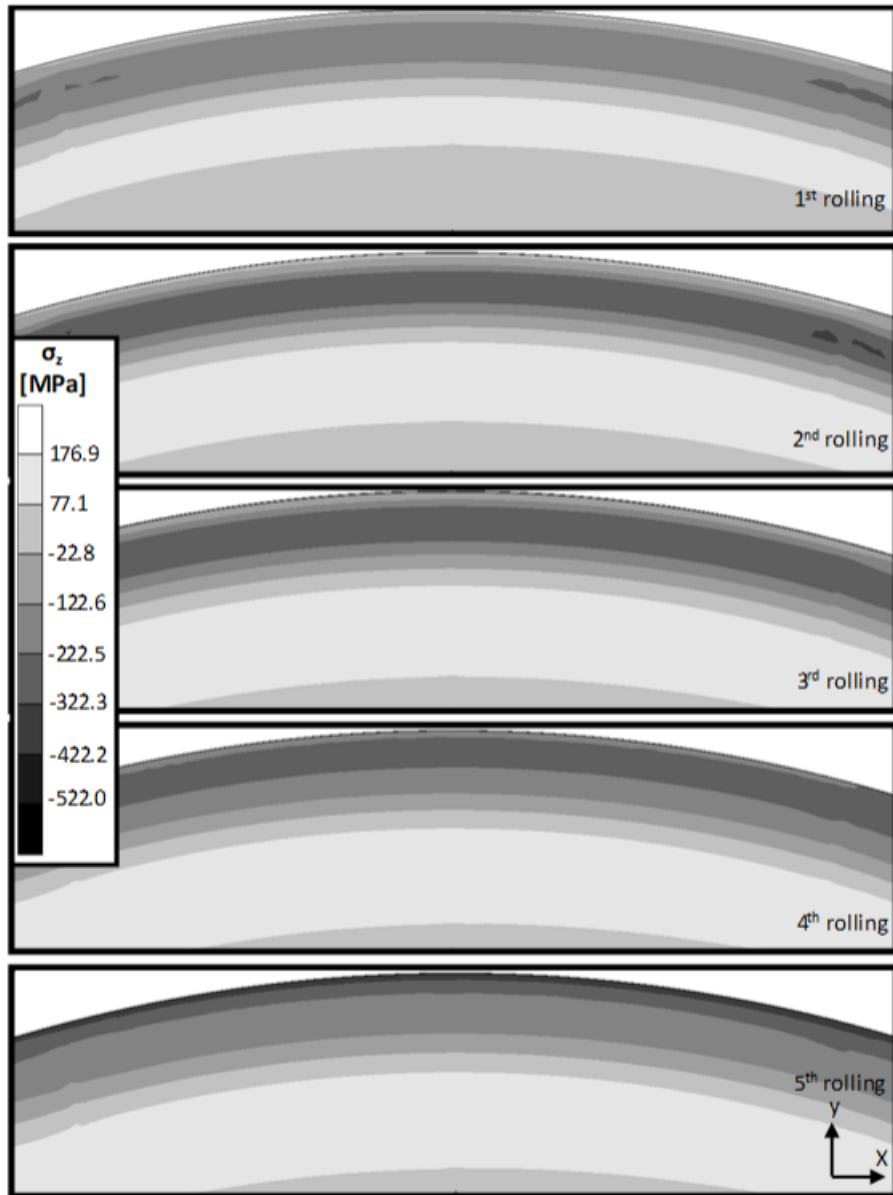


Figure 121 Residual Stress Distribution on Ø8 T. R. Model, σ_z , 125 N, 0.1 mm Feed
Parameter

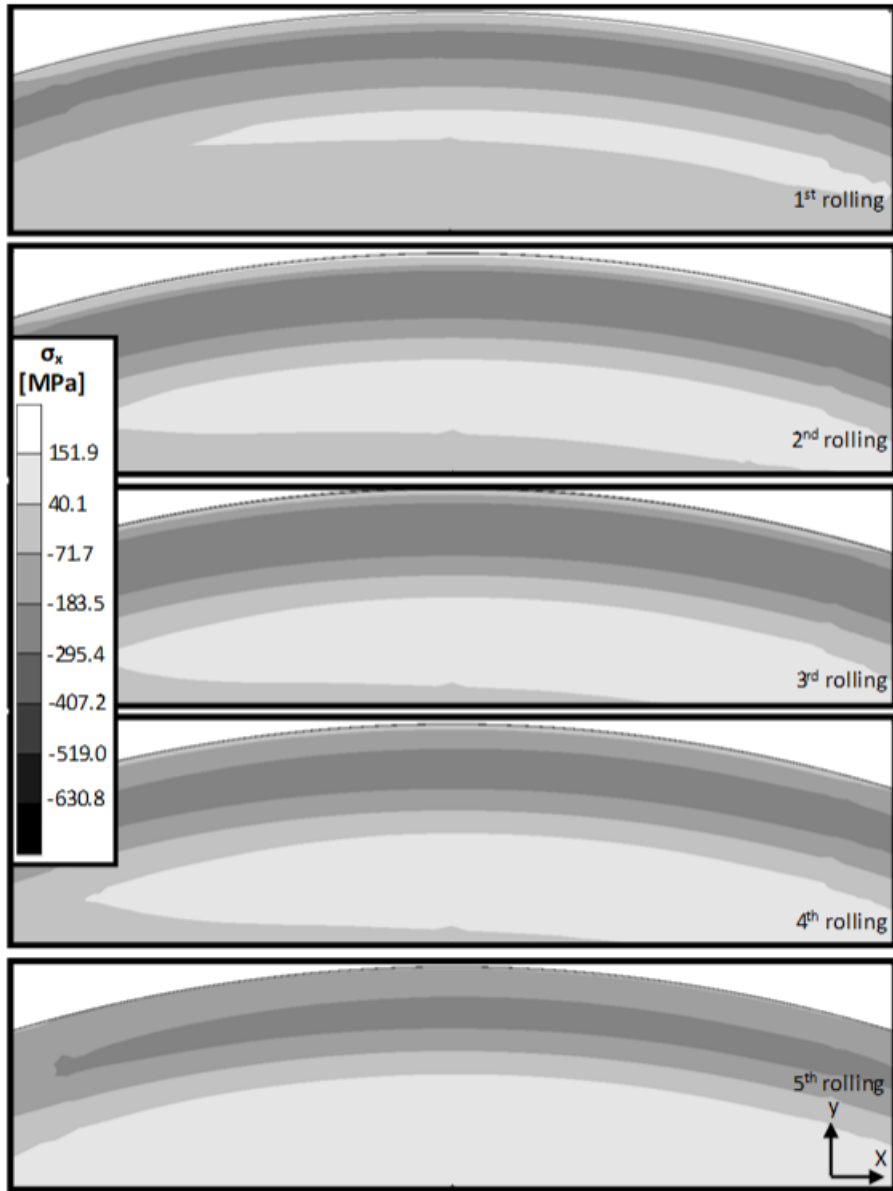


Figure 122 Residual Stress Distribution on Ø8 T. R. Model, σ_x , 125 N, 0.1 mm Feed
Parameter

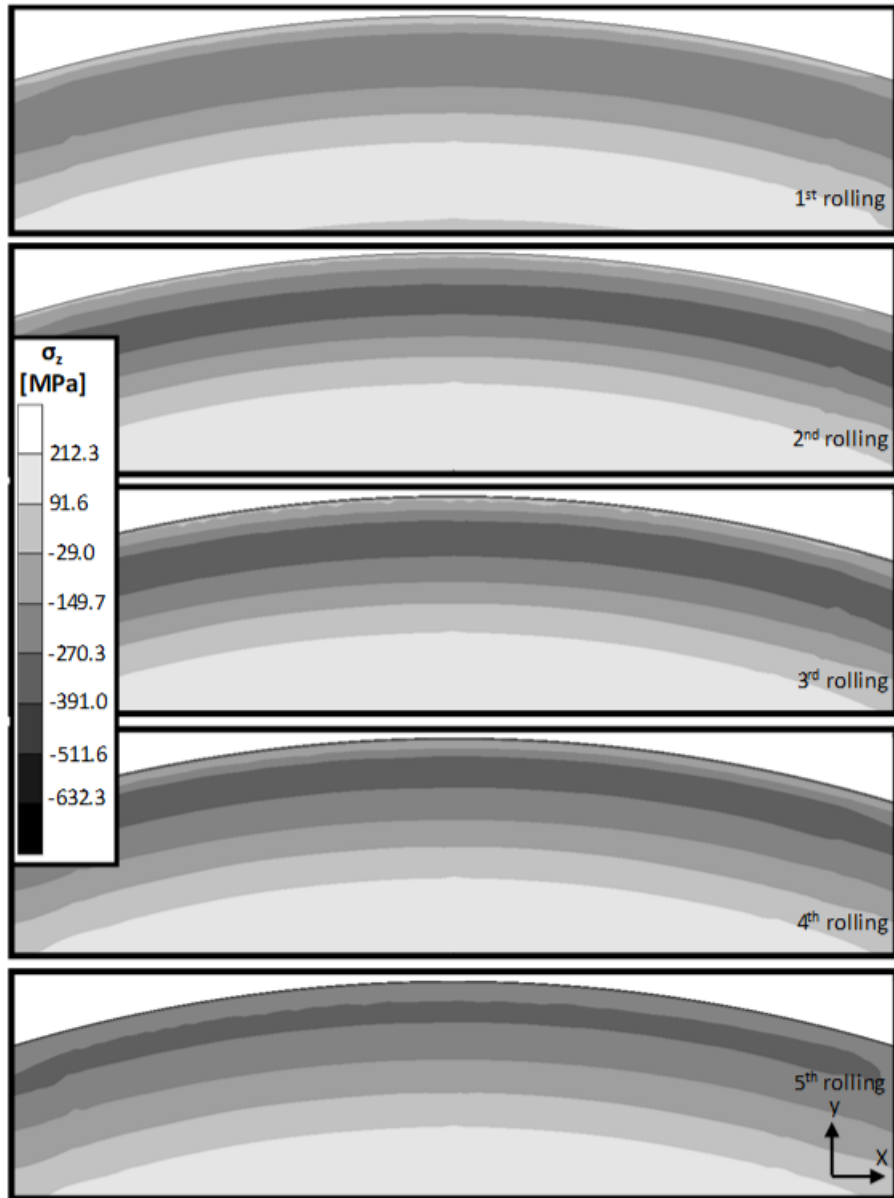


Figure 123 Residual Stress Distribution on Ø8 T. R. Model, σ_z , 250 N, 0.1 mm Feed
Parameter

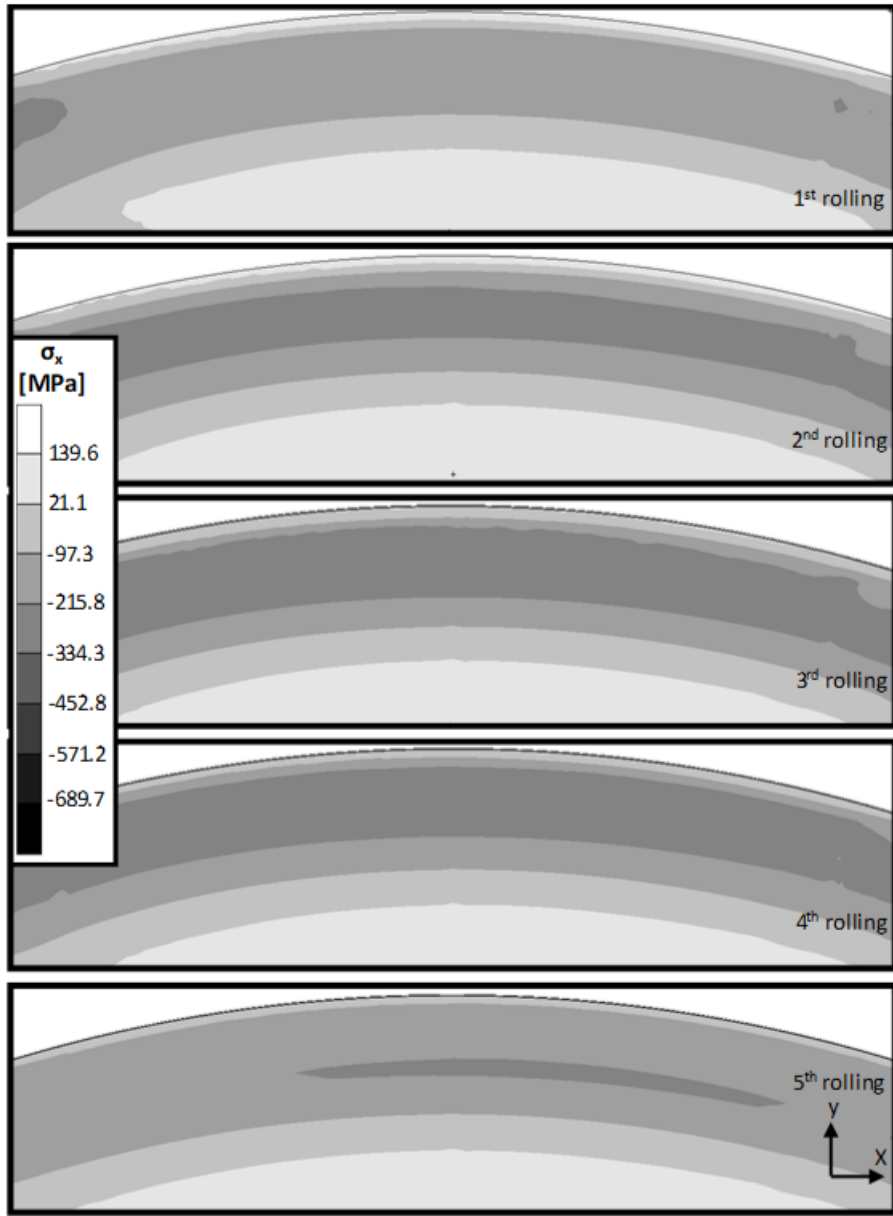


Figure 124 Residual Stress Distribution on Ø8 T. R. Model, σ_x , 250 N, 0.1 mm Feed
Parameter

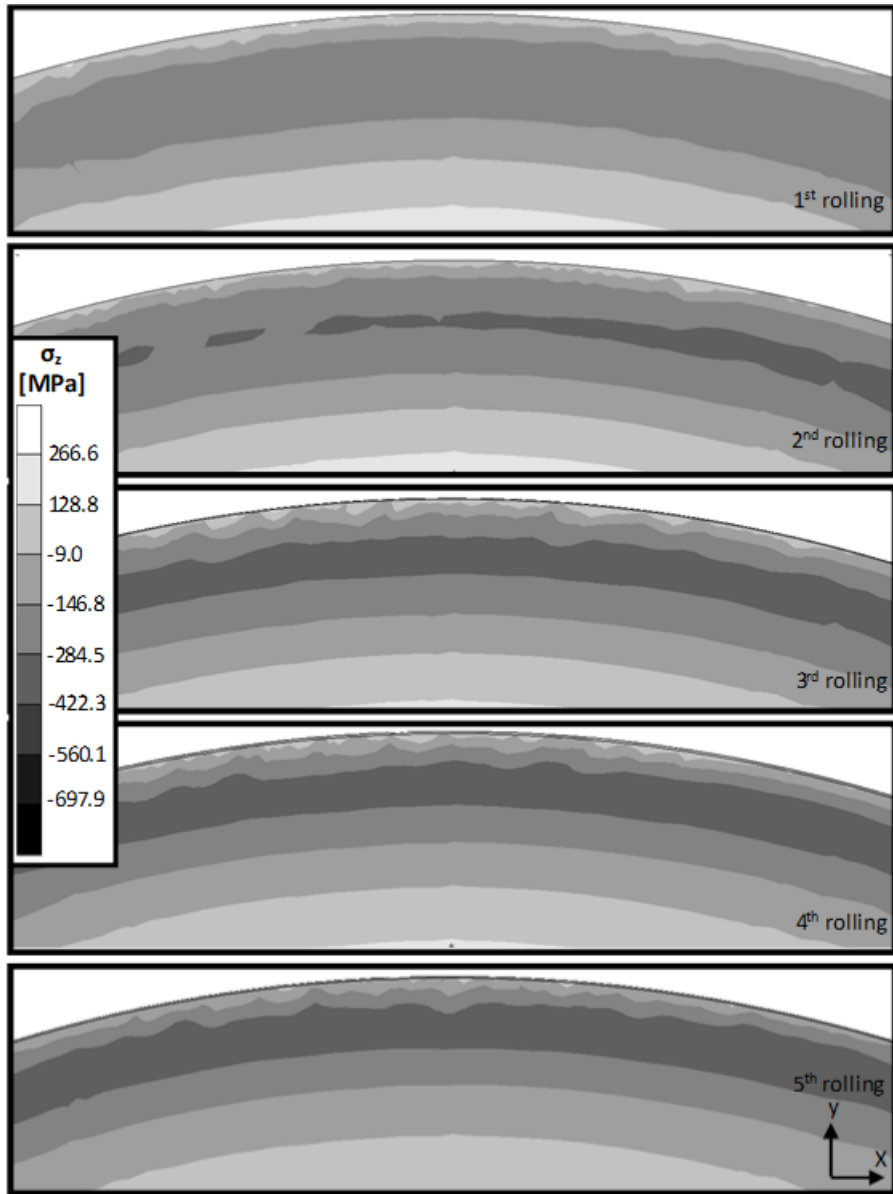


Figure 125 Residual Stress Distribution on Ø8 T. R. Model, σ_z , 500 N, 0.1 mm Feed
Parameter

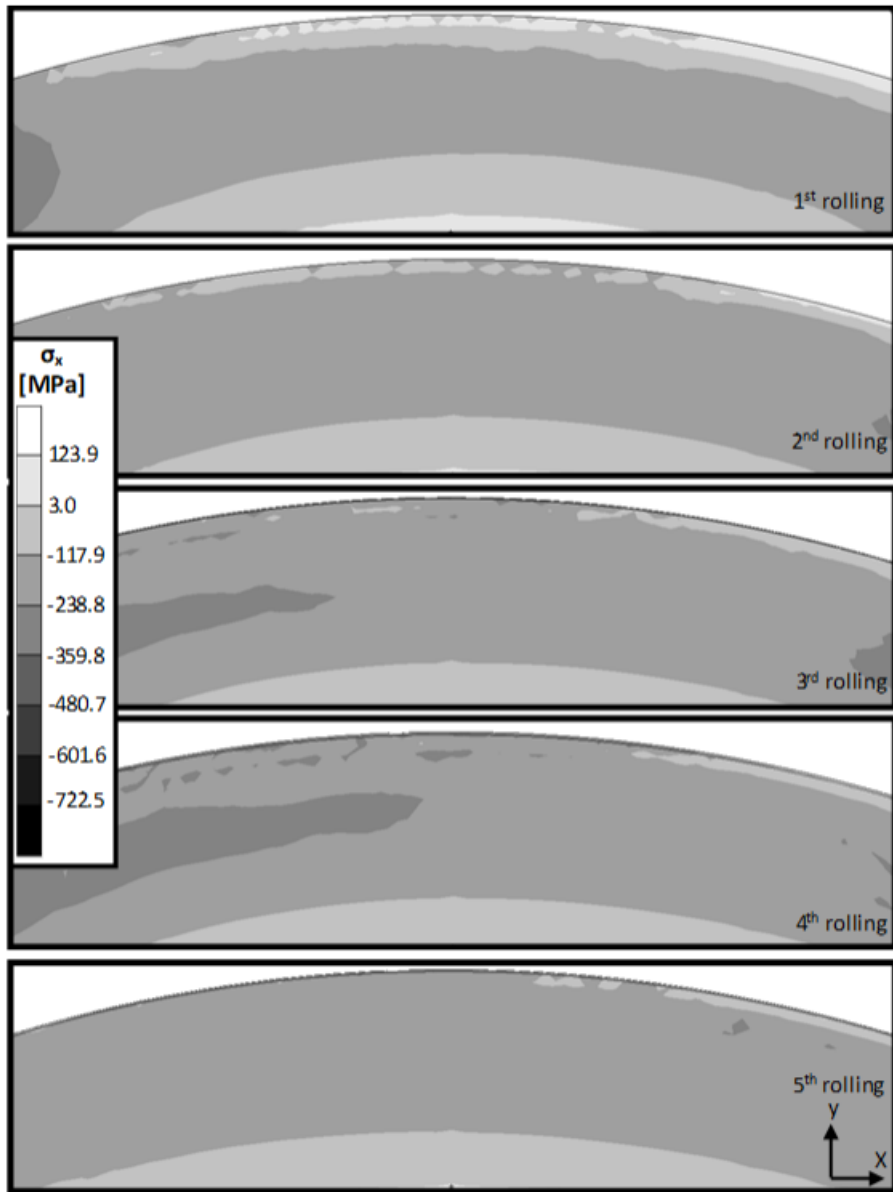


Figure 126 Residual Stress Distribution on Ø8 T. R. Model, σ_x , 500 N, 0.1 mm Feed
Parameter

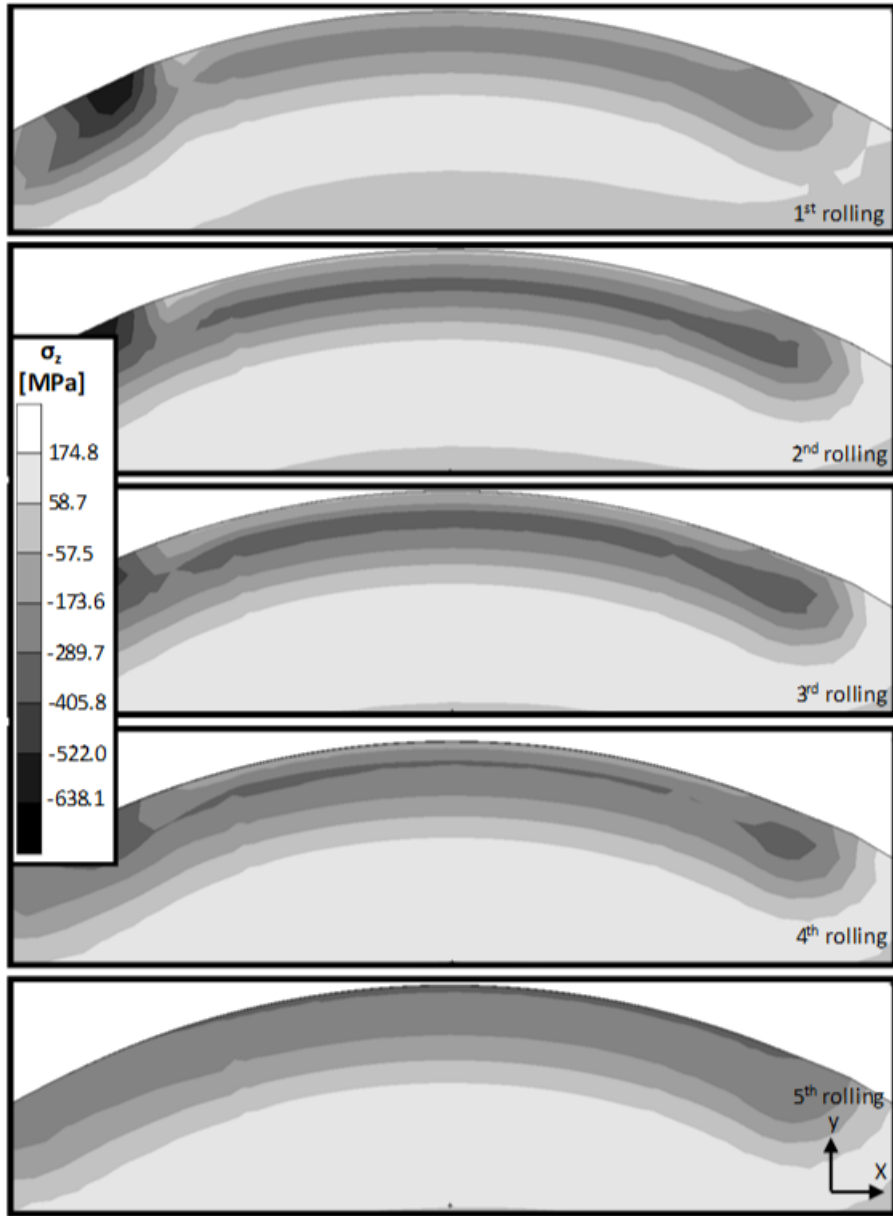


Figure 127 Residual Stress Distribution on Ø8 T. R. Model, σ_z , 125 N, 0.1 mm Feed
Parameter

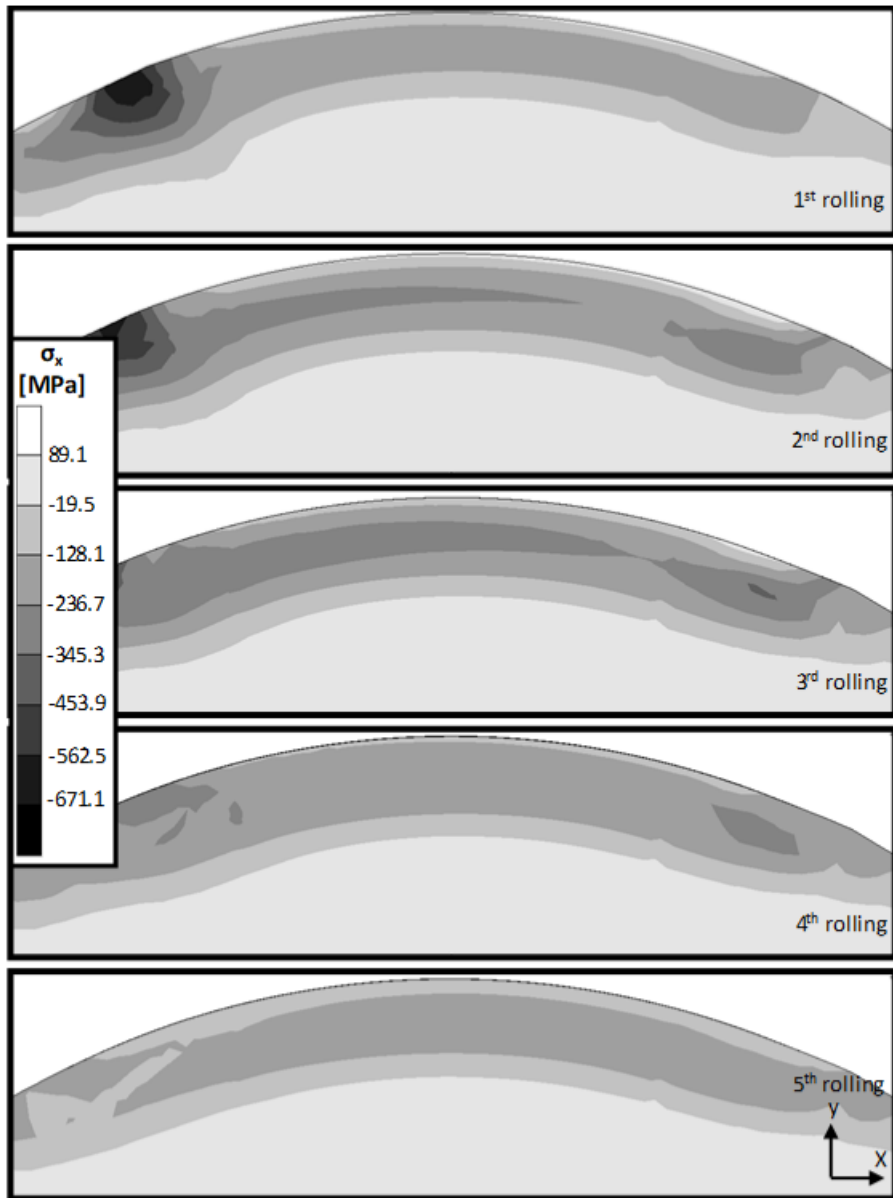


Figure 128 Residual Stress Distribution on Ø8 T. R. Model, σ_x , 125 N, 0.1 mm Feed
Parameter

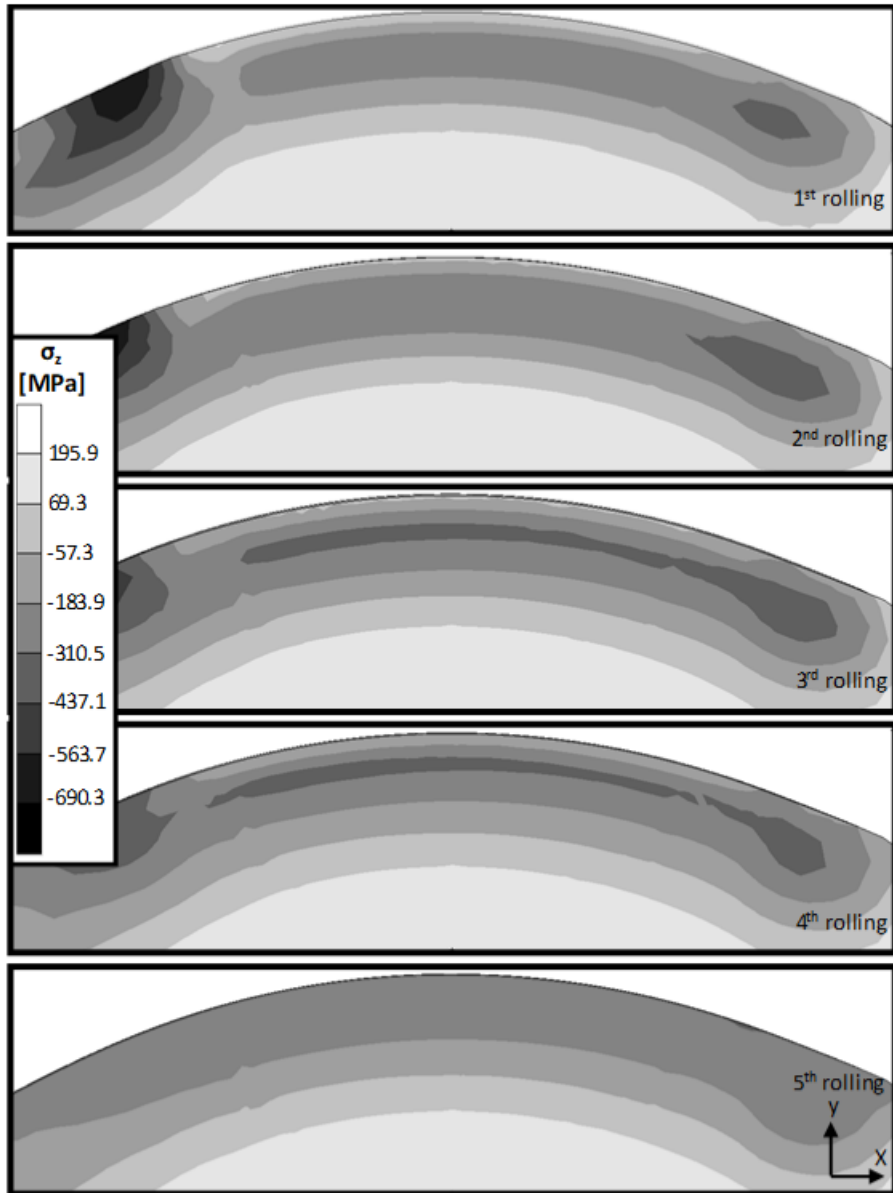


Figure 129 Residual Stress Distribution on Ø8 T. R. Model, σ_z , 250 N, 0.1 mm Feed
Parameter

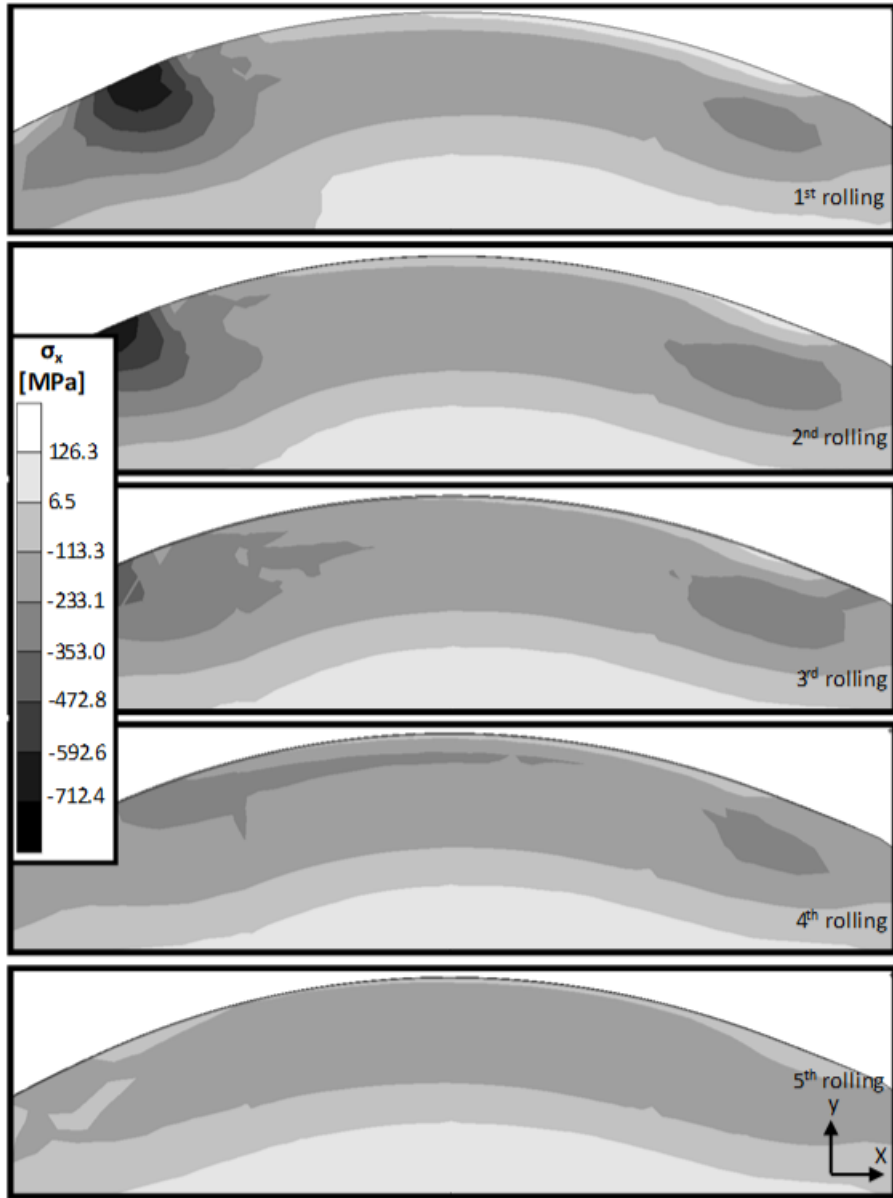


Figure 130 Residual Stress Distribution on Ø8 T. R. Model, σ_x , 250 N, 0.1 mm Feed
Parameter

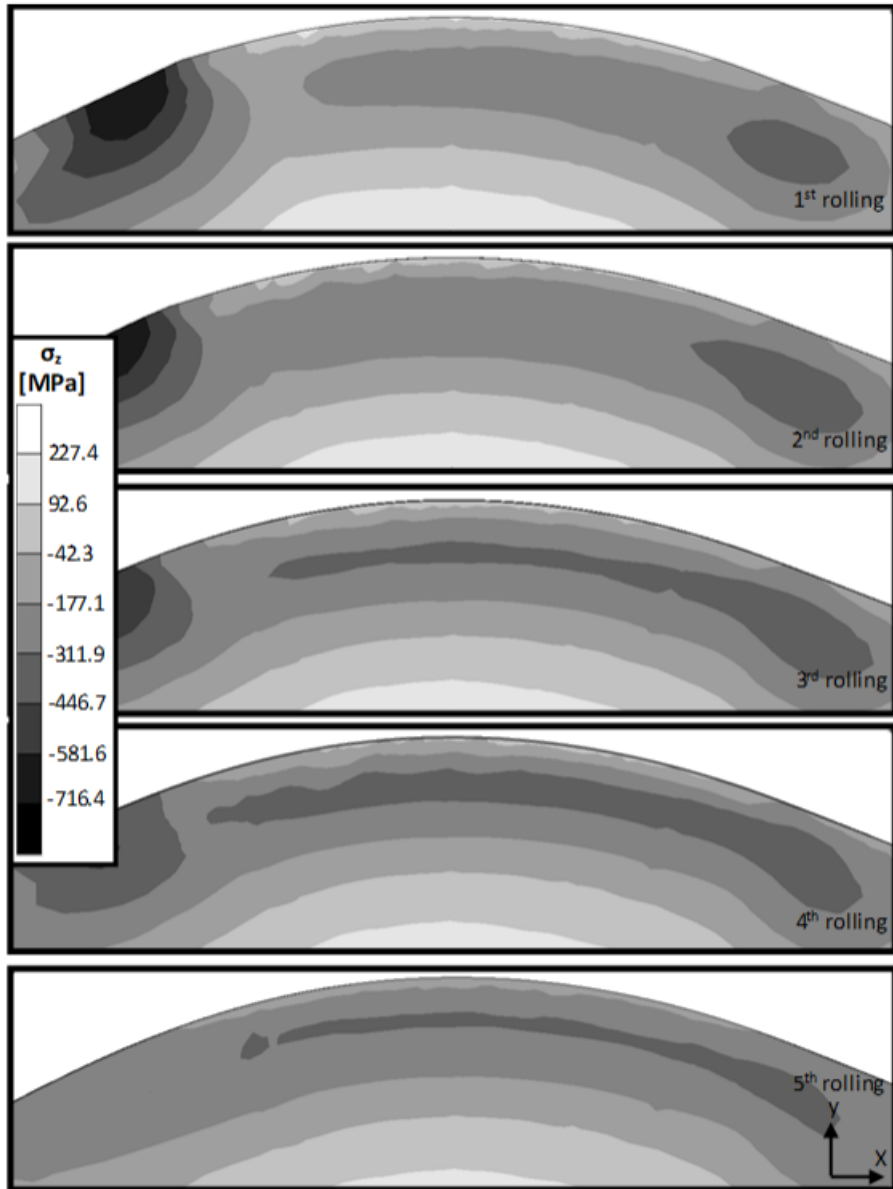


Figure 131 Residual Stress Distribution on Ø8 T. R. Model, σ_z , 500 N, 0.1 mm Feed
Parameter

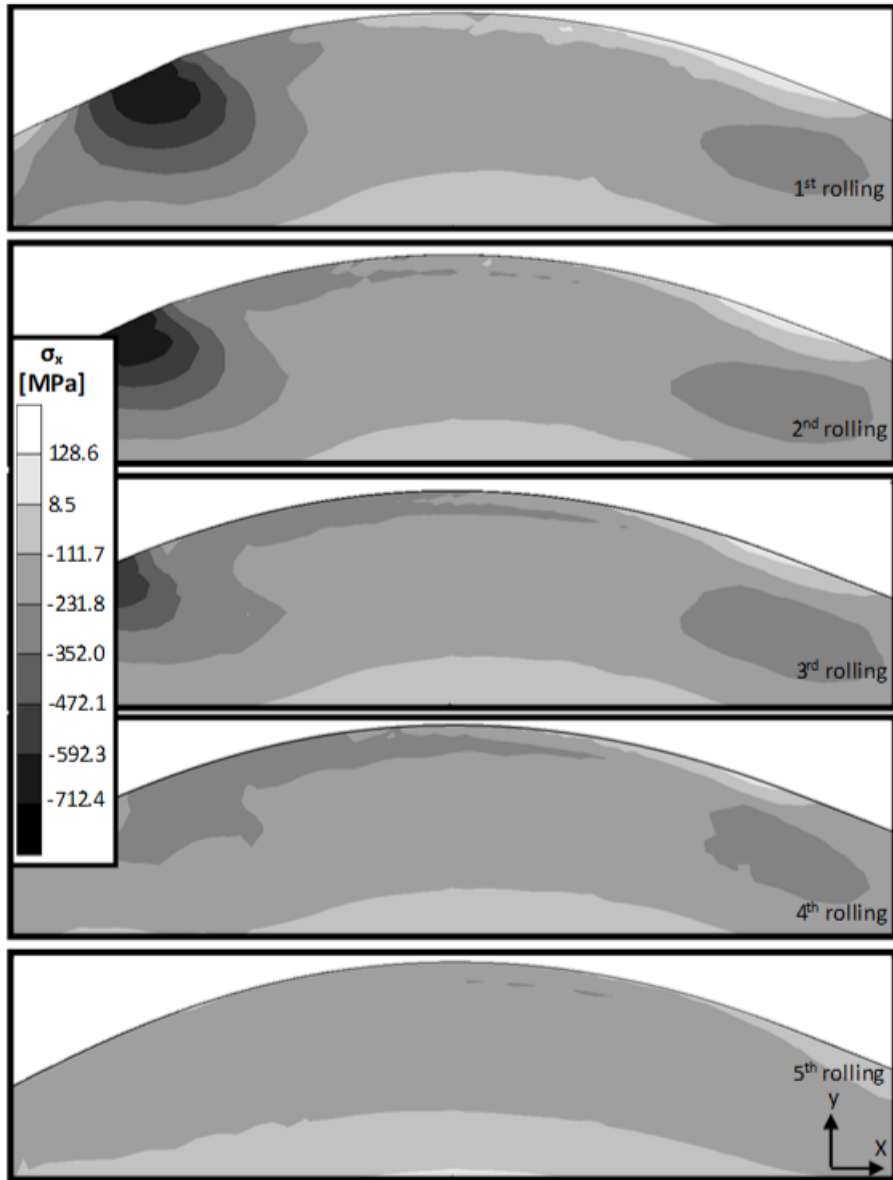


Figure 132 Residual Stress Distribution on Ø8 T. R. Model, σ_x , 500 N, 0.1 mm Feed
Parameter

8. REFERENCES

- [1] K. Kirkhopte, R. Bell, L. Caron, R. Basu and K.-T. Ma, "Weld Detail Fatigue Life Improvement Techniques. Part 1: Review," *Marine Structures*, no. 12, pp. 447-474, 1999.
- [2] M. Sticchi, D. Schnubel, N. Kashaev and N. Huber, "Review of Residual Stress Modification Techniques for Extending the Fatigue Life of Metallic Components," *Applied Mechanics Review*, no. 67, pp. 1-9, 2015.
- [3] P. Delgado, I. Cuesta, J. Alegre and A. Díaz, "State of the Art of Deep Rolling," *Presicion Engineering*, no. 46, pp. 1-10, 2016.
- [4] M. Beghini, L. Bertini, B. Monelli, C. Santus and M. Bandini, "Experimental Parameter Sensitivity Analysis of Residual Stresses Induced by Deep Rolling on 7075-T6 Aluminium Alloy," *Surface & Coatings Technology*, no. 254, pp. 175-186, 2014.
- [5] H. Coules, G. Horne, S. Kabra, P. Colegrove and D. Smith, "Three-dimensional Mapping of the Residual Stress Field in a Locally-Rolled Aluminium Alloy Specimen," *Journal of Manufacturing Processes*, no. 26, pp. 240-251, 2017.
- [6] Anonymous, "Advanced High-Strength Steel Applications Guidelines Version 6.0," *World Steel Association*, 2017.
- [7] M. Kleiner, S. Chatti and A. Klaus, "Metal Forming Techniques for Lightweight Construction," *Journal of Materials Processing Technology*, no. 177, pp. 2-7, 2006.
- [8] J. Jeswiet, M. Geiger, U. Engel, .. M. Kleiner, M. Schikorra, J. Duflou, R. Neugebauer, P. Bariani and S. Bruschi, "Metal Forming Progress Since 2000," *CIRP Journal of Manufacturing Science and Technology*, no. 1, pp. 2-17, 2008.
- [9] L. Kukielka, "Designating the Field Areas for the Contact of a Rotary Burnishing Element with the Rough Surface of a Part, Providing a High-Quality Product," *Journal of Mechanical Technology*, no. 19, pp. 319-356, 1989.
- [10] G. Lütjering and J. Williams, *Titanium*, Berlin-Heidelberg-New York: Springer, 2007.
- [11] V. Schulze, *Modern Mechanical Surface Treatment*, Weinheim: WILEY-VCH, 2006.
- [12] B. Scholtes and O. Voehringer, *Mechanical Surface Treatment*, Amsterdam: Elsevier, 2001, pp. 5253-5261.

- [13] H. Miao, D. Demers, S. Larose, C. Perron and M. Levesque, "Experimental Study of Shot Peening and Stress Peen Forming," *Journal of Materials Processing Technology*, no. 210, pp. 2089-2102, 2010.
- [14] J. Gonzalez, S. Bagherifard, M. Guagliano and I. Periente, "Influence of Different Shot Peening Treatments on Surface State and Fatigue Behaviour of Al 6063 Alloy," *Engineering Fracture Mechanics*, vol. 185, pp. 72-81, 2017.
- [15] J. Lessells and R. Brodrick, "Shot-Peening as Protection of Surface-Damaged Propeller-Blade Materials," in *Proceedings of the International Conference on Fatigue of Metals*, Londra, 1956.
- [16] D. Brunette, P. Tengvall, M. Textor and P. Thomsen, *Titanium in Medicine*, Berlin-Heidelberg: Springer, 2001.
- [17] Anonymous, "Shot Peening Applications," *Metal Improvement Company*, 2016.
- [18] T. Ludian and L. Wagner, "Coverage Effects in Shot Peening of Al 2024-T4," *ICSP9: Shot Peening*, 2005.
- [19] S. Bagherifard, I. Fernandez-Pariante, R. Ghelichi and M. Guagliano, "Effect of Severe Shot Peening on Microstructure and Fatigue Strength of Cast Iron," *International Journal of Fatigue*, no. 65, pp. 64-70, 2014.
- [20] F. Klocke and S. Mader, "Fundamentals of the Deep Rolling of Compressor Blades for Turbo Aircraft Engines," *Steel Research International*, no. 76, pp. 229-235, 2005.
- [21] P. Groche, M. Engels, M. Steitz, C. Mueller, J. Scheil and M. Heilmaier, "Potential of Mechanical Surface Treatment for Mould and Die Production," *International Journal of Materials Research*, no. 103, pp. 783-789, 2012.
- [22] M. Abdulstaar, M. Mhaede and L. Wagner, "Pre-corrosion and Surface Treatments Effects on the Fatigue Life of AA6082 T6," *Advanced Engineering Materials*, no. 15, pp. 1002-1006, 2013.
- [23] G. Majzoobi, K. Azadikhah and J. Nemati, "The Effects of deep Rolling and Shot Peening on Fretting Fatigue Resistance of Aluminum-7075-T6," *Materials Science and Engineering A*, no. 516, pp. 235-247, 2009.
- [24] P. Prevey and J. Cammett, "The Influence of Surface Enhancement by Low Plasticity Burnishing on the Corrosion Fatigue Performance of AA7075-T6," *International Journal of Fatigue*, no. 26, pp. 975-982, 2004.

- [25] P. Juijerm, I. Altenberger and B. Scholtes, "Fatigue and Residual Stress Relaxation of Deep Rolled Differently Aged aluminum Alloy AA6110," *Materials Science and Engineering A*, no. 426, pp. 4-10, 2006.
- [26] V. Backer, F. Klocke, H. Wegner, A. Timmer, R. Grzhibovskis and S. Rjasanow, "Analysis of the Deep Rolling Process on Turbine Blades Using the FEM/BEM-Coupling," *IOP Conference Series: Materials Science and Engineering*, no. 10, pp. 1-10, 2010.
- [27] S. Hassani-Gangaraj, M. Carboni and M. Guagliano, "Finite Element Approach Toward an Advanced Understanding of Deep Rolling Induced Residual Stresses, and an Application to Railway Axles," *Materials and Design*, no. 83, pp. 689-703, 2015.
- [28] H. Raedt, P. Groche, P. Grupp, G. Heimbürger, R. Koppensteiner, F. Müller, B. Nillies, E. Rauschnabel, K. Röttger, P. Strehmel, M. Türk and M. Görtan, "Recent Developments in Incremental Bulk Metal Forming," in *43rd ICFG Plenary Meeting*, Darmstadt, 2010.
- [29] D. K. Matlock, M. D. Richards and J. G. Speer, "Surface Modification to Enhance Fatigue Performance of Steel: Applications of Deep Rolling," *Material Science Forum Vols. 638-642*, pp. 142-147, 2010.
- [30] C. Sonsino, "Course of SN-Curves Especially in the High-Cycle Fatigue Regime with Regard to Component Design and Safety," *International Journal of Fatigue*, no. 29, pp. 2246-2258, 2007.
- [31] M. Frija, T. Hassine, R. Fathallah, C. Bouraoui and A. Dogui, "Finite Element Modelling of Shot Peening Process: Prediction of the Compressive Residual Stresses, the Plastic Deformations and the Surface Integrity," *Materials Science and Engineering A*, no. 426, pp. 173-180, 2006.
- [32] N.R. Tao, M. Suib., J. Lud and K. Lua, "Surface Nanocrystallization of Iron Induced by Ultrasonic Shot Peening," *Nanostructured Materials, Vol.11*, no. 4, pp. 433-440, 1999.
- [33] A. H. Clauer, "Laser Shock Peening for Fatigue Resistance," *LSP Technologies, Inc.*, 1996.
- [34] W. Braisted and R. Brockman, "Finite Element Simulation of Laser Shock Peening," *International Journal of Fatigue*, no. 7, pp. 719-724, 1999.
- [35] P. Balland, L. Tabourot, F. Degrea and V. Moreaub, "Mechanics of the Burnishing

- Process," *Precision Engineering*, no. 37, pp. 129-134, 2013.
- [36] W. B. Sai and K.Sai, "Finite Element Modeling of Burnishing of AISI 1042 Steel," *Int J Adv Manuf Technol*, no. 25, pp. 460-465, 2005.
- [37] A. Abrão, B. Denkena, J. Köhler, B. Breidenstein, T. Mörke and P. Rodrigues, "The Influence of Heat Treatment and Deep Rolling on the Mechanical Properties and Integrity of AISI 1060 Steel," *Materials Science and Engineering A* , no. 516, pp. 235-247, 2009.
- [38] G. Majzoubi, F. Z. Jouneghani and E. Khademi, "Experimental and numerical studies on the effect of deep rolling on bending fretting fatigue resistance of Al7075," *Int J Adv Manuf Technol.*, vol. 82, no. 9-12, pp. 2137-2148, 2015.
- [39] G. E. Totten and D. S. MacKenzie, *Handbook of Aluminum Volume 1 Physical Metallurgy and Processes*, New York- Basel: Marcel Dekker, Inc., 2003.
- [40] R.P. Garrett, J. J. Lin and T. Dean, "An Investigation of the Effects of Solution Heat Treatment on Mechanical Properties for AA 6xxx Alloys: Experimentation and Modelling," *International Journal of Plasticity*, no. 21, pp. 1640-1657, 2005.
- [41] Anonymus, "Aerospace Material Specification AMS 2770H, Heat Treatment of Wrought Aluminum Alloy Parts," SAE Aerospace, 1974.
- [42] G. Mrowka-Nowotnik and J. Sieniawski, "Influence of Heat Treatment on the Microstructure and Mechanical Properties of 6005 and 6082 Aluminium Alloys," *Journal of Materials Processing Technology* , no. 162-163, pp. 367-372, 2005.
- [43] Anonymous, DIN50125, Testing of Metallic Materials-Tensile Test Pieces, 2009.



HACETTEPE UNIVERSITY
GRADUATE SCHOOL OF SCIENCE AND ENGINEERING
THESIS/DISSERTATION ORIGINALITY REPORT

HACETTEPE UNIVERSITY
GRADUATE SCHOOL OF SCIENCE AND ENGINEERING
TO THE DEPARTMENT OF MECHANICAL ENGINEERING

Date: 28/06./2019

Thesis Title / Topic: INVESTIGATION OF PLASTIC DEFORMATION AND RESIDUAL STRESSES OCCURED AFTER DEEP ROLLING PROCESS ON ALUMINUM 6082 ALLOY USING FINITE ELEMENT ANALYSIS

According to the originality report obtained by my thesis advisor by using the *Turnitin* plagiarism detection software and by applying the filtering options stated below on 27/06/2019 for the total of 154. pages including the a) Title Page, b) Introduction, c) Main Chapters, d) Conclusion sections of my thesis entitled as above, the similarity index of my thesis is 5 %.

Filtering options applied:

1. Bibliography/Works Cited excluded
2. Quotes excluded / included
3. Match size up to 5 words excluded

I declare that I have carefully read Hacettepe University Graduate School of Science and Engineering Guidelines for Obtaining and Using Thesis Originality Reports; that according to the maximum similarity index values specified in the Guidelines, my thesis does not include any form of plagiarism; that in any future detection of possible infringement of the regulations I accept all legal responsibility; and that all the information I have provided is correct to the best of my knowledge.

I respectfully submit this for approval.

28.06.2019

Date and Signature

Name Surname: Ruhi Batuhan Savaşkan

Student No: N14320909

Department: Mechanical Engineering

Program: Graduate

Status: Masters Ph.D. Integrated Ph.D.

ADVISOR APPROVAL

APPROVED.

Dr. Öğr. Üyesi MEHMET OKAN GÖRTAN

(Title, Name Surname, Signature)

ÖZGEÇMİŞ

Adı Soyadı : Ruhi Batuhan Savaşkan
Doğum yeri : Eskişehir / Merkez
Doğum tarihi : 04 / 09 / 1991
Medeni hali : Bekar
Yazışma adresi : Şehit Osman Avcı Mah. 50.Sok. Cumhuriyet Apt. No:8
Daire:37 Eryaman- Etimesgut / Ankara
Telefon : 05062219379
Elektronik posta adresi : batuhan.svskan@gmail.com
Yabancı dili : İngilizce, Almanca

EĞİTİM DURUMU

Lisans : Hacettepe Üniversitesi Makina Mühendisliği
Yüksek Lisans : Hacettepe Üniversitesi Makina Mühendisliği (Devam Ediyor)
Doktora : -

İş Tecrübesi

2017 –	Türk Havacılık Uzay Sanayii A.Ş.	Mekanik Tasarım Mühendisi
2017 – 2017	Tübitak SAGE	Mekanik Tasarım ve Analiz Mühendisi
2016 – 2016	Proted Protez Ortez	Mekanik Tasarım ve Analiz Mühendisi
2016 – 2016	Artec Ltd.Şti.	Mekanik Tasarım ve Analiz Mühendisi
2015 – 2016	Inolab Bilişim Müh.	Mekanik Tasarım ve Analiz Mühendisi
2014 – 2015	Mercedes Benz Türk A.Ş.	Part Time Mühendis